OPTIMIZATION OF IMPACT RESISTANCE OF COMPOSITE PLATES AND PIPES

BY

MUHAMMAD HARIS MALIK

A Thesis Presented to the

DEANSHIP OF GRADUATE STUDIES

KING FAHD UNIVERSITY OF PETROLEUM & MINERALS

DHAHRAN, SAUDI ARABIA

In Partial Fulfillment of the

Requirements for the Degree of

MASTER OF SCIENCE

In

MECHANICAL ENGINEERING

DECEMBER 2012

KING FAHD UNIVERSITY OF PETROLEUM & MINERALS

DHAHRAN, SAUDI ARABIA

DEANSHIP OF GRADUATE STUDIES

This thesis, written by **Muhammad Haris Malik** under the direction of his thesis advisor and approved by his thesis committee, has been presented to and accepted by the Dean of Graduate Studies, in partial fulfillment of the requirements for the degree of **MASTER OF SCIENCE in MECHANICAL ENGINEERING**.

Thesis Committee

Thesis Advisor

Prof. Abul Fazal M. Arif

Member

Dr. Faleh A. Al-Sulaiman

Department Chairman

Prof. Amro M. Al-Qutub

Member

Prof. Zafarullah Khan

Dean of Graduate Studies

Prof. Salam A. Zummo

30/12/12

Date

Dedicated to my mother, my brother and my family

ACKNOWLEDGEMENTS

In the name of Allah, the Most Gracious and the Most Merciful

> Praise belongs to Allah, the Lord of all the worlds (2) The All-Merciful, the Very-Merciful. (3) The Master of the Day of Requital. (4) You alone do we worship, and from You alone do we seek help. (5) Take us on the straight path (6) The path of those on whom You have bestowed Your Grace, Not of those who have incurred Your wrath, nor of those who have gone astray. (7)
>
> Al-Fatiha

I begin with the name of Allah, the most beneficent, the most merciful. May Allah bestow peace on our beloved Prophet Mohammed (*peace and blessings of Allah be upon him*), and his family. Alhamdulillah, all praises to ALLAH for the strengths and His blessing upon me in completing this thesis. Without doubt, all my accomplishments are due to the countless blessings of ALLAH.

First of all, I would like to thank my mother and dedicate this work to her because without her presence I would not have been able to accomplish all this.

Special appreciation goes to my supervisor, Prof. Dr. Abul Fazal M. Arif, for his supervision, patience, motivation, immense knowledge and constant support. His invaluable help of constructive comments and suggestions throughout the courses and thesis work have contributed to the success of this research. His guidance helped me in all the time of research and writing of this thesis. Not forgotten, my appreciation to my co-supervisor, Dr. Faleh Abdullah Al-Sulaiman for his support and knowledge regarding this topic and for

providing me the opportunity to work on one of the fields I love to work. Also, I would like to thank Dr. Zafarullah Khan for his support and help. I could not have imagined having a better advising committee and mentors for my research.

Acknowledgements are due to *King Fahd University of Petroleum and Minerals* which gave me the opportunity to pursue a graduate degree and also for all the support I received in carrying out this research. I am also grateful to the graduate coordinator of Mechanical Engineering Department Dr. Esmail M. A. Mokheimer for his constant guidance and persuasion towards my postgraduate affairs. I would also like to express my appreciation to all the professors of Mechanical Engineering Department in particular and King Fahd University of Petroleum and Minerals in general. I would also like to mention special gratitude towards Dr. Sebestian Didierjean for his time and help while he visited KFUPM. His input was of great value as it made me understand this topic in detail.

Sincere thanks to all my friends especially the office mates at the graduate room and others for their kindness and moral support during my study. Thanks for the friendship and memories. By far, these are not the only people that helped me throughout my career and I would like to express my gratitude towards them all, they all helped me in their own way. Lastly, my deepest gratitude goes to my ex-boss Mr. Ahmad Safi from whom I learnt a lot of professional skills and for his support and encouragement for me to pursue my postgraduate studies.

TABLE OF CONTENTS

LIST OF TABLES

LIST OF FIGURES

ABSTRACT (ENGLISH)

NAME:	Muhammad Haris Malik
TITLE:	Optimization of Impact Resistance of Composite Plates and Pipes
MAJOR FIELD:	MECHANICAL ENGINEERING
DATE OF DEGREE:	DECEMBER 2012

Composite materials have seen a significant interest in the mechanical engineering applications in the past few decades. These materials provide excellent mechanical and thermal properties against the conventional materials. The properties required for certain applications of these materials can be tailored according to the needs and due to this ability composite materials have become popular choice against the conventional materials. Oil and gas industry is shifting quite rapidly towards the use of composite based pipes and replacing the conventional pipes due to their good corrosive and thermal properties. These composite based pipes are easy to manufacture, handle and install, but their behavior under impact loading is uncertain and cannot be described analytically or empirically. The lack of understanding of impact response of composite materials make it difficult to design the composite pipes to best handle the impact loading without losing the desired level of performance. The objective of the proposed work is to understand the characteristics of material and design parameters which have the most profound effect on the impact resistance of the composite plates and pipes. These factors will be then optimized such that the impact resistance will be maximized while keeping the cost as minimum as possible. A mathematical model will be developed based on artificial neural networks to optimize the impact resistance of the composite plates and pipes.

ABSTRACT (ARABIC)

ملخص الرسالة

الاسم: محمد حارث ملك

عنوان الرسالة: اتممة مقاومة الصدم للالواح المركبة والآنابيب.

التخصص العام : الهندسة الميكانيكية

تأريخ التخرج: 1434 هـ - (ديسمبر 2012 م)

المواد المركبه لها أهميه كبرى فى تطبيقات الهندسه الميكانيكيه فى العقود القليلة الماضية. وذلك لما لها من خصائص ميكانيكية وحرارية عالية مقارنة بالمواد التقليدية. خصائص المواد المركبه المطلوبه لتصميم معين يمكن تحقيقها طبقا لمتطلبات التصميم .ونظرا لهذه الخاصية أصبحت المواد المركبه الاختيار الأمثل والأفضل مقارنة بالمواد التقليدية. صناعة البترول والغاز الطبيعى توجهت سريعا إلى استخدام الأنابيب المصنوعة من المواد المركبة بدلا من الأنابيب المصنعة من المواد التقليديه نتيجة لمقاومتها الجيدة للتاكل و خصائص الحرارية الجيدة. توتميز عملية تصنيع الأنابيب من المواد المركبة بسهولة التصنيع والتداول والتركيب . ولكن خصائص هذه المواد تحت تاثير حمل الصدم غير معروف ولا يمكن تحديده تحليليا او تجريبيا. وهذا يجعل عملية تصميم الأنابيب من المواد المركبة صعبة من حيث عديد مقاومة حمل الصدم دون أن تفقد مستوى الأداء المطلوب . والهدف من هذه الرساله هو دراسة متغيرات التصميم وخصائص المواد التى تؤثر على مقاومة الصدم للألواح والأنابيب المصنعة من المواد المركبة . وكذلك البحث على الوضع الأمثل هذه المتغيرات لتحقيق اقصى مقاومة لحمل الصدم مع اقل تكلفة ممكنة.و سيتم تطوير نموذج رياضى باستخدام الشبكات العصبية الاصطناعية لاتممة مقاومة الصدم لالواح والأنابيب المصنعه من المواد المركبة.

CHAPTER 1

INTRODUCTION

Composite materials have been in human use in different forms for thousands of years, examples of earlier use of composite materials can be seen in the mud and straw bricks.

Composite materials for construction, engineering and other similar applications are formed by combination of two or more materials in order to enjoy the benefits of the properties of the constituents. A property of composite materials is that the materials are still distinguishable and don't blend completely unlike alloys, hence, normally exhibit an interface between one another. The constituent materials retain their physical and chemical properties, only to combine to give properties that are not offered by the individual constituents.

The majority of composite materials use two constituents: a binder or matrix and reinforcement. The reinforcement is stronger and stiffer, forming a sort of backbone, while the matrix keeps the reinforcement in a set place. The binder also protects the reinforcement, which may be brittle or breakable.

1.1 CLASSIFICATION OF COMPOSITE MATERIALS

Composites can be categorized in three main divisions according to the geometry of the reinforcements:

1. Particle-reinforced
2. Fiber-reinforced
3. Structural Composites

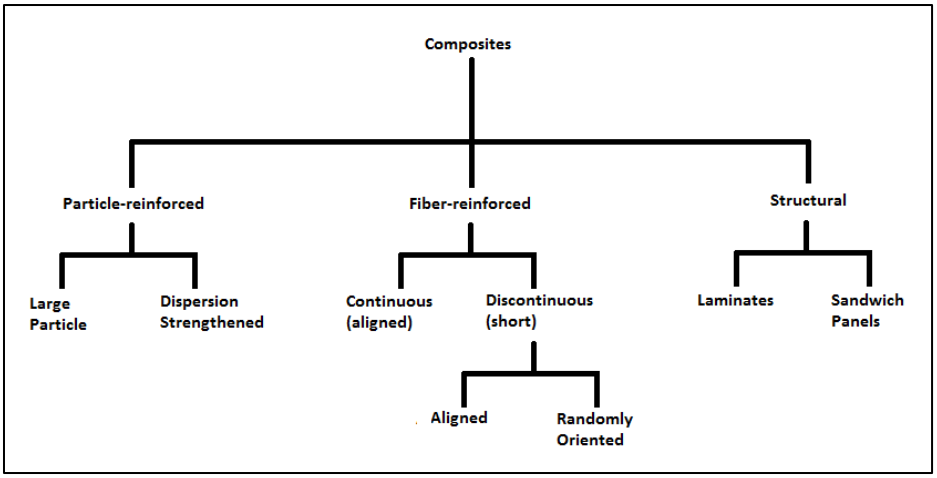

Figure 1.1: Classification scheme for the various composites types

According to the type of the matrix:

1. Polymer Matrix Composites
2. Metal Matrix Composites
3. Ceramic Matrix Composites

Technologically, the most important composites are those in which the dispersed phase is in the form of a fiber. Design goals of fiber-reinforced composites often include

high strength and/or stiffness on a weight basis. In fiber-reinforced composites, fibers are the phase that provides the strength and the ability to carry load while the matrix increases the ductility and also acts as binding agent for the fibers and also acts as load transfer medium.

Common fiber reinforcing agents include, Aluminum, Aluminum oxide, Aluminum silica, Asbestos, Beryllium, Beryllium carbide, Beryllium oxide, Carbon (Graphite), Glass (E-glass, S-glass, D-glass), Molybdenum, Polyamide (Aromatic polyamide, Aramid), e.g., Kevlar 29 and Kevlar 49, Polyester, Quartz (Fused silica), Steel, Tantalum, Titanium, Tungsten, Tungsten monocarbide.

Common resin materials include Epoxy, Phenolic, Polyester, Polyurethene, and Vinyl Ester.

1.2 COMPOSITE PIPES

Composite pipes are gradually replacing the conventional pipes in the industrial applications. Composite pipes show good resistance to corrosion compared to metallic pipes in applications where pipes are carrying fluids like water or highly corrosive sulphuric acid is present in it. This property makes them ideal for usage in pipe industry [37].

Composite pipes can be described in two categories depending upon the type of resin material.

1) Reinforced thermosetting resin pipes (RTRP)
2) Reinforced thermoplastic pipes (RTP)

Due to their superior mechanical and thermal properties over conventional materials, fiber reinforced composite materials are being preferred in the petroleum industry. Initially they were developed because of their high non-corrosive properties for onshore oil and gas industry, particularly in the Middle East. The characteristics of the fiber reinforced composites also attracted the deep-water offshore oil industry which was looking for strong, lightweight materials to replace the heavy alloy piping used on oil platforms in sea water. As an example of the advantage gained by replacing conventional material pipelines with composite materials is that a 6-inch diameter pipe weighs 4 pound per foot, whereas copper nickel pipe with the same diameter weighs 24 pound per foot [51].

Apart from the oil and gas industry, another major area of significant interest where composite pipes can be of use is the water related applications. Especially in the Middle East, lack of fresh water reservoirs put forward the need of desalination applications. The desalination application requires piping systems that are corrosion resistant [61]. Water losses due to degradation of traditional pipe systems present a significant financial and maintenance problem. Composite based piping systems provide good protection against the corrosion. Fiberglass pipe systems have become the material of choice in the desalination and water distribution industry.

1.1.1 Advantages of Composite Pipes

There are several major advantages composite pipes offer over conventional material pipes. Corrosion resistance is one of those, fiberglass pipes are resistant to corrosion for a long period of time and resists corrosion to a variety of media including seawater, hot brine, acids and other chemicals [61]. Also, the composite materials have a high strength to weight ratio compared to metals and the transportation and installation of the composite materials is easier. Large lengths of composite pipes can be easily manufactured and can be assembled with relative ease on sites.

Since, composite materials are corrosion resistant; the cost of maintenance is considerably lower. Also, the fatigue resistant capability of composite pipes is better than the metallic pipes. Also, low internal friction, fire resistance, torsional stiffness and good impact resistance combined with the flexibility in design as per strength and other requirements make them ideal replacement for the current conventional materials [61].

1.1.2 Mechanical Damages in Pipes

Mechanical damages to pipes occur frequently. These damages can cause leakage of oil and gas from pipes resulting from structural failure and may lead to reduced operating pressure or stopped production, human and environmental hazards and the heavy economic losses [7].

There are, however, some issues related to the use of composite piping systems primarily the lack of test data to support the materials' long term durability. The failure caused by the mechanical damages is one of the important aspects that need to be

addressed. The structural failure of these pipelines can be due to a number of effects as burst, impact, puncture, overload, buckling, fatigue and fracture.

One of the major causes of damages in pipes are considered as “External Damage” caused by foreign objects and third party damage such as caused by a farmer ploughing a drainage ditch, or a supply boat dragging its anchor around an offshore platform [24]. These structural components are often very susceptible to foreign object impact during service. These damages can be vulnerable and can go unseen especially in case of low velocity impacts since these are not visually observable. A small dent caused by such impacts can lead to significant underlying damages for example, delamination, matrix cracking, fiber breakage and fiber/matrix interfacial debonding induced within the laminate [27].

Outside forces are one of the major causes of pipeline failures. Figure 1.2 shows the data for USA.

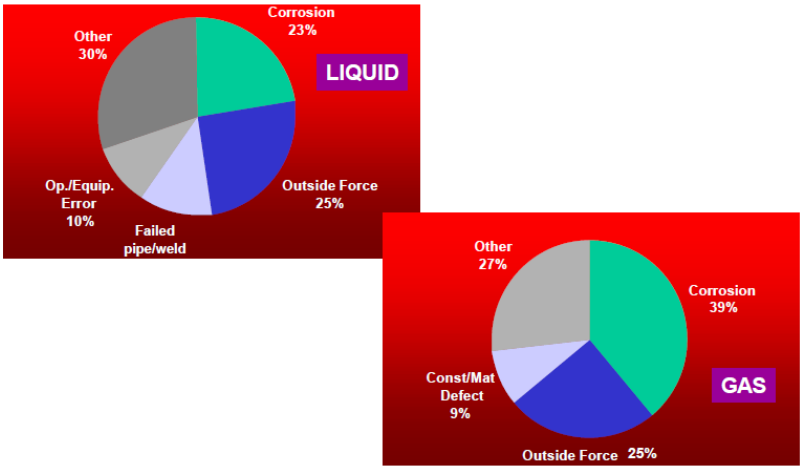

Figure 1.2: Data for pipelines damage in USA [24]

Historically, the pipelines used were made from steels. Steel is a ductile material and the specifications used in the industry are already set for its use. The ASME codes B31.4 for oil applications and B31.8 for gas applications provide measures for the different kind of damages and repairs [12]. These materials are tested for their ductile behavior. Impact tests are considered good method to measure toughness of pipelines.

1.1.3 Impact Damage

During the product lifecycle it is always expected that damages can occur due to impact by foreign objects. Mechanical damage can occur during handling, installation and service to the composite pipes. To ensure the reliability, we need good impact properties against low and intermediate velocity impacts. Due to the laminate structure of composite materials their behavior to impacts is different to the metallic structures. The modes of damage in composite structures due to impact can be categorized as matrix cracking, fiber breakage and/or delamination [14].

Impact generally causes low to medium energies which cause a global structural response, and often results in internal cracking and delamination, while at higher energy levels can cause penetration and excessive local shear damage [1].

The impact damage can be caused by a number of reasons some of which are listed as:

1) Dropped tool
2) Damage due to mishandling
3) In-service impacts
4) Hail and Debry

The composite materials are prone to low energy impacts that can be observed with the effect of delamination in the plies and can be indirectly responsible for the failure. Delamination result in lowering of the elastic moduli, strength, durability and damage tolerance [14]. Low velocity impacts can also cause matrix cracking which sometimes may not be on the surface of impact but on the internal or bottom surface, this is due to the fact that the laminate is flexible. Matrix cracking is in the perpendicular direction to the plane of the laminate and is a tensile crack. In thicker laminates, matrix cracking is near the top surface and characterized as the shear crack.

The damage in composite materials due to impact force is a complex mechanism and still there are no analytical methods that can be generally accepted to define the phenomenon.

In addition to these, the micro failure modes commonly observed in composite laminates are fiber breakage, fiber micro buckling and matrix crushing, transverse matrix cracking, transverse matrix crushing, debonding at the fiber-matrix interface and delamination [14].

1.2 MOTIVATION

The literature review presented in the following chapters of this document serves as the state of the art in the field of the impact resistance and behavior of composite laminated plates and shells. By studying in detail the available literature, a number of motivations have been found to continue the work in the field of optimization of the impact resistance of composite laminated plates and pipes. It is apparent that a lot of

effort by various researchers around the globe has been put into the study of the behavior and dynamic response of composite materials under low velocity impact loading. Most of the work has been focused on the damage characterization and the initiation and propagation of damage under certain conditions. These studies have provided a great insight into the behavior and response of composite laminates plates and shells when impacted by foreign objects having low-velocity impacts. While there have been a lot of parametric studies considering the effects of various factors involving both the composite structure and the impactor, there is no logical conclusion to the effects which enhances the impact resistance of such structures. It is known from these studies that the impact response of composite plates depend upon the size, shape, mass and velocity of the impactor, also the impact response is the characteristic of the material and geometric properties of the composite plate or shell itself. This is apparent that the properties and circumstances involving the impactor are not in the control of the designers; rather the composite plates or shells can be manipulated such that the impact performance of these structures can be enhanced.

The studies provide a general understanding of different effects material, geometric and boundary conditions of the composite structure have on the impact resistance. This provides the opportunity to further take these studies and develop such characteristics of materials and other factors related directly to the composite structure so that the impact performance can be increased. This study will focus on such factors that will give the optimized performance of composite laminated plates and pipes under low velocity impact.

1.3 OBJECTIVES AND APPROACH

The objectives of the thesis study are listed as:

1) To develop an optimization procedure for the fiber reinforced polymeric composite structures against the low velocity impact loads and resulting in an estimation model.
2) Apply the said developed model for the optimization of a composite laminated flat plate.
3) Apply the said developed model for the optimization of a composite pipe.

1.4 METHODOLOGY

The optimization of the composite plates and pipes is divided into two phases, in the initial phase a model is developed for the composite laminated plates and the study is based upon models and results from available literatures.

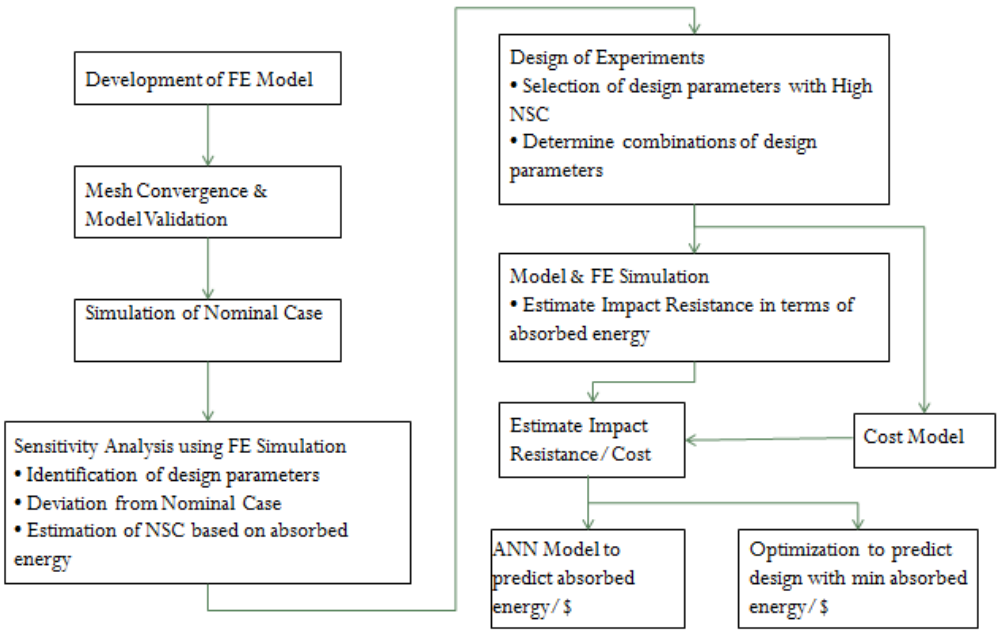

Figure 1.3: Flow Chart of the proposed methodology

CHAPTER 2

LITERATURE REVIEW

There have been a number of studies on the effect of different parameters on the impact characteristics of composite plates and pipes. These studies include experimental [2,5,13,25,58,63,66,69] numerical [6,40,41,66], and analytical [26] which discuss the impact behavior of different composite laminates and discuss the effects of various parameter changes and a number of studies which studied numerically [32,34,35,56,72,73] and a few experimental studies [43,72] have also been performed on laminated composite shells. There are a number of studies which have developed analytical or numerical techniques to study the impact response of composite plates and shells under low energy impact damage.

2.1 EXPERIMENTAL STUDIES ON PLATES AND LAMINATES

Yang & Cantwell [71] conducted a number of low velocity impact tests on (0^o, 90^o) glass fiber reinforced epoxy resin to study the effects of varying key parameters on the damage initiation threshold. The results show that the impact resistance is proportional to the thickness of the composite panel. Also, the tests show that the impact resistance was not affected by the plate's geometry. A further study by Yang et al was done to study the

effect of impactor shape. The focus of their study was the effect of key parameters, such as target size, projectile diameter and test temperature on damage initiation. The tests were carried out on samples of unidirectional E-glass fiber reinforced FM94 epoxy resin. The majority of tests were conducted on laminates of 1.8 mm thickness while few tests were carried out on laminates of thickness ranging from 0.8 mm to 3.6 mm. Tests were also undertaken to study the effect of temperature on the damage initiation. Tests were carried out at temperatures of 45, 60, 75 and 90^{o} C. In these tests, the damage initiation threshold was established by increasing the impact energy until delamination just became apparent in the test samples. The samples were not subjected to multiple impact tests considering that would result in fatigue and a lower value of damage threshold. The tests conducted by Yang and Cantwell, suggested that the damage initiation force is proportional to the target thickness. The tests demonstrated dependency in the order of $t^{3/2}$, where 't' is the thickness of the composite plate. This result was verified with the studies conducted earlier. They also carried out experimental studies on whether the geometry of the test specimen effects on the damage initiation threshold. This result was also supported by earlier studies that the damage initiation threshold does not depend upon the panel size. The final parameter studied was the effect of temperature and it was expected that temperature will have an effect on the matrix fracture. Tests were conducted at a number of temperatures between 23^{o} and 90^{o} C. A linear relationship was observed between the thickness of the panel and the damage initiation force at a particular temperature. It was observed that the damage threshold increased with temperature for thinner laminates.

Keršys, Keršienė, & Žiliukas [5] studied the impact response of woven carbon/epoxy and E-Glass/epoxy composite systems on vehicle body structures by considering energy profile diagrams and force-displacement curves. For low velocity impact tests, drop weight tests were performed. To determine the mechanism of impact damage the experiment was performed when laminated composite materials were deformed with low impact energy. The maximum energy used in the test was equal to 120 J by means of a vertically falling impactor. The total amount of energy introduced to a composite specimen and the energy absorbed by the composite specimen through the impact event are important parameters to assess impact response of the composite structures. The experiments demonstrated the fact that was also displayed by numerical studies was that the reduction in the stiffness of the composite plate. To estimate the energy absorbed during the impact a contact force F(t) was measured during the impact. This force depends upon the impactor mass 'm' and the velocity 'v'. Given an initial velocity 'v_0', that is a function of acceleration due to gravity and downfall height 'H'.

$$v_0 = \sqrt{2gH}$$

Impactor speed and displacement 's' as the function of time are given by integrating the impact force:

$$v(t) = v_0 - \left(\frac{1}{m}\right)\int_0^t F(t)dt$$

$$s(t) = \int_0^t \left(v_0 - \left(\frac{1}{m}\right)\int_0^t F(t)dt \right)$$

The kinetic energy of the impactor and the absorbed energy

$$E_{imp} = \frac{1}{2} m v^2$$

$$E_{ab}(t) = \frac{1}{2} m v_0^2 - \frac{1}{2} m \left(v_0 - \left(\frac{1}{m} \right) \int_0^t F(t) dt \right)^2$$

It was observed that the stiffness of E-Glass/Epoxy composites during impact decreased with the increasing displacement due to great specimen deflection related with non-linear membrane effect. Force-time relationships were almost symmetrical. But the area under the force-displacement curve showed the great part of impact energy absorbed with the laminar composite at low velocity impact energies. The results show that at low impact energies of 6 J, the force value of 3.08kN was maximum which gradually decreases to zero. But when the impact energy is greater, the maximum force value is reached when the damage under the impactor occurs after the greater total displacement.

Rilo & Ferreira [58] conducted their study on the experimental investigation of low velocity impacts on glass-epoxy laminated composite plates. The characterization of the damage was done in relation to the type of test, stacking sequence, dimensions and the maximum force of the impact.

2.2 NUMERICAL STUDIES FOR IMPACT ON COMPOSITE PLATES

A number of studies were also carried out using the numerical approach to investigate the impact response of composite laminates and plates.

Setoodeh et al. [62] used a three dimensional elasticity based approach coupled with the layer wise laminated plate theory by J.N. Reddy. The study considers the effects of low velocity impact of general fiber reinforced laminated composite plates. A custom finite element code was developed for the impact response based on 3-D elasticity approach. Hertzian nonlinear contact law used to model the contact forces between the impactor and the target surface. The effect of impact velocity, mass of the impactor and the material properties were studied. The method applied by Setoodeh et al adopts a combined two- and one-dimensional analysis, which reduces the number of manipulations and the complexity in the formulation of the 3-D finite element method. The procedure is not completely three-dimensional yet it is capable of describing the impact behavior economically and accurately at the same time. In the FE modeling of Setoodeh et al, 9 noded quadratic surface elements with 3 noded quadratic elements in the thickness direction were used.

Farooq & Gregory [18] developed a finite element computational model to study the impact behavior and the failure of CFRP panels that are impacted with low velocity drop-weight. The impactor used for the study is a flat-nosed tip object. Farooq et al used the commercially available software ABAQUS to to study the critical damage regions under and near the impact zone. In-plane stresses were calculated from the model and the transverse shear stress were calculated using Trapezium rule from the standard equilibrium equations. The method used in this study is different from the Setoodeh et al as it is a 2-D model to predict the 3-D transverse shear stress. The calculated and the predicted stresses were used with failure theories to predict possible failure modes.

Farooq & Gregory [17] in the paper titled “Finite Element Simulation of Low Velocity Impact Damage Morphology in Quasi Isotropic Composite Panels Under Variable Shape Impactors” studied the barely visible impact damage (BVID), its initiation, growth and tolerance in fiber based composites under the low velocity impact. The impact damage reduces the stiffness of the composite panel and this concept was used in the model. Quasi isotropic specimens were selected to model the damage in the fiber directions. Three different specimens and three different types of impactor nose shapes were used. It is predicted that under the same loading conditions different nozal tips produce different damages. The energy absorbed during the impact is dissipated in the form of matrix damage, fiber fracture and delamination, this result in significantly reduced stiffness. Low velocity impacts mean longer contact time between impactor and target surface which causes global deformation which can cause internal damage that can be difficult to detect. Farooq et al have studied the effect of such damages on the stiffness and the operational life of composite panels after low velocity impacts.

Tiberkak et al. [65] has investigated the response of Fiber reinforced composite under the low velocity impact loads. Mindlin’s plate theory is implemented in the FE model which uses a 9-noded Lagrangian element. The study suggests that the increase in 90 degree plies increase the contact force implying a reduction in the rigidity of the laminate. Initially, threshold velocities were evaluated for matrix crack initiation. Afterwards, using appropriate failure criteria will be used to predict matrix cracking at higher velocities. The results in this study suggest that the damage occurs in the upper 90 degree plies with the dominance of transverse shear stress. The study is based upon the impact of a spherical object with low velocity upon a composite laminated plate

containing a number of transversely thin layers and the contact force is applied at the center of the plate. The Mindlin plate theory takes into account the effect of transverse shear deformation and is applied in this study. The impact between the impactor and the composite plate is considered frictionless, the damping in the plate is neglected and the impactor is considered as a rigid body with isotropic properties. This study also applies the Hertzian law to calculate the contact force between the impactor and the composite plates. The study performs a parametric analysis by varying boundary conditions, stacking sequence, size of the composite plate and velocity of the impactor.

Tiberkak et al. observed no significant variations in the results with the change in boundary conditions. The effect of change of the stacking sequence shows that the contact force increases with the increase in the thickness of the 90 degree plies that mean the rigidity of the laminates is reduced. The contact forces increase with an increase in the percentage of fibers in the 90 degrees direction.

Heimbs et al. [22] conducted their analysis of impact on a composite plate with compressive preloads. Since, in real life systems the composite plates may be subjected to different stress states when it is being impacted and hence its behavior can be different from the unloaded or without stress behavior. The main issues covered by Heimbs et al are the modeling of composite laminate, its delamination and the implementation of preload. Impact loads are considered as a transient load and hence FE codes are based on explicit time integration, using small time step intervals. But the preloading is a static load making the use of implicit calculations more appropriate. That's why Heimbs et al have used specific numerical techniques for the solution of a combination of preloading and impact loadings. The results of the study were supported by a number of tests

conducted on the drop weight test method. The tests were conducted for both preloaded and unloaded composite laminates. The tests conducted on compressive preloaded specimens indicated that preloading results in increased deflection of the CFRP plates and hence more material damage. This is due to the fact that more energy is absorbed and less is rebounded as elastic spring back effect which is the case with unloaded CFRP plates. The FE model was developed in LS-DYNA and it was developed with the modeling of the composite material including the intra laminar failure and delamination failure, the modeling of the preload and the impactor. The composite laminate was modeled as 24 plies of unidirectional laminas as 2-D shell elements. A number of failure criteria were defined based on the loading and the material damage such as tensile failure in matrix direction, tensile failure in fiber direction, compressive failure in matrix direction and compressive failure in the fiber direction. Failure is considered as soon as one of these criteria was met. In addition to these, strain based failure was also defined.

Interlaminar failure is another major phenomenon in the low velocity impacts of composite laminates, delamination absorbs energy upon impact and as a result the stiffness of the laminate is reduced. In LS-DYNA, there are two methods to include delamination as described by [22]. One of the methods is to use the cohesive brick elements between separate layers of shell elements with material law that can describe the damage process of the laminate connection.

The literature survey showed that so far the majority of the work in the impact analysis of composite materials has been focused on the study of composite laminates and very few studies have considered composite shells such as pipes. There is a lot of potential in the research related to the impact response of composite pipes and need to

develop solutions for the improvement of impact characteristics of composite pipes subjected to low velocity impacts.

Naik and Meduri [53] studied the effect of laminate configuration on the impact behavior of composite laminates. Studies were carried out on different mixed composites, cross-ply laminates, woven-fabric composites and 3-D composites. The studies concentrated the effect of different laminate configurations on the impact response. The impactor mass, velocity and the incident impact energy were kept constant keeping in view of the typical tool drop scenario. From the study it is observed that the mixture of Unidirectional and woven fabrics demonstrates more resistance to impact damage.

2.3 STUDIES ON COMPOSITE SHELLS

A limited number of studies have also been done on the impact behavior of composite shells. A brief review of these studies is presented.

Ibekwe et al. [27] discussed the effect of a thin metallic shell bonded to the outer surface of a laminated composite shell as a bumper layer. The experimental study revealed that the inclusion of a thin aluminum sheet increased the initiation energy that is the metallic sheet was able to absorb some of the impact energy. The maximum impact load and the deflection at maximum load were increased and the impact duration reduced. The higher impact loads did not cause considerable damage in the specimens with bonded aluminum sheet and only a slight reduction in the bending strength of the specimen was observed compared to the specimen without the aluminum sheet. The

study by Ibekwe et al. showed that the damage was primarily in the bumper layer i.e. the aluminum sheet and it has served its purpose of absorbing the impact energy.

Yokoyama, Donadon, & de Almeida [72] presented an energy based failure model to study the impact resistance of the composite shell laminates. The damage model is formulated using a combination of stress based, continuum damage mechanics and fracture mechanics approaches within a unified procedure by using a smeared cracking formulation. The damage model was implemented in ABAQUS as a user defined material for shell elements and the damage model was validated with experimental results from previously available studies. In total five failure criterions were used in the study namely, tensile and compression fiber failure, tensile and compression matrix cracking and in-plane shear failure modes defined as:

Tensile fiber failure $$\frac{\sigma_{11}}{X_t} \geq 1$$

Compression fiber failure $$\frac{|\sigma_{11}|}{X_c} \geq 1$$

Tensile matrix cracking $$\frac{\sigma_{22}}{Y_t} \geq 1$$

Compression matrix cracking $$\frac{|\sigma_{22}|}{Y_c} \geq 1$$

In-plane shear failure $$\frac{|\tau_{12}|}{S_{12}} \geq 1$$

Based on these failure criterions, damage evolution laws were developed for fiber breakage and matrix cracking. They studied the effects of three parameters namely the presence of pressure loading, the laminate thickness and curvature. The main contribution of the paper is the development of damage models and the verification. The numerical results indicated that thickness, curvature and pressure significantly affect the damage extent on pressurized composite laminates under impact loading. This becomes more visible for plates, which shows a greater susceptibility to the pressure effects. The damage extent under impact loading decreases when combined with internal pressure effects. The results indicated that larger the plate curvature higher is the amount of dissipated energy during the impact loading. Moreover, the amount of dissipated energy decreases as the plate thickness increases.

Her et al. [23] studied the effects of low velocity impacts on shell structures using ANSYS/LS-DYNA as well as the effect on the composite laminates. The effects of parameters like shell curvature, type of support boundary conditions and impactor velocity were analyzed. The results show that the structures which have smaller curvature and clamped boundary condition result in a larger contact force and less deflection. In the study by Her et al., the focus was on the evaluation of transient response of the impact on composite laminates, cylindrical and spherical shells.

Krishnamurthy et al. [36] discussed the impact response and the damage of laminated composite shells by a metallic impactor using Finite Element Method. The important parameters that formed the basis of study were impactor mass and velocity, shell curvature and stacking sequence. Also, studied was the effect of presence of initial stress.

The paper by Pinnoji and Mahajan [56] presents a numerical study on the impact resistance of composite shells laminates using energy based failure model. The damage model formulation is based on a methodology that combines stress based, continuum damage mechanics (CDM) and fracture mechanics approaches. The damage model has been implemented as a user defined material model in ABAQUS FE code within shell elements. [56]

Krishnamurthy et al. [34] studied the impact response using the classical Fourier series and the FEM. Impact response determined by the finite element method also includes a prediction of the impact-induced damage deploying the semi-empirical damage prediction model of Choi–Chang. A parametric study was carried out by the finite element method to determine the effect of varying the controlling parameters such as impactor mass, its approach velocity, curvature of the shell, on both the impact response and on the impact-induced damage. A reduction of the stiffnesses of the failed laminas on the impact response concurrently as the solution proceeded has also been incorporated.

The study by Zhao et al. focuses on the impact-induced damage initiation and propagation for laminated composite shells under low velocity impacts. The damage analysis is performed by using Tsai–Wu quadratic failure criterion, Tsai's damage modes and additional delamination formula at all Gaussian points. The damage modes considered are matrix cracking, fiber breakage and delamination. The progressive failure is expressed by reducing stiffness of the material at all failed Gaussian points. The analyses of the flat and curved laminates are compared for discussing their different

damage mechanism. In addition, the influence of the stacking sequence, the thickness and the radius of curvature on damage behavior of composite shells is studied [73].

2.4 SENSITIVITY ANALYSIS

Sensitivity analysis is a tool employed in engineering problems to identify the influence of input parameters on the state variables such as displacements, stresses, strains and temperature etc. The result of sensitivity analysis is the identification of a limited set of state or input variables that have greater influence on the output of the system. The main aim of the sensitivity analysis is the calculation of the sensitivity coefficients [54] which is obtained by the variation of input variables one at a time or in groups and study the variation in the output variable [57].

The sensitivity coefficient is computed by partially differentiating the state function; defining the output; with respect to the input parameters. These derivatives can be computed numerically using the basic equations defining the system output or can be calculated analytically if a closed form solution exists. This sensitivity coefficient can be calculated using analytical functions, also some combined numerical and analytical methods for calculation are available in the literature [19]. The computation of sensitivity coefficients is suggested to be normalized so that a direct comparison of all the input variables can be deduced. The actual benefit of normalized sensitivity coefficient (NSC) is that it provides an information about the order of magnitude of variation in the output variable with the change of one order of magnitude in the input variables [47].

The methodology of using sensitivity analysis is a common practice in for almost all types of numerical techniques [31]; Boundary Element Method (BEM) [33], Finite Difference Method (FDM) [33], Finite Element Method (FEM) [9] as well as hybrid and meshless strategies [15,41]. This technique provides a very helpful tool in narrowing down the complex variables involved in the design of composite structures.

Finite Element Methods are one of the best developed numerical tools for the structural analysis and the use of sensitivity analysis along with FEM has been quite common. In a study from 1993, Noor and Shah [54] used the technique to estimate the sensitivity coefficients of unidirectional fiber-reinforced composites for the effective thermal and thermoelastic properties.

The sensitivity analysis approach is successfully used in a wide range of applications. Bilal et al. [57] used the approach to identify important model parameters in their study of evaporative coolers and condensers. They use the normalized sensitivity coefficients to study the effects of input variables that have the most influence on the response variables of the condensers and cooler systems. The method used to calculate the normalized sensitivity coefficient in this study is based upon the formulation presented by Bilal et al. in their paper, which will be discussed in detail later on.

2.5 ARTIFICIAL NEURAL NETWORKS

Artificial Neural Networks (ANN) models are a very powerful method since they can be applied to any generic problem with few inputs and can be trained to learn from them with the expected outputs. These networks mimic the behavior of the neurons inside a

human brain and it is argued that even at 0.1% of its performance, it is still an extraordinary processing system [29]. ANN models proved to be excellent tool in the approximation and interpolation in a variety of applications [10,11,21,28,39,42,44–46,55,67,70]. ANN has been used in function fitting and prediction of various mechanical properties and damage mechanisms in composite materials. ANN models are very efficient for modeling and predicting the non-linear behavior of different systems.

El Kadi [29] has presented a comprehensive review of the neural networks and the different approaches within them. ANNs are generally composed of a number of neurons spread over few layers that are interconnected. These models are trained against some target data and response set and the model are trained such that it is able to predict the output to a certain range of the training set. The progress is measured against either the mean-square error (MSE), root-mean-square error (RMSE), or normal-mean-square error (NMSE) between the observed output and the target output. The applications of ANN are in the manufacturing process optimization as well as in the monitoring and modeling the manufacturing and the mechanical behavior of fiber-reinforced composites. El Kadi has presented a brief review of all the applications of ANN in the field of fiber reinforced polymeric composites.

Bezerra et al. [11] used ANN to predict the shear stress-strain behavior of carbon/epoxy and glass/epoxy fabric composites. The authors used the multi-layered neural network model and demonstrated that about 80% of standard error of prediction was ≥ 0.9. In their study, they considered the stress as a function of the orientation angle by layers, specimen of fiber and the shear strain, while certain other factors like porosity, number of layers, matrix type and volumetric fraction of fibers were not studied.

Vassilopoulos et al. [67] used ANN to model the fatigue life of multidirectional GFRP composite laminates. The benefit that ANN provided the authors was the approach saved around 50% experimental effort for the whole analysis as compared to conventional methods and that too without the loss of considerable accuracy. It is mentioned that the artificial neural networks are effective tools to model fatigue life of composite materials and also to build the constant life diagrams. The authors have used the error back propagation (EBP) algorithm for the training of the neural network. The neural network used was a multilayer feed forward network having four inputs namely θ (off axis angle), R (stress ratio), σ_{max} (maximum stress), and σ_a (stress amplitude).

Jiang et al [28] applied the ANN model to predict the mechanical and wear properties of the short fiber reinforced polyamide composites. The polyamide composites were reinforced by short carbon and glass fibers and then optimization of the neural networks was performed. The neural network was used to predict the mechanical and wear properties as a function of the content of fibers and testing conditions. In this study, the authors have also used the back propagation neural network algorithm.

2.6 DESIGN OF EXPERIMENTS

Design of experiments, or experimental design, is the design of all information-gathering exercises where variation is present, whether under the full control of the experimenter or not. The purpose of it is to study the effect of some processes or intervention on some objects. Design of experiment is a discipline which has broad applications across all the natural and social sciences. A methodology for designing

experiments was proposed by Ronald A. Fisher, in his innovative book The Design of Experiments (1935).

Design of experiments is a very efficient statistical technique which can be employed in various experimental investigations [3]. The design of experiments provides the capability to understand the design effects of various factors and their statistical significance as well [50]. The design of experiments is useful at the stage of data collection as it provides a systematic and rigorous approach which generates valid, defensible and supportable data sets.

2.7 DESIGN OPTIMIZATION AND ALGORITHMS

Optimization is an integral part of design and is very beneficial for the commercial production of structures. The ability design engineers possess using composite materials is the custom made properties tailored exactly according to the needs of the structures. But, the composite materials involve more design variables compared to conventional materials which make it difficult to optimize the design and achieve maximum performance. This difficulty induces the need to use optimization techniques in the design process of composite materials.

Almeida et al. [4] used genetic algorithms for the design optimization of the composite laminated structures. The authors have discussed the adaptation of the terminologies and developing codes to use them with GA. The technique is used to study multi-objective optimization of plates under transverse or in-plane loads. The objectives of the study were the weight and the cost or the deflection and weight.

Lee et al [38] have used evolutionary algorithms for the multilayered composite structure design optimization. The objective of their study was the optimization of the stacking sequence of the composite plates. The authors have shown that the optimal solutions have lower weight, higher stiffness and affordable costs compared to other cases. They also discussed the benefits of parallel optimization systems.

Swaroop et al [68] used the optimization techniques to optimize the ply angles and the internal geometry of the helicopter rotor blades made using composite materials. The authors studied the multi objective optimization of several conflicting objectives which included the stiffness parameters, blade mass and the distance between mass center and the aerodynamic center of the blades. They discussed the transformation of multi-objective optimization to a single optimization problem and then applying a Particle Swarm Optimization technique to find the optimal solution.

Suresh et al. [64] also used the Particle Swarm Optimization for multi objective optimization of the design of box beam made of composite materials. The optimal solution was used to design a helicopter rotor blade. The ply angles and the cross-sectional area are considered the design parameters needed to optimize.

CHAPTER 3

NUMERICAL MODEL

Initially, a numerical model of a flat plate was developed in ABAQUS Explicit environment and used to verify against the available results from the literature. We chose the model from the study of Yokoyama et al [72], the study by Yokoyama et al. was based upon experimental and numerical results. The experimental results were based upon the thesis of Biase EHC., and the same model was developed in the ABAQUS to verify the model.

The numerical model was based on the same assumptions and material models as the one for the composite flat plates. The results were validated for the filament wound composite pipes against the experimental results available in the thesis by Mohammed Khaliq Naik [52]. The study by Naik was experimental and performed in the Advanced Material Science Lab at King Fahd University of Petroleum and Minerals, and hence will be better correlated.

In the following sections, the basic parameters and characteristics of the numerical model for both the flat plates and pipes will be discussed simultaneously.

3.1 IDEALIZATIONS AND ASSUMPTIONS

The plate and the pipe are assumed to be a 2-D shell with the layers defined in the composite section, while the impactor was considered as a 3-D rigid element with a reference point (pilot node) defined at the tip of the impactor. The initial velocity was given to the reference point of the impactor just before the impact as it is assumed to be under a free fall motion from a certain height achieving the velocity due to gravitational acceleration.

The contact is assumed to be frictionless without loss of much accuracy. It is assumed that the kinetic energy of the impactor just before the event of impact begins will be transferred to the specimen as the impact energy and this will be transferred to the subject in the form of internal energy, the amount of increase in the internal energy should be equal to the amount of decrease in the kinetic energy of the impactor as it bounces back. The amount of damage caused to the specimen as a result of impact will be evident from the amount of energy absorbed by the plate or the pipe. This energy absorbed will describe the damage to the composite specimen.

3.2 GEOMETRIC MODEL

In this research work, the impact performances of both composite plates and pipes have been studied. The composite plate model is modeled as the study of Yokoyama et al. [72], while the composite pipes were modeled as the experimental setup of Naik [52].

3.2.1 Geometric Model for Composite Flat Plate

The geometric dimensions of the composite plate and the impactor and also the stacking sequence of the plate are defined as:

Table 3.1: Geometric Dimensions of the composite plate and impactor for model validation

Composite Plate		**Impactor**	
Length	102 mm	Diameter	12.7 mm
Width	152 mm	Mass	1.5 kg
Thickness	4.2 mm	Velocity	6.0608 m/s

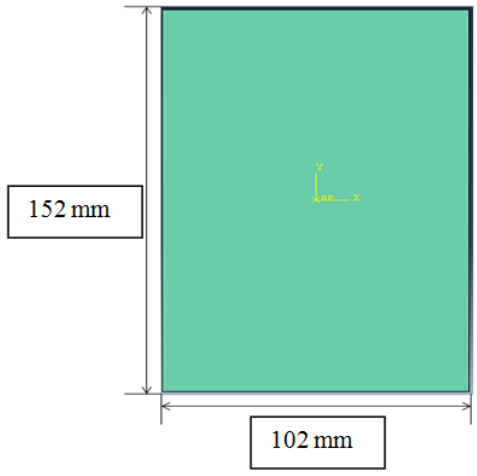

Figure 3.1: Model showing the length and height of the plate

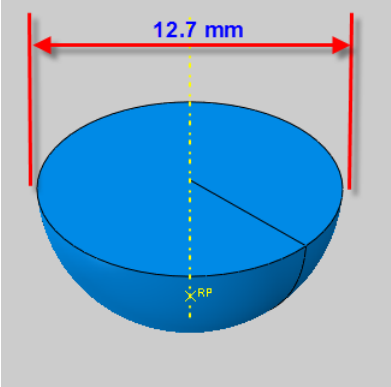

Figure 3.2: Tip Geometry of the Impactor

For the case of model validation, the laminate is consisted of 20 layers of equal thickness of 0.21 mm having the stacking sequence of $[(\pm45)/(0,90)/(\pm45)/(0,90)/(\pm45)]_{2s}$. Initially, a full model was developed for the model validation purposes, which was then reduced to quarter symmetry to save the computational efforts. The results were not much affected with the quarter symmetry.

As shown in Figure 3.2, only the nose tip of the impactor is modeled due to the reason that the impactor is assumed to be a rigid material and we are not interested in the stress distribution in the impactor. Therefore, it is appropriate to model only the nose tip of the impactor which comes into contact with the specimen and avoid the added complexity of the whole impactor geometry. The nose of the impactor has the dimensions as prescribed in the ASTM D2444 standards.

The layers are defined as symmetric about the middle plane, and hence only the half number of layers are defined and using the option in ABAQUS of symmetric plies. The layers are defined such that the primary direction of fibers is coincident with the global x-axis, these layers and the orientation can be visualized as represented in Figure 3.3.

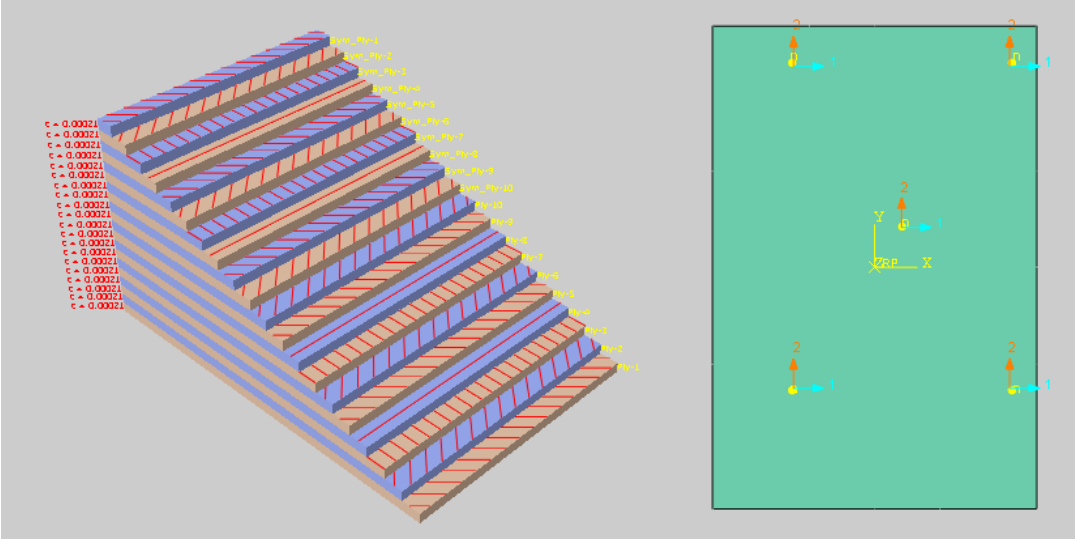

Figure 3.3: Layup plot and material orientation

3.2.2 Geometric Model for Composite Pipes

The dimensions of the composite pipes were selected so that it can be validated with the experimental results from the thesis of Mohammed Khaliq Naik [52]. These experiments and the thesis study were carried out in the King Fahd University of Petroleum and Minerals and hence have a better correlation with the future experimental works if performed. Also, the dimensions are dictated by the ASTM Standards ASTM D2444.

According to the ASTM D2444 standards, the pipe length should be at least equal to the nominal outside diameter but not less than 6 in. (152 mm) [48]. Since, the diameter of the pipe in our case is 150 mm; the length of the pipe is taken as twice the diameter as suggested.

Table 3.2: Geometric Dimensions of the Composite Pipe and the Impactor for the Model Validation

Composite Pipe		**Impactor**	
Length	300 mm	Diameter	12.7 mm
Internal Diameter	150 mm	Mass	10 kg
Thickness	6 mm	Velocity	2.8284 m/s

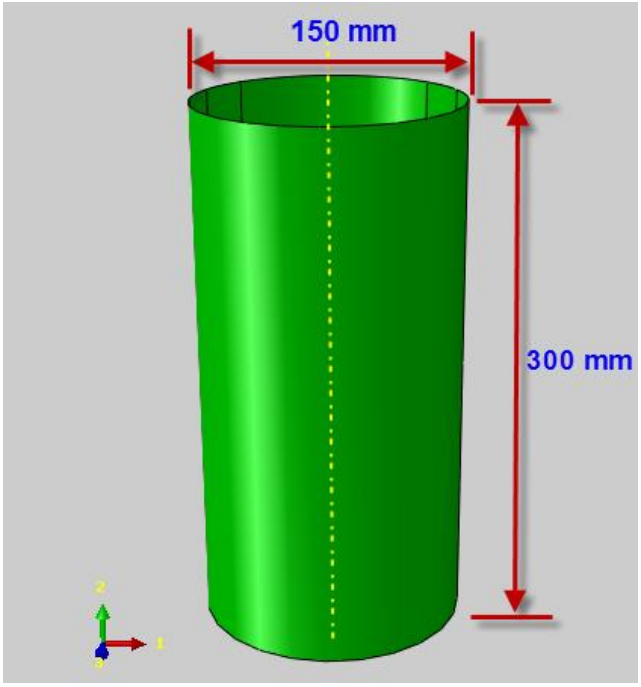

Figure 3.4: Pipe Geometry representing the major dimensions

The specimen is considered to be manufactured using filament winding technology, which generally winds fiber around a sand mandrel at a specific angle. Since, the process of winding goes from end to end on the mandrel, the winding angle varies from +θ to –θ. This kind of layers are defined in ABAQUS using the composite section without the

usage of symmetric layers option as there is no mid-plane about which the layers are symmetric.

For the case of model validation, the winding angle is kept at 55˚ as reported in the work of Naik. The winding angle of 55˚ is a preferred choice of winding angle among the industry as it is known to have good performance against both the axial loading and internal pressure [8]. The number of layers is assumed to be 24 with each layer having thickness of 0.25 mm, as this is the popular layer thickness from available literature and the supplier's information in the market.

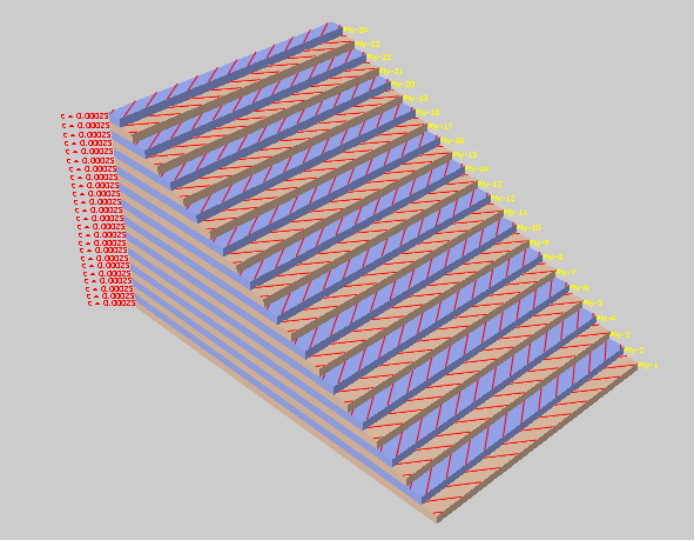

Figure 3.5: Layer orientation of a composite pipe

3.3 MATERIAL MODELING

Composite materials as explained in the introduction are anisotropic material having different material properties in different directions. For a layered composite, it is considered to be orthotropic with material properties in the fiber direction higher than the

material properties in the two transverse directions. Most commonly, the material properties in the two transverse directions are considered to be equal, this kind of material is considered to be transversely isotropic material. The material used in the study is either carbon fiber impregnated with epoxy resin or glass fiber. Generally, flat plates are constructed using woven fabrics and the pipes are manufactured using the filament winding technology. The material properties and behavior is therefore, different as the woven fabric is usually available in the form of cross-ply woven form which makes it different from the layers from filament winding which is essentially a uni-directional construction.

Hooke's law for transversely isotropic materials defines five independent elastic constants, which are the Young's modulus and Poisson's ratio in the y-z symmetry plane, Young's modulus and Poisson's ratio in the perpendicular direction and the shear modulus in the perpendicular direction. The compliance matrix is given as the Eq. (3.1)

$$\begin{bmatrix} \varepsilon_{xx} \\ \varepsilon_{yy} \\ \varepsilon_{zz} \\ \varepsilon_{yz} \\ \varepsilon_{zx} \\ \varepsilon_{xy} \end{bmatrix} = \begin{bmatrix} \frac{1}{E_x} & -\frac{\nu_{yx}}{E_y} & -\frac{\nu_{yx}}{E_y} & 0 & 0 & 0 \\ -\frac{\nu_{xy}}{E_x} & \frac{1}{E_y} & -\frac{\nu_{zy}}{E_y} & 0 & 0 & 0 \\ -\frac{\nu_{xy}}{E_x} & -\frac{\nu_{yz}}{E_y} & \frac{1}{E_y} & 0 & 0 & 0 \\ 0 & 0 & 0 & \frac{1}{2G_{yz}} & 0 & 0 \\ 0 & 0 & 0 & 0 & \frac{1}{2G_{xy}} & 0 \\ 0 & 0 & 0 & 0 & 0 & \frac{1}{2G_{xy}} \end{bmatrix} \begin{bmatrix} \sigma_{xx} \\ \sigma_{yy} \\ \sigma_{zz} \\ \sigma_{yz} \\ \sigma_{zx} \\ \sigma_{xy} \end{bmatrix} \tag{3.1}$$

As y-z plane was considered the plane of symmetry, $E_y = E_z$, $\nu_{xy} = \nu_{xz}$, and $\nu_{yx} = \nu_{zx}$. The symmetry of the stress and strain tensors dictates that

$$\frac{\nu_{xy}}{E_x} = \frac{\nu_{yx}}{E_y}, \nu_{yz} = \nu_{zy} \tag{3.2}$$

However, both woven fabric and uni-directional laminates are considered transversely isotropic, a special subcategory of orthotropic materials and following are the damage initiation models and the damage evolution models for these materials.

3.3.1 Damage Initiation Modeling

Since, the impact of the striker will cause damage; a damage model is needed in order to describe when this damage begins and also once the damage initiates how it will progress. In this study, we will use the damage initiation model as proposed by Hashin (1980). The model as proposed by Hashin considers damage initiation in four different modes, namely,

Tensile Matrix Mode:

$$\frac{1}{Y_t^2}\left(\sigma_{22}+\sigma_{33}\right)^2 + \frac{1}{S_{23}^2}\left(\sigma_{23}^2 - \sigma_{22}\sigma_{33}\right) + \frac{1}{S_{12}^2}\left(\sigma_{12}^2 + \sigma_{31}^2\right) \le 1 \tag{3.3}$$

Compressive Matrix Mode:

$$\begin{aligned}&\frac{1}{Y_c}\left[\left(\frac{Y_c}{2S_{23}}\right)^2 - 1\right]\left(\sigma_{22}+\sigma_{33}\right) + \frac{1}{4S_{23}^2}\left(\sigma_{22}+\sigma_{33}\right)^2 + \\ &\frac{1}{S_{23}^2}\left(\sigma_{23}^2 - \sigma_{22}\sigma_{33}\right) + \frac{1}{S_{12}^2}\left(\sigma_{12}^2 + \sigma_{31}^2\right) \le 1\end{aligned} \tag{3.4}$$

Tensile Fiber Mode:

$$\left(\frac{\sigma_{11}}{X_t}\right)^2 + \frac{1}{S_{12}^2}\left(\sigma_{12}^2 + \sigma_{31}^2\right) \leq 1 \tag{3.5}$$

Compressive Fiber Mode:

$$\left(\frac{\sigma_{11}}{X_c}\right)^2 \leq 1 \tag{3.6}$$

Where Y_t, Y_c, X_t, X_c represents the longitudinal tensile and compressive and transverse tensile and compressive strengths respectively while S_{12} and S_{23} represents the longitudinal and transverse shear strength.

3.3.2 Damage Evolution Model

Damage initiation is the event at which the initial damage is caused in the laminate but once it is initiated this damage will progressively spread with further impact force. This is known as the damage evolution and this will cause the strength of the composite laminate to deteriorate and hence the resulting product will be weaker compared to earlier before impact.

A simple energy based linear softening model is used as the damage evolution model. Energy damage evolution defines damage in terms of the energy required for failure (fracture energy) after the initiation of damage. Linear softening specifies a linear softening stress-strain response for linear elastic materials or a linear evolution of the damage variable with deformation for elastic-plastic materials.

For the damage initiation in plane stress fiber reinforced composites, the damage evolution law is available in ABAQUS; it assumes that before damage initiation the material was linearly elastic, with the stiffness matrix of a plane stress orthotropic material. After, the response of the material is computed from

$$\sigma = C_d \varepsilon \tag{3.7}$$

Where ε is the strain and C_d is the damaged elasticity matrix, given as

$$C_d = \frac{1}{D}\begin{bmatrix} (1-d_f)E_1 & (1-d_f)(1-d_m)\nu_{21}E_1 & 0 \\ (1-d_f)(1-d_m)\nu_{21}E_1 & (1-d_m)E_2 & 0 \\ 0 & 0 & (1-d_s)GD \end{bmatrix} \tag{3.8}$$

Where $D = 1-(1-d_f)(1-d_m)\nu_{12}\nu_{21}, d_f$ gives the current state of fiber damage, d_m gives the current state of matrix damage and d_s gives the current state of shear damage. The damage variables d_f , d_m and d_s are derived from damage variables $d_f^t, d_f^c, d_m^t,$ and d_m^c corresponding to the four failure modes described for Hashin model.

$$\begin{aligned} d_f &= \begin{cases} d_f^t \text{ if } \sigma_{11} \geq 0, \\ d_f^c \text{ if } \sigma_{11} < 0, \end{cases} \\ d_m &= \begin{cases} d_m^t \text{ if } \sigma_{22} \geq 0, \\ d_m^c \text{ if } \sigma_{22} < 0, \end{cases} \\ d_s &= 1-(1-d_f^t)(1-d_f^c)(1-d_m^t)(1-d_m^c) \end{aligned} \tag{3.9}$$

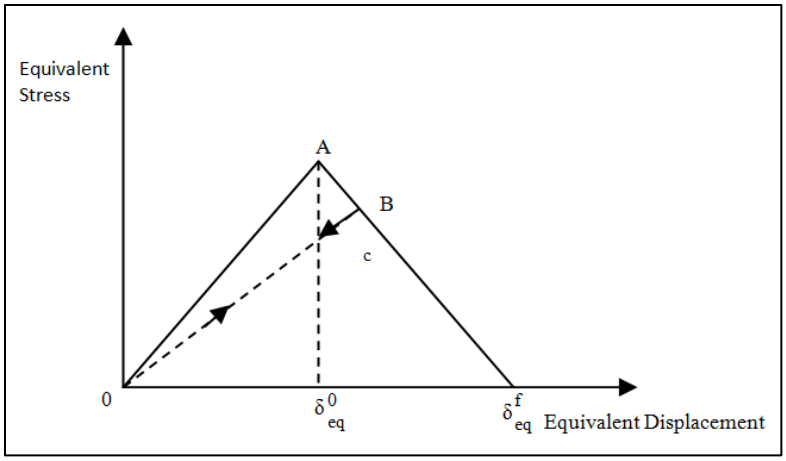

Figure 3.6: Linear damage evolution

Where G_f^t , G_f^c , G_m^t , G_m^c and G_s are the energies dissipated during damage for fiber tension, fiber compression, matrix tension, matrix compression and in-plane shear damage modes respectively. The built-in damage evolution model in ABAQUS doesn't support the in-plane shear damage.

3.3.3 Material Model for Composite Plates

The composite plates are manufactured using the woven fabric of carbon fiber or glass fiber impregnated with epoxy resin. The elastic material properties for the plates are listed in Table 3.3 for Carbon/Epoxy system and in Table 3.4 for the Glass/Epoxy system.

The material properties used for the Carbon/Epoxy composite system is taken from the study of Yokoyama et al. [72] and is also used for the validation purposes. These values are quite close to the values cited in other literatures e.g. in the study by Pinnoji et al. [56], but as stated in the study by Yokoyama et al. the values are calculated experimentally. One of the points to note here is that the elastic modulus in the z-

direction demonstrated by subscript 3 is missing, but this value has no consequence as the laminate material properties that affect the overall solution are the in-plane properties and the material properties that ABAQUS requires are the laminate properties which does not include E_3. Also, generally this modulus is considerably lower than the moduli in the other two directions for the case of woven fabric composites.

Table 3.3: Mechanical elastic properties for orthotropic layer of Carbon/Epoxy woven fabric used in composite plate modeling [72]

E_1 (GPa)	E_2 (GPa)	E_3 (GPa)	G_{12} (GPa)	G_{13} (GPa)	G_{23} (GPa)	ν_{12}	ν_{13}	ν_{23}
60.8	58.25	-	4.55	4.55	5	0.07	0.07	0.4

The material properties for the Glass/Epoxy system are selected from the study of Menna et al. [49].

Table 3.4: Mechanical elastic properties for orthotropic layer of Glass/Epoxy woven fabric used in composite plate modeling [49]

E_1 (GPa)	E_2 (GPa)	E_3 (GPa)	G_{12} (GPa)	G_{13} (GPa)	G_{23} (GPa)	ν_{12}	ν_{13}	ν_{23}
26	26	8	3.8	2.8	2.8	0.1	0.25	0.25

The damage initiation as described in the section (3.3.1) is defined in terms of the stress values compared to the strength of the lamina in a particular direction under a particular loading condition. The strength values for the Carbon/Epoxy are defined as Table 3.5 and for the Glass/Epoxy as Table 3.7.

Table 3.5: Strength of composite layer in various directions for Carbon/Epoxy

Ply Strengths	X_t (MPa)	X_c (MPa)	Y_t (MPa)	Y_c (MPa)	S_{12} (MPa)	S_{23} (MPa)
	621	760	594	707	125	125

Table 3.6: Strength of composite layer in various directions for Glass/Epoxy

Ply Strengths	X_t (MPa)	X_c (MPa)	Y_t (MPa)	Y_c (MPa)	S_{12} (MPa)	S_{23} (MPa)
	414	458	414	458	105	65

The amount of damage due to the impact loads depend upon how the damage propagates through the sample. The damage is said to initiate when the critical strength limits were crossed and as more energy was applied by the impactor the damage progressed through the sample. The amount of energy released or the amount of energy required to propagate the damage in the composite plate depends upon the intralaminar fracture energies given in Table 3.7 for the Carbon/Epoxy system.

Table 3.7: Energy value for the damage evolution for Carbon/Epoxy

Intralaminar Fracture Toughness	G_f^t (KJ/m^2)	G_f^c (KJ/m^2)	G_m^t (KJ/m^2)	G_m^c (KJ/m^2)	G_s (KJ/m^2)
	160	25	10	2.25	2.25

The fracture toughness is not available widely and if found most of the literature studies only the critical value of the fracture toughness that is the value at which the damage or the crack initiates. For this study, we have selected stress limit as the damage initiation and the use of energy release rates for modeling the propagation of damage. The value for the energy release rate in the fiber direction during tension was selected

from the study of [16]. The rest of the values though have less impact on the overall performance as will be shown in the later sections. Therefore, a simple ratio was adopted for the fracture energy in the fiber direction during compression and the matrix materials and is listed in Table 3.8.

Table 3.8: Energy value for the damage evolution for Glass/Epoxy

Intralaminar Fracture Toughness	G_f^t (KJ/m^2)	G_f^c (KJ/m^2)	G_m^t (KJ/m^2)	G_m^c (KJ/m^2)	G_s (KJ/m^2)
	10	1.562	0.625	0.14	0.14

3.3.4 Material Model for Composite Pipes

The composite pipes are manufactured using the filament winding technology. This process of manufacturing pipes means that the layers are considered unidirectional lamina and hence the material properties and the plane of symmetry are different than the woven fabric. The elastic material properties for the Carbon/Epoxy composite pipes are selected from the study of Yokoyama et al. [72] are listed in Table 3.9.

Table 3.9: Mechanical elastic properties for orthotropic layer of Carbon/Epoxy unidirectional lamina used in composite plate modeling [72]

E_1 (GPa)	E_2 (GPa)	E_3 (GPa)	G_{12} (GPa)	G_{13} (GPa)	G_{23} (GPa)	ν_{12}	ν_{13}	ν_{23}
100	8.11	8.11	4.65	4.65	5	0.3	0.3	0.4

The elastic material properties for the Glass/Epoxy composite pipes are used from the study of Li et al. [41]. The model validation of the GFRP (Glass Fiber Reinforced

Polymers) pipes was carried out with the experimental study of Naik [52], but the thesis was mainly experimental and all the material properties were not provided. Therefore, the material properties were calibrated and validated and it was found that the material properties given in the study of Li et al. [41] closely matched the results. These material properties are tabulated in Table 3.10.

Table 3.10: Mechanical elastic properties for orthotropic layer of Glass/Epoxy unidirectional lamina used in composite plate modeling [41]

E_1 (GPa)	E_2 (GPa)	E_3 (GPa)	G_{12} (GPa)	G_{13} (GPa)	G_{23} (GPa)	ν_{12}	ν_{13}	ν_{23}
30.5	6.9	6.9	4.65	4.65	1.6	0.344	0.344	0.4

The strength properties of the Carbon/Epoxy lamina are given in Table 3.11 and the strength properties of the Glass/Epoxy lamina are given in Table 3.12.

Table 3.11: Strength of composite layer in various directions for Carbon/Epoxy

Ply Strengths	X_t (MPa)	X_c (MPa)	Y_t (MPa)	Y_c (MPa)	S_{12} (MPa)	S_{23} (MPa)
	2000	1000	100	160	140	140

Table 3.12: Strength of composite layer in various directions for Glass/Epoxy

Ply Strengths	X_t (MPa)	X_c (MPa)	Y_t (MPa)	Y_c (MPa)	S_{12} (MPa)	S_{23} (MPa)
	700	300	100	237	64	64

As it is described earlier, the damage propagation is modeled using the energy release rates. These values for the CFRP are listed in the study of Yokoyama et al. [72] and are

listed in the Table 3.13. The intralaminar fracture toughness for the GFRP pipes are used from the study of Gershom and Marom [20].

Table 3.13: Energy value for the damage evolution for Carbon/Epoxy

Intralaminar Fracture Toughness	G_f^t (KJ/m^2)	G_f^c (KJ/m^2)	G_m^t (KJ/m^2)	G_m^c (KJ/m^2)	G_s (KJ/m^2)
	100	25	2	2	2

Table 3.14: Energy value for the damage evolution for Glass/Epoxy

Intralaminar Fracture Toughness	G_f^t (KJ/m^2)	G_f^c (KJ/m^2)	G_m^t (KJ/m^2)	G_m^c (KJ/m^2)	G_s (KJ/m^2)
	52.5	20	2	2	2

3.4 LOADS AND BOUNDARY CONDITIONS

This study is based on the damage caused due to the low-velocity impact loads. These loads are applied to the striker in the form of initial velocity, which has kinetic energy equivalent to the amount of impact energy intended to hit the specimen with. During experimentation, the impact energy is controlled by the height from which the striker is dropped. The striker achieves the desired impact energy by virtue of the potential energy transferred to the kinetic energy in the free fall.

$$P.E. = mgh$$
$$K.E. = \frac{1}{2}mv^2 \qquad (3.10)$$

Where, '*m*' is the mass of the impactor, '*h*' the drop height of the impactor and '*v*' is the velocity of the impactor just before it hits the test specimen.

In ABAQUS, a reference point on the striker geometry is modeled and is given the mass and the velocity with which to impact the test specimen.

3.4.1 Case for Flat Plates

The impact load of 27.55 J was applied in the initial step of the explicit dynamic analysis. This energy is provided to the striker of mass 1.5 kg with an initial velocity of 6.0608 m/s.

The boundary conditions are such that the shorter edges of the plate were fully constrained while the longer edges were set to be free. The impact energy and the mass of the impactor and the boundary conditions are set according to the model from the study of Yokoyama et al. [72].

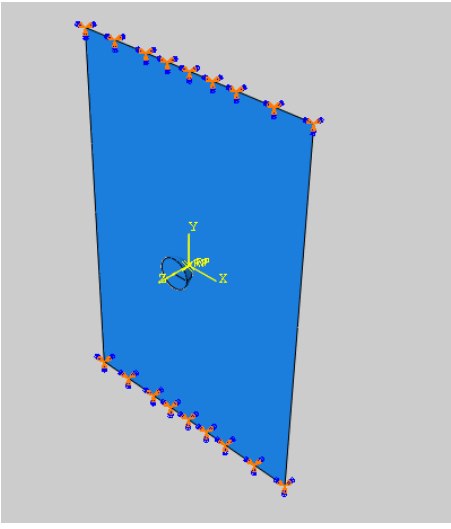

Figure 3.7: Boundary Conditions on the full plate model

The quarter plate symmetry model was developed to reduce the size of the problem, the loads were also reduced by ¼ which is achieved by dividing the mass of the impactor by 4 such that the mass will be 0.375 kg. To apply the symmetric boundary conditions, the two edges were constrained to move in the direction of the axis of symmetry, this is shown in the Figure 3.8.

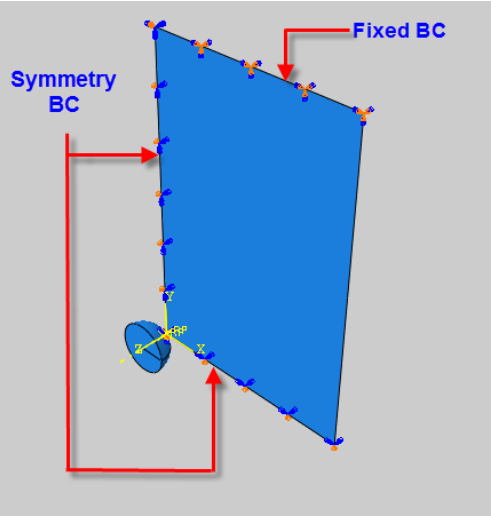

Figure 3.8: Boundary Conditions on the quarter plate model

3.4.2 Case for Composite Pipes

The boundary conditions for the impact analysis of composite pipes are dictated by the standards provided in the ASTM D2444. It is mentioned in the standards that the pipe is supported with the help of a V-block. The design of V-block should be such that it should be equal to the length of the pipe and has a 90˚ included angle. The support in the numerical model is provided at approximately the patches of the pipe where the V-block is supposed to be in contact with the pipe. The results in the model validation proved that this simplification in the model was accurate.

The impact loads for the composite pipe are applied in the same way as for the plates' impact analysis. The initial velocity is provided to the striker which equates to 40 J of impact energy. The mass of the striker is selected as 10 kg and the velocity to achieve the impact energy of 40 J is 2.82843 m/s.

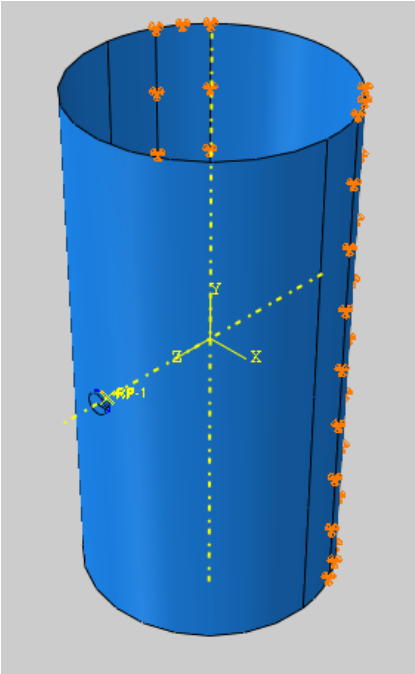

Figure 3.9: Boundary Conditions on the Composite Pipe Model

3.5 ELEMENT TYPE AND MESH

The composite plate and the pipe were modeled as the shell element, while the impactor was modeled as a rigid element. The element type S4R was used to mesh the composite plate and the pipes. The area near the impact point was more refinely meshed rather than the whole model. It is obvious that the areas away from the impact point had less influence on the numerical result. Hence, it was necessary to keep the mesh as coarse

as possible in those regions so as to keep the number of nodes and elements to be solved to a minimum. This approach results in a high quality result with a much lesser amount of computational time spent.

The mesh for the striker is not required as it is a rigid element and we are not interested in the deformation and stress in the striker. A brief introduction about the element type used for the composite plate is discussed further.

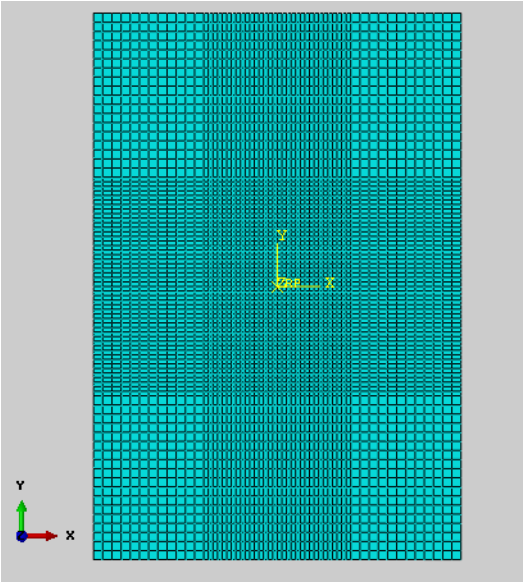

Figure 3.10: Mesh for the full composite plate model

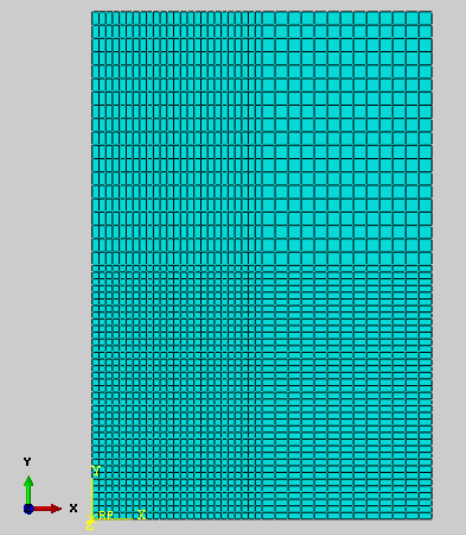

Figure 3.11: Mesh for the quarter plate model

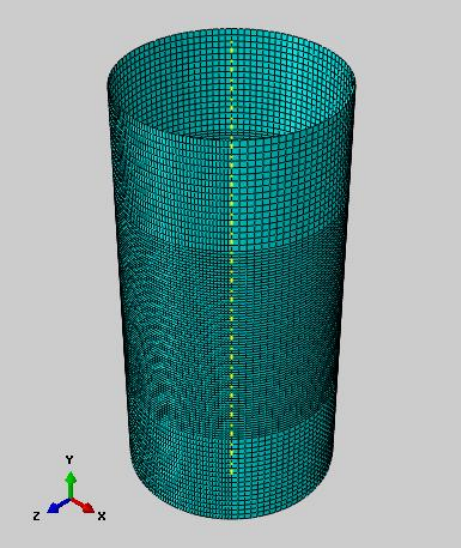

Figure 3.12: Mesh for the composite pipe model

3.5.1 Element Type - S4R

The thickness of the plate in this study is comparatively small than the length and the width of the plate. For such structures, shell elements are used. ABAQUS offers two types of shell elements, namely, conventional shell elements and the continuum shell elements.

S4R is a 4-node, quadrilateral, stress/displacement shell element with reduced integration and a large-strain formulation. This element is from the family of conventional shell elements and allows transverse shear deformation and uses thick shell theory as the shell thickness increases and become discrete Kirchhoff thin shell elements as the thickness decreases; the transverse shear deformation becomes very small as the shell thickness decreases.

This element type accounts for finite membrane strains and arbitrarily large rotations; therefore, they are suitable for large-strain analysis as in the case of impact analysis. Therefore, for our case where we expect finite strains and transverse shear deformation, S4R element has been chosen for the simulation.

CHAPTER 4

MODEL VALIDATION AND SENSITIVITY ANALYSIS

Model validation is an important step of every numerical analysis. If the numerical model is able to predict the results from the similar model from other studies either numerical or experimental, it gives the confidence to use the model for the further analysis with the surety of results.

4.1 MODEL VALIDATION OF COMPOSITE FLAT PLATE

The model validation for the composite plates is carried out with the study by Yokoyama et al. [72]. The model geometry is described in the Table 3.1, which is the same as the model used in the study of Yokoyama. In that study, Yokoyama et al. proposed a new damage initiation and evolution model to better predict the impact damage and the energy absorbed during the impact event. For this study, we started with the built-in model for the damage initiation and the damage evolution as described earlier. It was found out that the results in our study are more closely matched from the results of the proposed model by Yokoyama et al. and also with the experimental results presented in their study.

4.1.1 Mesh Convergence

Mesh convergence is required to eliminate the numerical errors induced due to finite element method which approximates the whole domain in a finite number of smaller elements. The results for the mesh convergence are presented in the Table 4.1. The mesh was generated at two refinement levels, with a refined central region where the impactor strikes the composite plate. The composite plate is meshed using the mapped meshing technique. Initially a constant element edge length of 3 mm was used throughout the plate which resulted in the generation of 2400 elements with 2501 nodes, referred to as the refinement level 1 in the Table 4.1. The element edge length or edge seeds as better known in the ABAQUS environment were reduced to 2.5 mm for the refinement level 2.

At this point, the further reduction of element sizes would have resulted in a large number of elements costing computational time, a central region near the impact point was then refined further without reducing the edge lengths of the outer edges. In the first run, the central region edge length of elements was 1.25 mm and 2.5 mm for outer edges. The mesh at level 3 gave almost the double number of elements as previous level with only about 3% improvement in the dissipated energy and less than 1% of the maximum displacement. However, a further refinement was tried to make sure the convergence. Here to keep the mapped meshing, the outer element edges were reduced to seed size of 2 mm and central region to 1 mm.

Table 4.1: Mesh Convergence based on Maximum Displacement and Dissipated Energy

Refinement Level	Elements	Nodes	Dissipated Energy (J)	Maximum Displacement (mm)	%age Difference in Dissipated Energy	%age Difference in Displacement
1	1700	1785	6.167	6.2060	-	-
2	2400	2501	5.0089	6.104	18.7	1.64
3	4704	4845	4.8674	6.062	2.82	0.688
4	7420	7597	4.7867	6.082	1.66	0.33

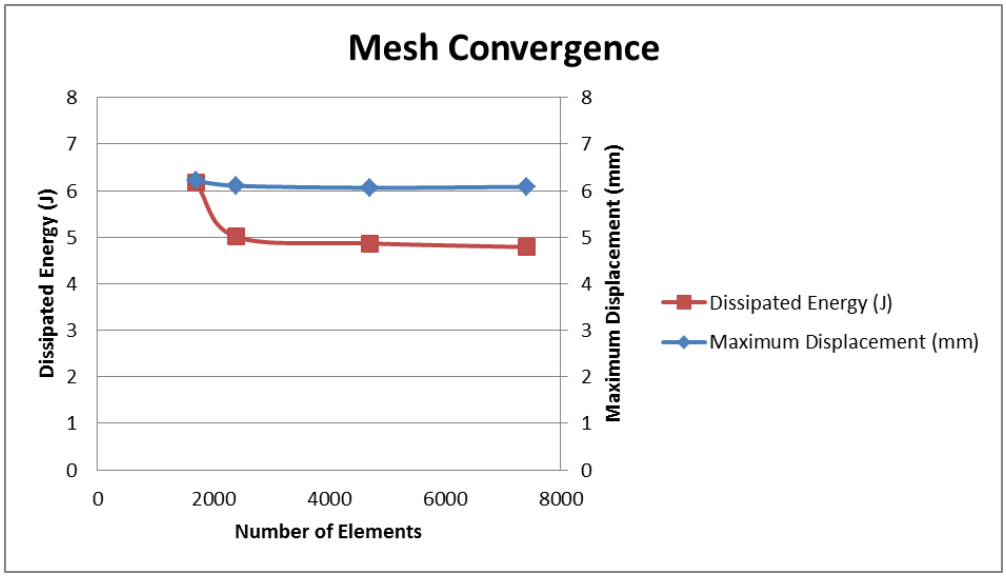

Figure 4.1: Mesh Convergence Check for Dissipated Energy and the Maximum Displacement

From the mesh convergence Table 4.1 and the related graph in Figure 4.1, it is evident that the further refinement of mesh is not required and the mesh at the refinement level 3 is sufficient. However, the refinement level 4 was preferred once the model was reduced to ¼ of the original size using the quarter symmetry model.

4.1.2 Validated Results

The results reported in the study by Yokoyama et al. are used to validate the model. Our study reveals a much closer result to the experimental values than the result from the proposed model. [72]

In the Table 4.2 below, the results are shown for the experimental and numerical results from the previous studies for both the Hashin model and the model proposed by Yokoyama et al. and compared with our results from ABAQUS using the built-in Hashin model.

Table 4.2: Results from Yokoyama et al. and the comparison with our results

	Experimental (Biase)	**Numerical (Yokoyama)**	**Numerical (Hashin Model)**	**Our Result**	**Error (%age)**
Maximum Displacement (m)	0.006018	0.00611	0.00592	0.006062	0.7%
Time of Impact Event (sec)	0.0036	0.00354	0.00328	0.00338	3.05%

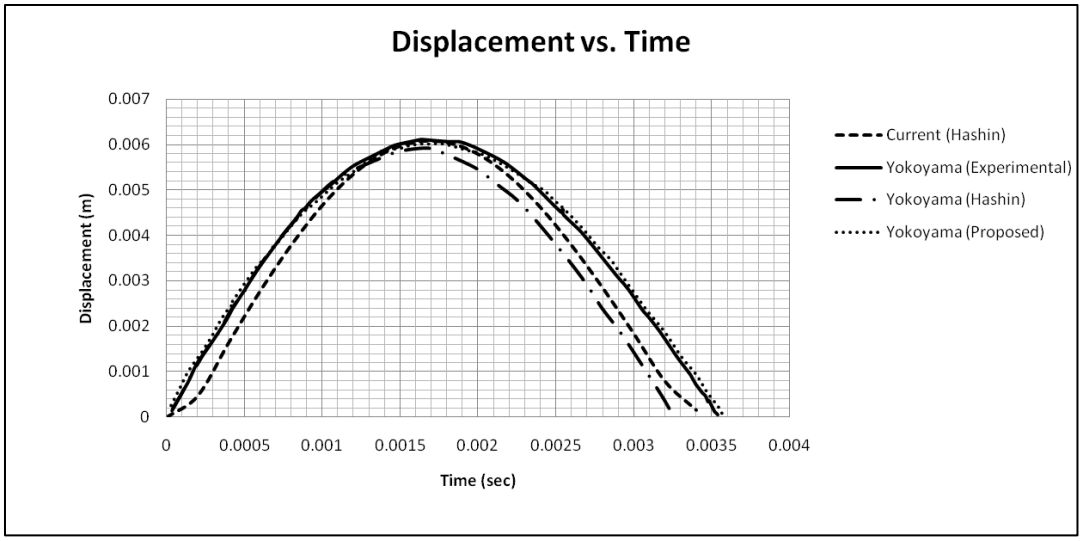

Figure 4.2: Maximum displacement for the composite plate with respect to time. Experimental and numerical results for displacement-time curve from Yokoyama et al. [72]

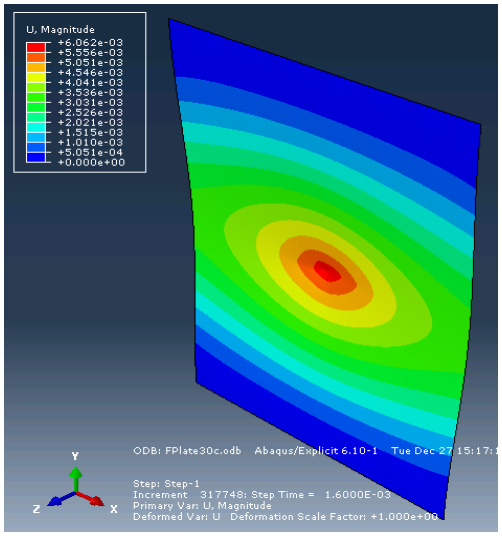

Figure 4.3: Displacement contour at the instant of 1.6 msec when the kinetic energy was zero

The results show that the maximum displacement occurs around 1.6 msec, after that the impactor bounced back with reduced velocity. This reduced velocity resulted in the loss of kinetic energy which was absorbed as internal energy in the composite plate. The kinetic energy of the impactor as it bounces back reduces to just around 22.7 J which is equal to the amount of energy absorbed in damaging the plate.

There was very little difference in the values of the full plate and the quarter plate model as it is listed in Table 4.3.

Table 4.3: Comparison of results between full and quarter model

	Full Model	**Quarter Model**	**%age Difference**
Number of Elements	7420	2166	71 %
Number of Nodes	7597	2262	70 %
Dissipated Energy (J)	4.7867	4.7433	0.91 %
Maximum Displacement (mm)	6.082	6.068	0.23 %
Time of Impact Event (msec)	3.38	3.32	1.78 %

4.2 MODEL VALIDATION OF COMPOSITE PIPE

The model validation of the composite pipe case was done using the experimental study conducted by Naik for his thesis work at Mechanical Engineering Department, King Fahd University of Petroleum and Minerals [52]. The geometry of the pipe and the impactor are already defined in Chapter 3 Table 3.2. The material elastic properties, the strength values and the fracture energies are listed in Table 3.10, Table 3.12 and Table 3.14 respectively for the glass/epoxy system used in the study by Naik. The boundary conditions are considered as defined by the ASTM standards D2444.

In the study by Naik, they conducted the experiments at different energy levels for different pipe materials. We selected the glass/epoxy composite pipes under the impact load of 20 J for the case of model validation. The geometric conditions and the loads are selected to be similar to the experimental setup. The experimental study by Naik presented the results in terms of peak force and therefore, we based our validation parameter to be the peak force rather than the maximum displacement as was the case with flat plate's model validation.

4.2.1 Mesh Convergence

Mesh convergence is an important aspect of finite element analysis. It is necessary to refine the mesh to such a size that generates minimum amount of elements with a reasonable level of accuracy of results. For the composite pipes, the mesh convergence was carried out in two steps; initially a uniform mapped meshing was used throughout the pipe. This kind of meshing results in a very large number of elements costing a lot of computing time. To save the computing effort, a similar kind of approach was adopted as with the composite plates, that is, a finer mesh in the central region where the impactor strikes the pipe and a more coarse mesh outside. Initially, mesh convergence was carried out for a reduced number of layers in order to save computational time required to solve large number of integration points due to more layers. During the mesh convergence, the total numbers of layers were considered to be 8 with the winding angle of $\pm 55^{\circ}$, each layer of 0.75 mm thickness.

For the uniform meshing, meshing was started with an element edge length of 10 mm and reducing it at each level where an element edge length was reduced to just 2.2 mm. At this mesh refinement, as can be observed from the graphs of Figures (Figure 4.4-

Figure 4.7) most of the values have reached the constant value and further mesh refinement was not necessary. From the Table 4.4, it can be noticed that at the seed level of 1.8 mm, there is a sudden jump in the maximum displacement but further mesh refinement resulted in the displacement value to go the earlier level of around 4.27 mm. Similary, peak force also had one or two mesh levels where it increased suddenly but overall it is constant around 7000 N.

Table 4.4: Mesh Convergence with Uniform Mesh Technique

Seed	**Elements**	**Nodes**	**Max Von Mises (MPa)**	**Max Disp (mm)**	**Peak Force (N)**	**Rebound Velocity (m/s)**
0.01	1536	1584	548	4.06	8163	1.70581
0.005	5700	5795	687	4.10	7157	1.67173
0.004	8816	8932	645	4.14	7229	1.65949
0.0025	23040	23232	710	4.28	6950	1.6705
0.0022	28832	29040	690	4.26	7100	1.68511
0.002	35636	35872	727	4.27	7090	1.70144
0.0018	43680	43940	692	5.92	7292	1.70984
0.0016	54896	55188	694	4.24	7523	1.73724
0.0015	63200	63516	693	5.97	7269	1.69964
0.0012	99396	99792	700	4.26	7106	1.67946
0.001	140400	140868	695	4.18	7631	1.73527

As it is evident, from the Table 4.4 and the graphs showing mesh convergence that the refinement level with seed size of 2.2 mm having mesh of about 30000 elements is appropriate for further studies. But, as shown in the graphs and Table 4.5, using the two level mesh refinements is beneficial as it reduces the element numbers by almost half and without losing major accuracy. As a result, the further study was carried out with the outer seed size of 4.4 mm and a 2.2 mm element edge length for the central near the impact zone.

Table 4.5: Mesh Convergence with Non-Uniform Mesh Technique

Seed	Elements	Nodes	Max Von Mises (MPa)	Max Disp (mm)	Peak Force (N)	Rebound Velocity (m/s)
0.005-0.0025	12520	12640	696	4.34	6916	1.66958
0.0044-0.0022	13872	14008	698	4.26	7019	1.6841
0.004-0.002	16272	16416	709	4.27	6994	1.68893

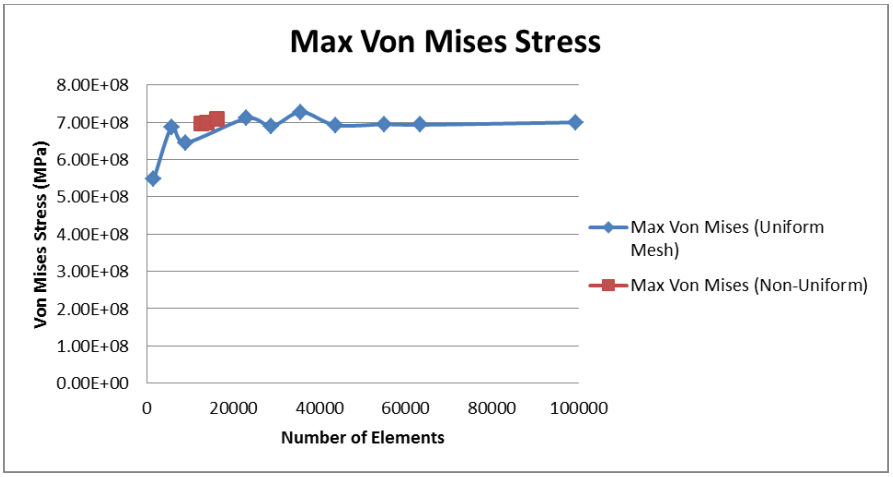

Figure 4.4: Mesh Convergence showing Maximum Von-Mises Stress

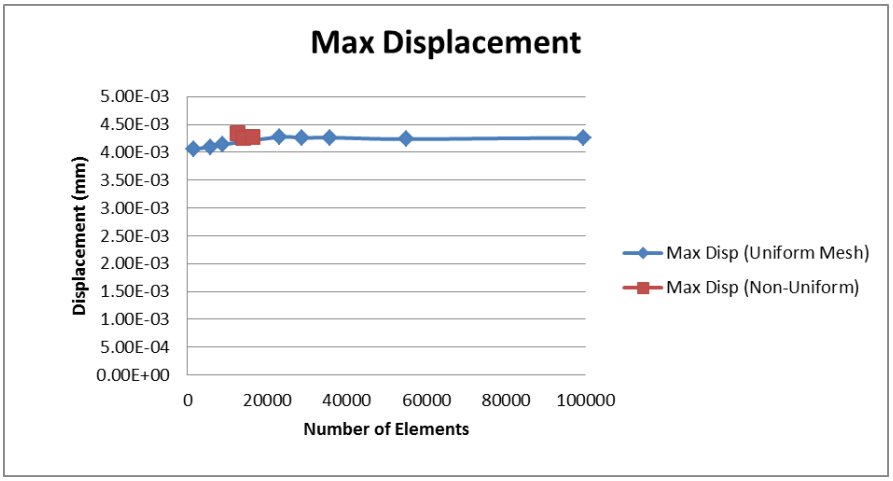

Figure 4.5: Mesh Convergence showing Maximum Displacement

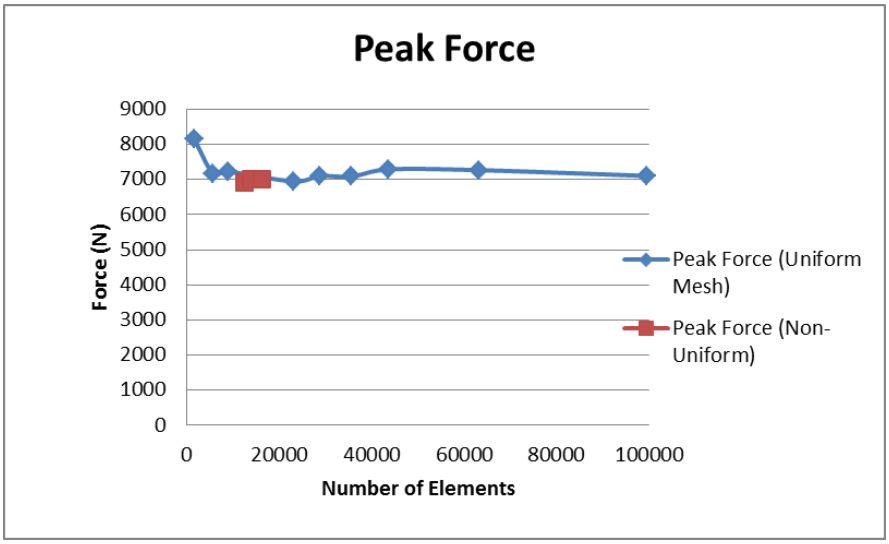

Figure 4.6: Mesh Convergence showing Maximum Peak Force

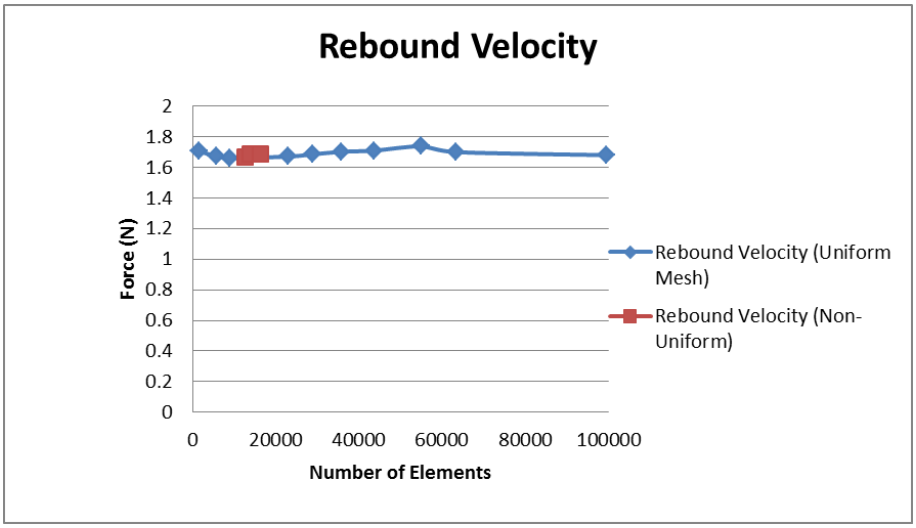

Figure 4.7: Mesh Convergence showing Rebound Velocity of the Impactor

4.2.2 Validated Results

The composite pipe model was validated with the experimental results from the thesis of Naik [52]. The validation was carried out against the impact load of 20 J with a striker of 10 kg weight. The numerical model requires the material properties for the validation

which were not provided in the thesis. These values were then obtained from the available literature for similar kind of composite materials provided in the study of Li et al. [40]. In the model validation phase, the geometric dimensions were kept the same as reported in the work of Naik, but due to the fact that it doesn't provide the material properties as well as the exact number of layers and the thickness of each layer. An assumption was made considering the number of layers and thickness based on the literature available on the subject. It was assumed that the layers were 0.25 mm thick and the total numbers of layer were 24. The results are reported in Table 4.6.

Table 4.6: Model Validation results for the Glass/Epoxy Composite Pipe at 20 J

	Peak Force (N)	Deformation at Peak Force (mm)	Time of Impact Event (msec)
Naik Thesis	6640	3.59 (12 J Impact)	7.4
Current Work	6970	3.95 (20 J Impact)	7.76
% age Difference	4.9 %	-	4.86 %

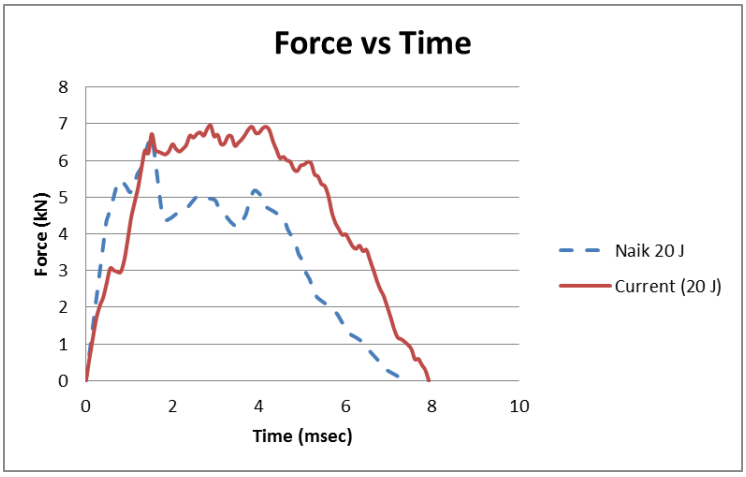

Figure 4.8: Force vs. time graph comparison between Naik and current work

The results in the above Table 4.6, shows that there is only about 5% difference between the results from Naik and the current numerical work, which is a sufficient level considering the above justified assumptions. In the table, the deformation at the peak force is mentioned for 12 J as there was no value for deformation at the 20 J impact tests in the thesis by Naik.

In the graph Figure 4.8, the comparison between the force vs. time plot is presented. One aspect that can be noticed that in the graph displaying the Naik's result, it shows that after the first peak force the force value remains less than the force values from the current work. This can be explained on the basis that the sudden drops occurs when the force is such that it initiates the damage and hence in the further contact the specimen is unable to offer more resistance. On the contrary, the peak force in the current research work reaches at the same point of time but it didn't dip down below enough to meet the experimental results. This may be due to the fact that the material used for experimental study has a lower tensile strength in the fiber direction compared to the material properties used in the numerical research. Nevertheless, the results as shown are close enough and the model can be safely validated.

4.3 SENSITIVITY ANALYSIS

This study employs a sensitivity analysis approach to identify the parameters and quantitatively describe their degree of influence on the impact resistance of the fiber reinforced polymer composite plates. The results were then used to optimize the factors in order to achieve the best impact resistance for a certain case of composite laminate under certain conditions of impact load and boundary conditions. The studies prior to the

current work have studied almost all the parameters in detail such as the thickness of the ply, stacking sequence and effect of materials etc. as discussed in the literature review, but the current focus is to know how big the effect of one parameter is with respect to others. This is needed in order to use the results in optimization studies where keeping the costs minimum is one criterion. It is well established that increasing thickness and using stronger fiber material increases the impact performance but to optimize with cost in mind, it is important to know how to maximize the performance without increasing the material costs. Hence, the needs to understand which parameter in addition to thickness have greater effects. Also, once known which material properties have greater influence, it would be beneficial to search from the available materials with the least cost and best properties.

4.3.1 Sensitivity Analysis Formulation

In general, the sensitivity analysis is performed by varying one input variable at a time and observing its effect on the overall output. Let's denote the independent variables or the input variables with Xi and the vector X denotes the set of these variables.

$$X = \overline{X} \pm U_X \tag{4.1}$$

Where $\overline{X}$ denotes the nominal value of the independent variable and the U_X is the small change about the nominal value. The range of $\pm U_X$ is defined such that the value of X can occur within this range with a certainty of about 95%. Since the output parameter Y depends upon the input variables X, an uncertainty in X can be related to the output variable as:

$$U_Y = \frac{dY}{dX} U_X \tag{4.2}$$

Since, the input variable X is a vector of many different variables, the output variable Y must be a function of all the input variables such that;

$$Y = Y\left(X_1, X_2, \ldots, X_N\right) \tag{4.3}$$

The uncertainty in Y can be expressed in terms of the root sum square of all the individual uncertainties due to the input variables, that is;

$$U_Y = \left[\sum_{i=1}^{N} \left(\frac{\partial Y}{\partial X_i} U_{X_i} \right)^2 \right]^{1/2} \tag{4.4}$$

To normalize the sensitivity coefficients, we divide with the nominal value of the output

$$\left(\frac{U_Y}{\overline{Y}} \right) = \left\{ \sum_{i=1}^{N} \left[\left(\frac{\partial Y}{\overline{Y}} \frac{\overline{X}_i}{\partial X_i} \right) \left(\frac{U_{X_i}}{\overline{X}_i} \right) \right]^2 \right\}^{1/2} \tag{4.5}$$

The normalized sensitivity coefficient NSC is the term in the first bracket on the right side of the equation, which is

$$NSC_{X_i} = \left(\frac{\partial Y}{\overline{Y}} \frac{\overline{X}_i}{\partial X_i} \right)^2 \tag{4.6}$$

This normalized sensitivity coefficient gives an opportunity to compare all the input variables and their effects with respect to one normalized value of the nominal output

variable. Figure 4.9 represents the nominal system whose values and results are selected as reference and Figure 4.10 graphically represents the variation in one parameter and its effect on the output parameter.

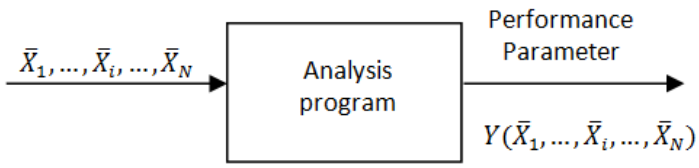

Figure 4.9: Nominal system

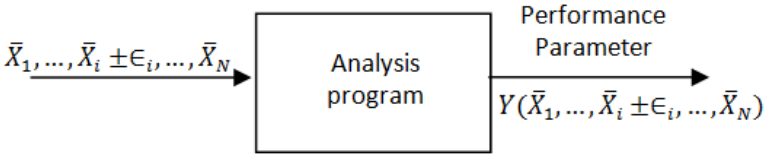

Figure 4.10: Perturbed system

For the sensitivity analysis of the structural problem, the general output responses are the displacements, stresses, strains or velocities [30]. The output variable in the case of impact problem is taken as amount of energy absorbed during the impact event. This is considered as during the impact event, the incident kinetic energy of the impactor is transferred to the specimen. This energy is absorbed in the form of internal energy of the specimen, which results in some of it used in the elastic deformation, some proportion of it used for plastic deformation of the fiber and epoxy while some of energy is dissipated in the damage mechanics as described by the Hashin Model. The energy used for the plastic deformation and damage is termed as the absorbed impact energy as it cannot be recovered while the energy stored in the elastic deformation is returned to the impactor.

The sensitivity coefficients are computed numerically using the finite element method, the sensitivity analysis takes the amount of absorbed energy as the output variable;

$$\{F\} = [K]\{d\} + [M]\left\{\ddot{d}\right\} \tag{4.7}$$

The stiffness matrix is defined as:

$$[K] = \iiint [B]^T [D][B] dV \tag{4.8}$$

Where [D] is the material properties matrix and the matrix [B] is the geometric properties matrix of the sample.

For a case of composite plate, the stiffness matrix can be given as;

$$[K] = tA[B]^T [D][B] \tag{4.9}$$

And the Mass matrix [M] is given by,

$$[M] = \int_V [N]^T [\rho][N] dV \tag{4.10}$$

Where, the nodal mass matrix [ρ] includes the rotary inertia terms.

For a unidirectional lamina, the material properties matrix is given by

$$[D] = \begin{bmatrix} \frac{E_1}{1-\nu_{12}\nu_{21}} & \frac{\nu_{12}E_2}{1-\nu_{12}\nu_{21}} & 0 \\ \frac{\nu_{21}E_1}{1-\nu_{12}\nu_{21}} & \frac{E_2}{1-\nu_{12}\nu_{21}} & 0 \\ 0 & 0 & G_{12} \end{bmatrix} \tag{4.11}$$

4.3.2 Input Variables for Sensitivity Coefficient Calculations

From the literature review, it was noted that the state variables upon which the response of the composite plate depends upon can be a number of different parameters which included, the shell thickness, number of layers and the material of the composite plate.

The studies show that the thickness of the plate, number of layers, thickness of each individual layer, stacking sequence and type of material are some of the factors influencing the impact properties. Also, some studies have been conducted with varying the impact energy by varying impactor mass or velocity. Some other variables were studied in other researches, but the parameters that considered to effect the sensitivity coefficient are the material and geometric properties as explained above because the output parameter “absorbed energy” is related to the material and geometric properties of the plate and is not directly related although effected by the constraint conditions and the impactor properties and energy.

The material properties are studied in detail individually in order to understand the material properties which have the most profound effect on the impact behavior of the composite plate. All the material properties like elastic moduli in the fiber and transverse

direction, shear modulus and strength under various conditions etc. are analyzed using sensitivity analysis. The variables that are studied by this approach are listed in Table 4.7.

Table 4.7: List of Variables for Sensitivity Analysis

No.	**Variable**	**Description**
1	Tp	Thickness of layer/ply
2	Tl	Thickness of laminate
3	N	Number of layers
4	St	Stacking Sequence
5	E_{11}	Elastic Modulus in Longitudinal Direction
6	E_{22}, E_{33}	Elastic Modulus in Transverse Direction
7	v_{12}, v_{13}	Poisson's Ratio in plane containing fiber
8	v_{23}	Poisson's Ratio in transverse plane
9	G_{12}, G_{13}	Shear Modulus in plane containing fiber
10	G_{23}	Shear Modulus in transverse plane
11	X_t	Tensile strength in longitudinal direction
12	X_c	Compressive strength in longitudinal direction
13	Y_t	Tensile strength in transverse direction
14	Y_c	Compressive strength in transverse direction
15	S_{12}	In-Plane Shear Strength
16	G_f^t	Fracture Toughness in longitudinal tensile direction
17	G_f^c	Fracture Toughness in longitudinal compressive direction
18	G_m^t	Fracture Toughness in transverse tensile fracture mode
19	G_m^c	Fracture Toughness in transverse compressive fracture mode

From variable 5 to variable 18, all are related to the selection of material and the sensitivity analysis is performed on these variables to get an informative guess for future material selection.

4.3.3 Validated Flat Plate Model as Nominal Case

The method developed in the sensitivity analysis is considering a case to be nominal and then varying the input variables from this nominal case by ±5%. The nominal case selected for this analysis was the same as the one used for model validation and compared with the results of Yokoyama et al [72]. The advantage of applying sensitivity analysis using a validated model is because of the possibility to isolate single answers to single perturbation of a process parameter [47].

The results and the input parameters used in the model validation were selected as the nominal and the nominal values for the variables are listed in the Table 4.8.

Table 4.8: Nominal Values for the input variables

No.	Variable	Nominal Values
1	Tp	0.21 mm
2	Tl	4.2 mm
3	N	20
4	St	$[45/-45/0/90/45/-45/0/90/45/-45]_s$
5	E_{11}	60.8 GPa
6	$E_{22} = E_{33}$	58.25 GPa
7	$v_{12} = v_{13}$	0.07
8	v_{23}	0.4
9	$G_{12} = G_{13}$	4.55 GPa
10	G_{23}	5 GPa
11	X_t	621 MPa
12	X_c	760 MPa
13	Y_t	594 MPa
14	Y_c	707 MPa
15	S_{12}	125 MPa
16	G_f^t	160 KJ/m^2
17	G_f^c	25 KJ/m^2
18	G_m^t	10 KJ/m^2
19	G_m^c	2.25 KJ/m^2

The output variable for sensitivity analysis is chosen to be the dissipated impact energy or the energy absorbed during the impact event. The absorbed energy gives an account of the damage done to the composite plate in the event of impact. The less this energy the better the design, considering this it is best suited for the study as

improvement in the impact performance of the composite plate is sought. The impact energy absorbed for the nominal case is 4.74 J.

4.3.3 Equivalent Elastic Modulus

The input variables like thickness of plate or the thickness of a single layer can be easily varied by 5% as defined in the approach. But, the variables like the stacking sequence or the number of layers which are not defined by a scalar cannot be varied in the same sense as other variables. For the stated reason, there was a need to develop an understanding to vary these parameters in order to better estimate their effects.

The material properties given in the Table 1 for the nominal case are for a unidirectional lamina i.e. a single ply of composite materials with all the fibers aligned in one direction. With more than one layers stacked at different orientations, they have an overall effect on the physical properties of the whole composite plate.

The stacking sequence for the nominal case corresponds to the concept of "Quasi-Isotropic" laminate, which is the case when the equivalent modulus of elasticity of the whole plate is same in the plane containing fibers, the other case happens to be when the modulus of elasticity in the plane containing fibers is not equal.

The laminate stiffness matrix is given by,

$$[K] = \begin{bmatrix} A & B \\ B & D \end{bmatrix} \tag{4.12}$$

Where each A, B and D is sub-matrices defined as the Extensional Stiffness, Coupling Stiffness and the Bending Stiffness matrices. [60]

The terms of these matrices are given by:

$$A = \sum_{k=1}^{N} \overline{D}\left(z_{k+1} - z_k\right) \tag{4.13}$$

$$B = \frac{1}{2}\sum_{k=1}^{N} \overline{D}\left(z_{k+1}^2 - z_k^2\right) \tag{4.14}$$

And

$$D = \frac{1}{3}\sum_{k=1}^{N} \overline{D}\left(z_{k+1}^3 - z_k^3\right) \tag{4.15}$$

Hence,

$$\begin{Bmatrix} N_x \\ N_y \\ N_{xy} \end{Bmatrix} = \begin{bmatrix} A_{11} & A_{12} & A_{16} \\ & A_{22} & A_{26} \\ sym & & A_{66} \end{bmatrix} \begin{Bmatrix} \varepsilon_x^0 \\ \varepsilon_y^0 \\ \gamma_{xy}^0 \end{Bmatrix} + \begin{bmatrix} B_{11} & B_{12} & B_{16} \\ & B_{22} & B_{26} \\ sym & & B_{66} \end{bmatrix} \begin{Bmatrix} \kappa_x \\ \kappa_y \\ 2\kappa_{xy} \end{Bmatrix} \tag{4.16}$$

For the case of Quasi-Isotropic laminates, the terms A_{11} and A_{22} must be equal. The nominal case selected had the quasi isotropic behavior. In order to study the effect of stacking sequence, it was assumed that the variation in the overall elastic modulus should be studied. Hence, the overall elastic modulus was considered to be varied to study the effect of stacking sequence. For the positive variation, a stacking sequence was designed such that the elastic modulus of the laminate increases by about 5%.

The nominal stacking sequence as listed in table 1 is $[45/-45/0/90/45/-45/0/90/45/-45]_s$ had the modulus of elasticity in the longitudinal direction is equal to be 38.7 GPa, the stacking sequence corresponding to 5% increase in the longitudinal elastic modulus

which is 40.635 GPa is $[30/-60/0/90/30/-60/0/90/30/-60]_s$. Similarly, for the variation of -5% in the longitudinal elastic modulus which is about 36.765 GPa, the stacking sequence is $[60/0/45/-45/60/0/45/-45/60/0]_s$. These layer configurations give the required equivalent longitudinal elastic modulus which is very close to the 5% variation.

Also, the number of layers was also selected as an input parameter, which means the variation would cause the number of layers in the laminate to increase and decrease by 1 layer; this would result in the change of elastic modulus of the laminate. But, it is varied in such a way that the quasi-isotropic behavior of the laminate didn't change.

The change in the parameters for the sake of sensitivity analysis is tabulated in Table 4.7 and the results of all the variables and their sensitivity coefficient are discussed in the next section.

Table 4.9: Variation in the nominal values of the input parameters

No.	Factor	Units	Nominal Value	5% Change	X + ΔX	X – ΔX
X1	Tp	mm	0.21	0.0105	0.2205	0.1995
X2	N	Unitless	20	1	21	19
X3	St	GPa	[45/-45/0/90/45/-45/0/90/45/-45]s ≈ 38.7	1.935	[30,-60,0,90,30,-60,0,90,30,-60]s ≈ 40.7	[60,0,45,-45,60,0,45,-45,60,0]s ≈ 36.8
X4	E_{11}	GPa	60.8	3.04	63.84	57.76
X5	E_{22} = E_{33}	GPa	58.25	2.913	61.1625	55.3375
X6	$v_{12} = v_{13}$		0.07	0.0035	0.0735	0.0665
X7	v_{23}		0.4	0.02	0.42	0.38
X8	G_{12} = G_{13}	GPa	4.55	$227.5X10^{-3}$	4.7775	4.3225
X9	G_{23}	GPa	5	$250\ X10^{-3}$	5.25	4.75
X10	X_t	MPa	621	31.05	652.05	58.995
X11	X_c	MPa	760	38	798	722
X12	Y_t	MPa	594	29.7	623.7	564.3
X13	Y_c	MPa	707	35.35	742.35	671.65
X14	S_{12}	MPa	125	6.25	131.25	118.75
X15	G_f^t	KJ/m^2	160	8	168	152
X16	G_f^c	KJ/m^2	25	1.25	26.25	23.75
X17	G_m^t	KJ/m^2	10	$500\ X10^{-3}$	10.5	9.5
X18	G_m^c	KJ/m^2	2.25	$112.5\ X10^{-3}$	2.3625	2.1375

The point to note here is that the values represented in Table 4.9, does not represent the realistic values of any material in terms of the elastic moduli and the strength values. Rather these values has been adjusted according to the criteria of sensitivity analysis

which states one variable is changed at a time by a some percentage and others keep constant and the same process is repeated for all the variables.

4.4 RESULTS AND DISCUSSIONS

As per the procedure described above a total of 36 simulations were performed using the commercial FEA software ABAQUS to determine the amount of impact energy lost in damage during the impact process for each of the above defined cases. The results for few of the parameter variations were as expected while there were some results that helped understand the role of certain variables play in the impact behavior of the composite laminate.

The results for all the different cases were compiled and sorted in the order of the calculated normalized sensitivity coefficients (NSCs). The order of the list provides with the information that which variable has how much effect. The larger the NSC value, the more that variable influences the output variable which in this case is the amount of the absorbed energy. The results are tabulated as shown in the table in the descending order of NSC.

As mentioned earlier, the amount of energy absorbed in the nominal case was 4.74 J. It is observed that based on the amount of energy absorbed in each variation of variables, the NSC has different orders of magnitude.

Table 4.10 provides a list of parameters in descending order with respect to the NSC.

Table 4.10: Sorted list of the parameters according to normalized sensitivity coefficient (NSC)

No.	Symbol	Energy absorbed in X+ΔX (J)	Energy absorbed in X-ΔX (J)	NSC
X1	Tp	4.59	5.16	1.4096
X3	St	5.59	5.34	0.2899
X10	X_t	4.66	4.87	0.2001
X2	N	4.77	4.88	0.0609
X15	G_f^t	4.70	4.81	0.0479
X5	$E_{22} = E_{33}$	4.80	4.70	0.0440
X4	E_{11}	4.77	4.72	0.0117
X6	$v_{12} = v_{13}$	4.78	4.75	0.0056
X16	G_f^c	4.74	4.77	0.0042
X8	$G_{12} = G_{13}$	4.74	4.76	0.0024
X11	X_c	4.77	4.75	0.0015
X17	G_m^t	4.76	4.74	0.0014
X13	Y_c	4.77	4.75	8.22×10^{-4}
X14	S_{12}	4.74	4.75	3.89×10^{-4}
X12	Y_t	4.75	4.76	3.35×10^{-4}
X18	G_m^c	4.76	4.76	1.69×10^{-4}
X7	v_{23}	4.76	4.76	1.28×10^{-4}
X9	G_{23}	4.74	4.73	6.4×10^{-6}

The results of the calculated NSC are graphically represented in the Figure 4.11. The results listed in Table 4.10 indicates that there is a large dependence of the impact performance of composite plates on some parameters such as the thickness of the layer, number of layers, stacking sequence and the material properties like the tensile strength and the fracture toughness in the fiber direction. The other material properties studied showed dependence of the impact performance does not vary that much with the variation of standard 5% from the nominal values.

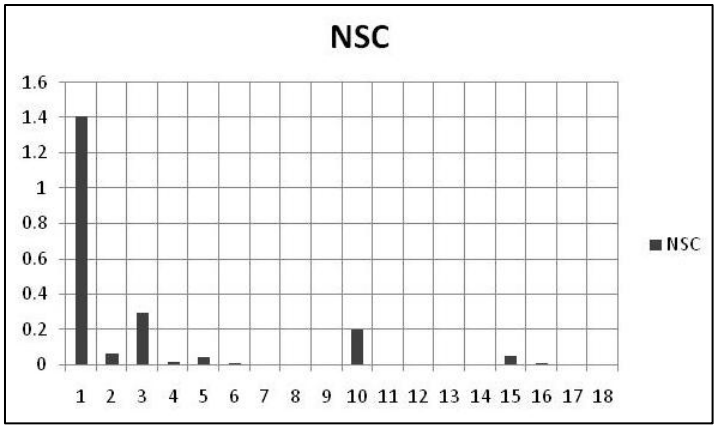

Figure 4.11: NSC for all the variables demonstrating the relative effect of each on the absorbed impact energy

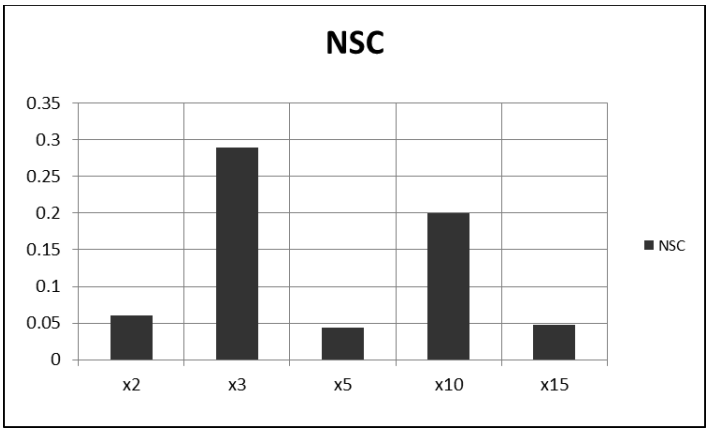

Figure 4.12: NSC for the variables having greater influence on the amount of absorbed energy except thickness

According the values listed in Table 4.10, the parameters considered to have significant effect are:

1) Thickness of each layer/ply

2) Stacking Sequence

3) Tensile strength in the fiber direction

4) Number of layers

5) Fracture toughness in the fiber direction during tensile loading

The parameters 3 and 5 are related to the material properties and are hence dependent upon the material selection. These parameters will help in selection of material for the fiber and matrix material.

The effect of thickness of individual layers show that the increase in thickness results in the decrease in absorbed energy and of all the parameters considered the effect of thickness is most profound on the impact performance of the composite plate. This result is intuitive and in accordance with the available studies in the different literature. The effect of increasing thickness of individual layers has been studied extensively and is the most effective parameter to increase the impact resistance of composite plates. This result is backed by the available results from the studies of Zhao et al. [73]. Zhao et al. demonstrated that with the increasing thickness the damage is considerably reduced while the stacking sequence was kept constant. As discussed in the literature, the effect of thickness is most prominent among all the variables considered, is also supported by the fact that the value of NSC for the case of thickness variation is the highest which characterizes a strong dependence on the thickness of the layer.

The first parameter to study was the thickness of the individual layer, the effect of the variation reveals that the impact performance improves as the thickness is increased, i.e.,

the amount of energy absorbed/dissipated decreases as the thickness is increased and vice versa.

The second most important parameter is found to be the stacking sequence, one important aspect to understand is that the stacking sequence effect is not linear considering that in this study the stacking sequence is studied in terms of the equivalent elastic modulus of the whole laminate. The nominal case that was selected to be the quasi isotropic behavior has the best performance in terms of minimum impact energy absorption.

The results show that the minimum amount of energy absorbed is for the case where the laminate configuration is such that the laminate behaves as quasi-isotropic material. This result agrees with the result from the study of Aktas et al. [2]. The value of the NSC calculated for the variation in the stacking sequence suggests that the impact resistance of composite laminated plates is highly dependent upon the stacking sequence. The dependence is not linear and as the stacking sequence converges to a quasi-isotropic behavior the amount of impact energy absorbed is significantly reduced.

The other important factors were the tensile strength and the fracture toughness in the fiber direction, increasing these parameters result in lower impact energy absorption while lowering these values has inverse effect. The tensile strength of the fiber is the third most significant variable as observed by the NSC and is quite close to the NSC of stacking sequence. This has a significant effect on the understanding in the design process of structures with composite materials that are susceptible to the impact loading

due to low velocity impacts. It is suggested that the material should be chosen as such which offers greater tensile strength as compared to the other material properties.

The tensile strength of the fiber has a significant effect on the absorbed impact energy as described by the damage initiation equations by Hashin (1980) given by equation (3.5), during the impact loading the plate is stretched and due to plate in tension as evident in Figure 4.2, the tensile strength of fiber plays an important role in the impact behavior of the composite plates. As evident by equation (3.5), the higher the strength value, the more stress it can bear before breakage hence less absorbed energy and better impact resistance.

Similarly, the effect of fracture toughness can be observed from the damage evolution laws described by Hashin. As shown in Figure 3.6, the amount of dissipated energy is the area under the curve for the equivalent stress-displacement curve, the higher the fracture toughness the more stress composite plate can withstand before the damage.

Finally, the last factor considered was the number of layers; it similarly has not a linear relation like the stacking sequence. Increasing and decreasing by 5% the number of layers while keeping the total laminate thickness constant result in increased impact energy absorption. Hence, it can be deduced that there must be an optimal number of layers for a fixed thickness which will give the better impact performance. This observation can be related to the fact that from various studies it is observed that increasing layers with 90° orientation results in the increase in contact force as described by Tiberkak et al. [65]. Thus, there must be an optimum condition for which the amount of absorbed energy and the resulting damage will be minimum.

The other material properties that have slight influence on the impact resistance are the fracture toughness of the material in the tensile loading in the longitudinal direction and the transverse elastic modulus. Both these variables have the NSC values in the same order as the NSC for the number of layers but slightly less. Besides, both these variables having similar NSC values, their behavior is completely different. The increase in the fracture toughness G_f^t results in better impact performance while the increase in transverse elastic modulus results in the increase in impact energy absorption hence it is desirable to have transverse elastic modulus low.

The rest of the material properties like the longitudinal elastic modulus, the shear modulus and the strength of the lamina in the transverse direction have very small effect on the overall impact performance of the composite plate. This can be observed by the fact that the value of NSC is of one or more order less than the NSC of stacking sequence and number of layers etc.

4.5 CONCLUSIONS

This chapter presented the model validation and the sensitivity analysis approach to ascertain the effects of various geometrical and material properties of composite materials on the impact performance of the composite laminated plates. Initial numerical model was selected from the literature and the results verified against the available numerical and experimental results. The results show quite a good agreement with the experimental results. The model was then selected as the nominal case for further evaluation of NSC using the commercial finite element solver ABAQUS explicit.

The results presented in the current study gives an insight about the effects of the considered parameters on the impact performance in terms of a normalized coefficient. The advantage of such a coefficient is that an equal amount of variation in any of the parameters will be highlighted in varying effect on the output; hence, it can be classified according to the order. ABAQUS explicit solver was used to perform the finite element simulations to find the effect of variations in all the input variables one at a time on the absorbed impact energy. The amount of energy absorbed varies significantly for the variations in the thickness of a single layer, number of layers, stacking sequence and the material properties that have significant effect were the tensile strength of the layer in the fiber direction, fracture toughness of the laminate in the tensile loading in the longitudinal direction and to some extent the elastic modulus of the transverse direction has effect on the absorbed impact energy. The only peculiar behavior is of the stacking sequence, as the stacking sequence is changed the overall elastic modulus of the laminate varies and as the behavior of the laminate moves away from that of the quasi-isotropic the amount of energy absorbed increased resulting in a poor performance compared to the nominal case.

The results from this study will help the authors in the future work in designing composite laminated plates having better impact resistance. The results will allow a more methodical approach in selecting the parameters to vary in order to achieve better impact performance of composite laminates against the low velocity impact loadings. The results from this chapter for the improvement of impact performance of composite plates can be summarized as:

- The layer thickness has the most prominent effect with the more the thickness, the better the impact resistance.

- Stacking sequence should be such that the overall behavior of the laminate should be close to quasi-isotropic.

- The most important material property for selection of material is the tensile strength of the fiber in the longitudinal direction.

- The number of layers has an effect on the impact resistance and should be selected carefully as to not just increase the layers which result in more contact force and hence greater damage.

CHAPTER 5

PARAMETRIC STUDY OF DESIGN VARIABLES

The main idea of this current study was to investigate the relation of the amount of damage occurring during an impact load with the number of factors such as the thickness of the layers, number of layers, orientation angles, material types and inclusion of other materials. These factors were identified using the sensitivity analysis approach discussed in the previous chapter. This way a more knowledgeable design criterion can be developed which will be optimal in terms of performance and the cost of the material. For a comprehensive study of effects of these factors, a design of experiments approach was adopted where all the possible combinations can be tried.

In this chapter, design of experiments approach is presented along with the discussion of the effects of these factors on the impact performance of both the composite plates and the pipes.

5.1 DESIGN OF EXPERIMENTS

Design of experiments is a very useful tool to investigate the causes and effects of various factors spread over a domain. The use of design of experiments along with the finite element analysis gives an analyst a powerful tool to understand deeply the

variations of the outcomes of a process and the factors causing these variations. In addition to the effects on the design or process, design of experiments gives statistical significance to understand them. The combination of finite element analysis with the design of experiments provides the opportunity for the current work to study the complete domain of the identified variables from sensitivity analysis and their relationship with the impact performance. It is evident from the literature review that so far the experimental studies conducted in the low-velocity impacts on the composite materials have not been comprehensive. This is due to the obvious reasons that the production of such large number of samples is costly and the experiments for impact loads can be classified as destructive analysis. Therefore, most of the studies conducted experimentally considered few variations in the factors like thickness or the stacking sequence.

The use of finite element analysis is therefore beneficial and advantageous to combine with the large number of experiments designed using DOE.

5.2 NUMERICAL EXPERIMENTS FOR FLAT PLATE

In the study discussed in Chapter 4 by the author, the sensitivity analysis characterized four variables namely the thickness of the single layer, number of layers, stacking sequence and the material type to be of most significance considering the impact behavior. Therefore, here these four factors are considered in the DOE study and the different levels studied are listed in the Table 5.1 and Table 5.2. Here, the materials considered are only carbon/epoxy and the glass/epoxy and the tables are listed separately for both these materials. This is due to the fact that the carbon being the stronger material

has different thickness ranges in which it varies from completely damaged, i.e., penetration of the striker to the complete survival, i.e., the striker bounces back with the same speed. The stacking sequence is kept the same for both of these materials as the effect of stacking sequence in both the materials had to be compared.

An initial DOE was fashioned with three discrete levels of thickness and four discrete levels for the number of layers. These were from levels ‘5’ to ‘7’ for the thickness and levels from ‘1’ to ‘4’ for the number of layers. This combination of factors results in total 96 experiments for both types of the materials. But after the initial simulations it occurred that there are two shortcomings in this design. One, in this range the variation was not from complete damage to complete survival; it only showed the intermediate behavior. Two, the number of experiments were not sufficient enough for a good training of neural networks. Therefore, additional levels were added for both carbon and glass fiber plates to observe the complete spectrum. The results were calculated in terms of the absorbed energy with the impact energy fixed at 27.55 J. The impactor dimensions, weight and velocity are being kept constant in all the cases. The boundary conditions are also kept the same throughout all the experiments. The simulations were performed in ABAQUS Explicit environment.

Table 5.1: DOE Table for Carbon/Epoxy Composite Plates

Thickness (mm)	Number of Layers	Stacking Sequence
0.12	16	[0/30/60/90]
0.14	20	[45/-45/0/90]
0.16	24	[45/30/-30/-45]
0.18	28	[60/45/-45/-60]
0.2	32	
0.25	36	
0.3		
0.35		
0.4		

In total, 108 experiments were performed using the carbon/epoxy as the material for the plate. The results are quite large and are listed in the Appendix A.

Table 5.2: DOE Table for Glass/Epoxy Composite Plates

Thickness (mm)	Number of Layers	Stacking Sequence
0.25	24	[0/30/60/90]
0.3	28	[45/-45/0/90]
0.35	32	[45/30/-30/-45]
0.4	36	[60/45/-45/-60]
0.45		
0.5		
0.6		

Similar to the experiments conducted numerically for the carbon/epoxy plates, 108 experiments were performed for the glass/epoxy plates as well. The combinations were not all similar but the initial 48 experiments were kept. All the results are listed in the Appendix A from Table A. 1 to Table A. 8.

5.2.1 Effects of Fiber Material

In this study, only two materials have been selected for the comparison. The material properties are listed in the Tables Table 3.3, Table 3.5 and Table 3.7 for the carbon/epoxy composite plate and for the glass/epoxy in the Tables Table 3.4, Table 3.6 and Table 3.8. The simulations were designed such that a direct comparison can be obtained between the absorbed energy by the two materials. The elastic moduli of the carbon fiber system are greater than the glass fiber system. Also, the difference in the strength levels is also considerably high in favor of carbon based composites as well as the intralaminar fracture toughness values. The damage mechanism mentioned in the equations (3.3) to (3.6) is based upon the strength levels of the composite. Once, the damage is initiated the cracks propagate through the material which is modeled using the linear energy based damage evolution model. According to the material properties, the carbon/epoxy system should be better than the glass/epoxy system in terms of impact performance as both the strength and the fracture energies for carbon/epoxy is higher.

The results from the simulation were intuitive as the carbon/epoxy composite plate has better impact resistance compared to glass/epoxy composite plate at the same conditions of thickness, stacking sequence and boundary conditions.

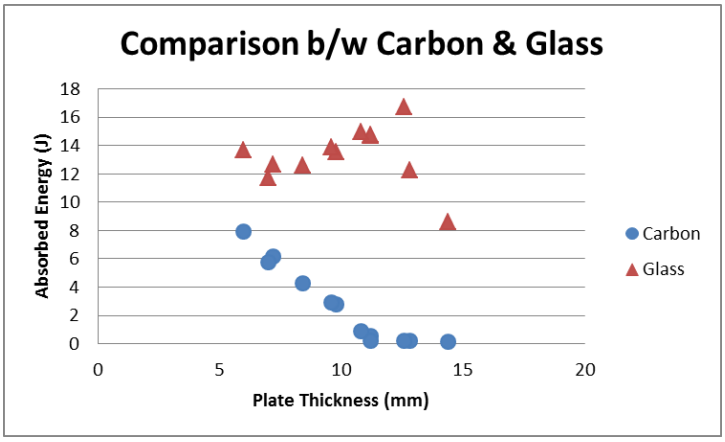

Figure 5.1: Comparison of Carbon and Glass composite plates at different thickness with stacking sequence 1

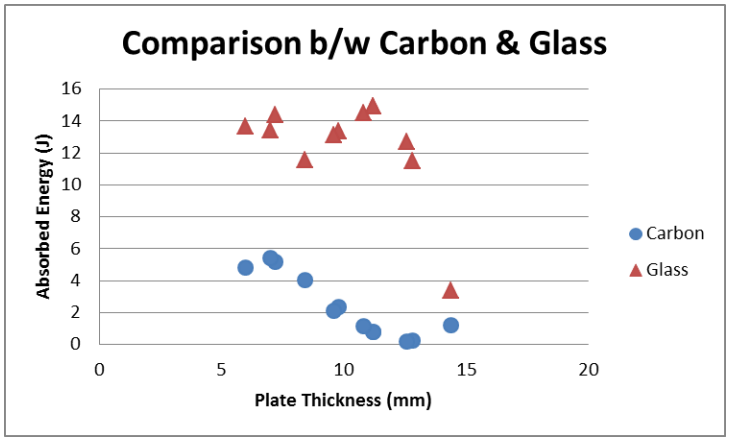

Figure 5.2: Comparison of Carbon and Glass composite plates at different thickness with stacking sequence 2

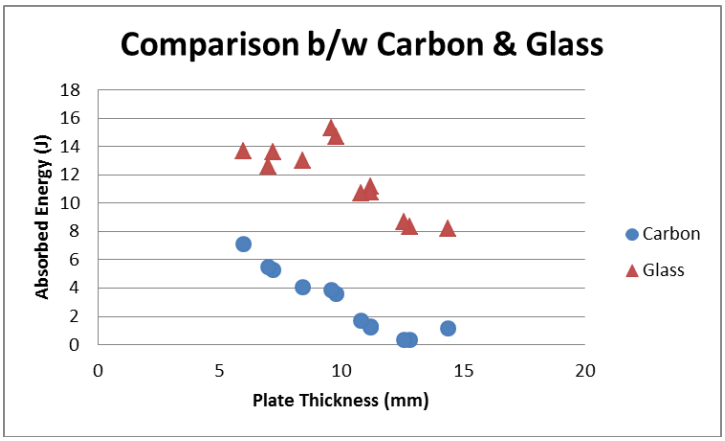

Figure 5.3: Comparison of Carbon and Glass composite plates at different thickness with stacking sequence 3

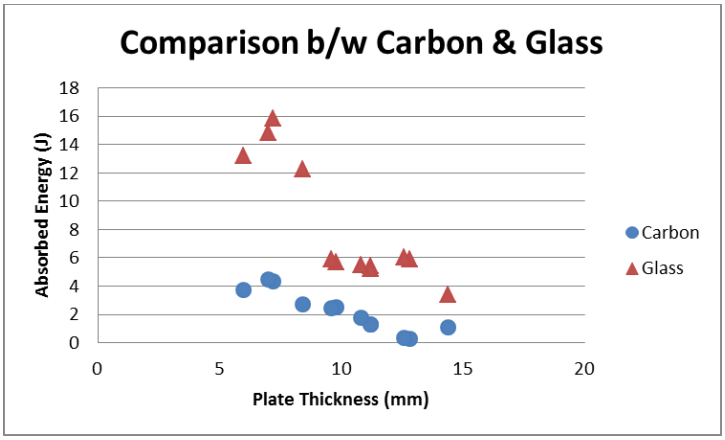

Figure 5.4: Comparison of Carbon and Glass composite plates at different thickness with stacking sequence 4

Figure 5.1 to Figure 5.4 shows that the composite plates of CFRP are better against impact loads compared with the GFRP. This has already been explained above is due to the higher strength and the fracture energies of the carbon/epoxy. The results listed in the tables in Appendix A for the composite plates demonstrates that the composite plates fail

completely at the thickness level of less than 6 mm for GFRP while that of CFRP can withstand the same impact load at around 2 mm.

5.2.2 Effects of Thickness of Plate

The sensitivity analysis showed that the biggest single factor in the impact performance of composite structures is the overall thickness of the plate or the pipe. In this section, the effect of thickness of both CFRP and GFRP plates are discussed.

From the results of sensitivity analysis, it is observed that the increasing thickness reduces the amount of absorbed energy.

A) Carbon/Epoxy Plates

This trend can be observed in the graphs for the various thicknesses for carbon/epoxy plates shown in the figures Figure 5.5 to Figure 5.8.

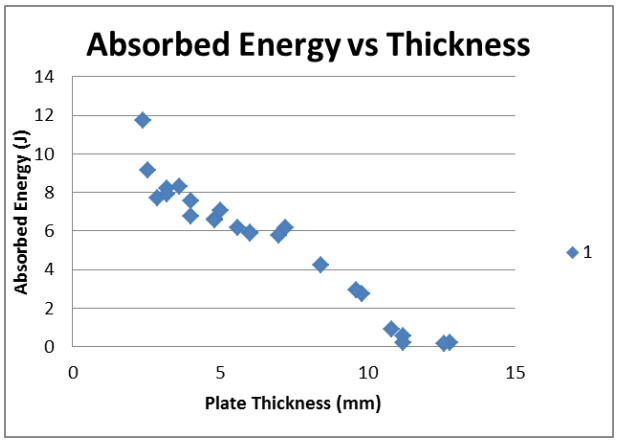

Figure 5.5: Scatter data for the layer configuration 1 for carbon/epoxy plates

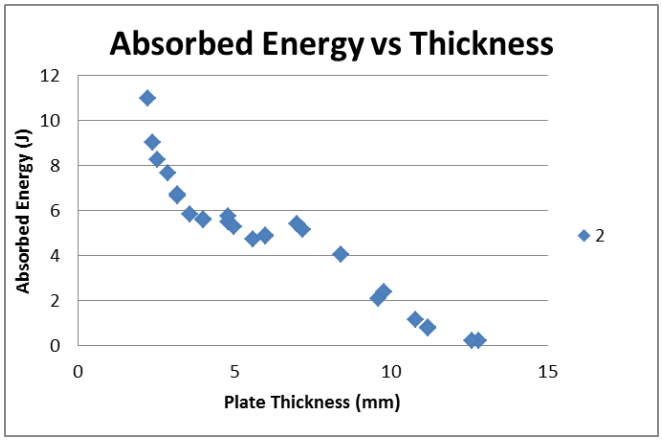

Figure 5.6: Scatter data for the layer configuration 2 for carbon/epoxy plates

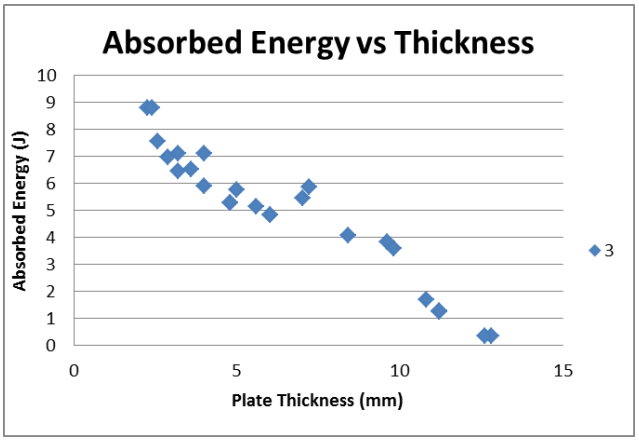

Figure 5.7: Scatter data for the layer configuration 3 for carbon/epoxy plates

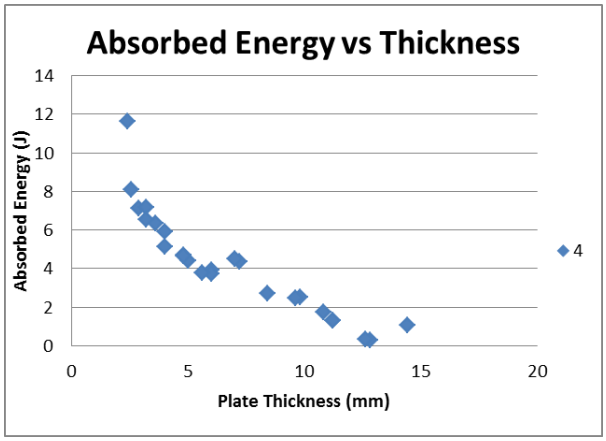

Figure 5.8: Scatter data for the layer configuration 4 for carbon/epoxy plates

The results from the ABAQUS analysis follow the intuition that with the increasing thickness the amount of absorbed energy will decrease i.e. an improvement in the impact performance of the composite plate. The results as plotted against the overall thickness of the plate show that they follow a certain trend and as a basic trial, a simple fourth order polynomial was fitted over the scattered data. The curve approximates quite accurately except for a few results which were away from the trend line.

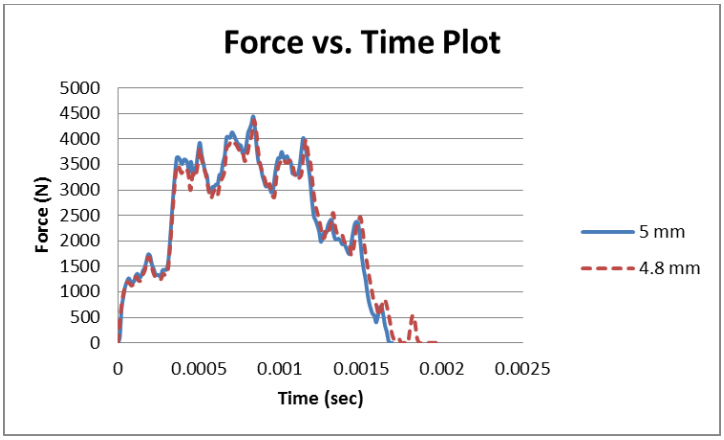

Figure 5.9: Force vs. time plots for two different thickness of CFRP plates using the [0/30/60/90] laminate configurations

B) Glass/Epoxy Plates

It was expected that the composite plates with glass fiber as the reinforcement material will behave in a similar fashion as the carbon fiber based plates did. However, it was found that the behavior of the glass/epoxy plates was a little peculiar as initially with the increase in thickness the absorbed energy reduced, therefore, improving the performance of the composite plates against the low velocity impact loads. However, a further increase in the overall thickness of the plate either by means of increase in layer thickness or by increasing the number of layers resulted in the decrease in performance. This behavior is strange and as compared with carbon/epoxy system was not observed in those cases. This behavior is clearly seen for all the different cases of stacking sequence. But, there is a thickness value beyond which the impact resistance starts to increase again and eventually the plate although at very large thickness performed without significant damage. These results are presented in the graphical form in the Figure 5.10 to Figure 5.13.

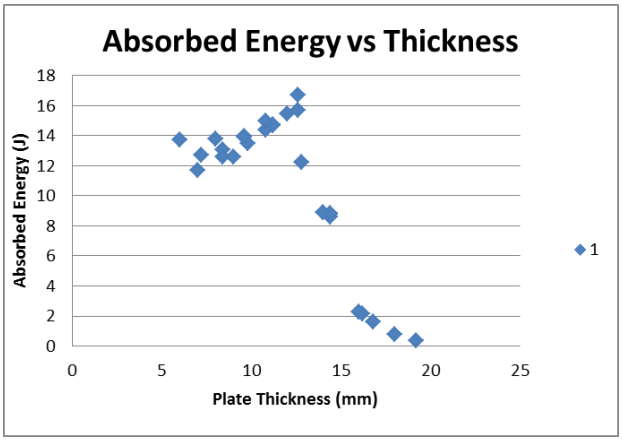

Figure 5.10: Scatter data for the layer configuration 1 for glass/epoxy plates

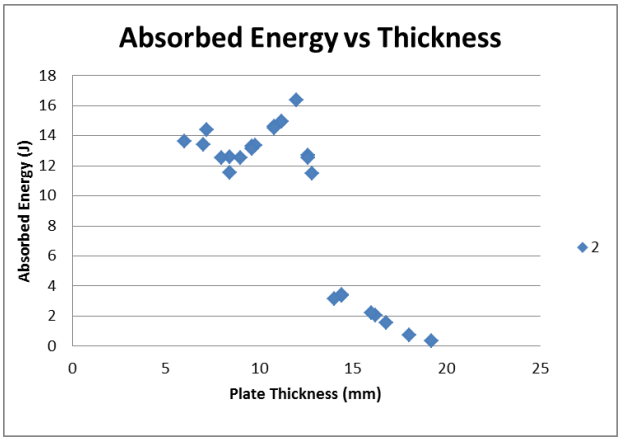

Figure 5.11: Scatter data for the layer configuration 2 for glass/epoxy plates

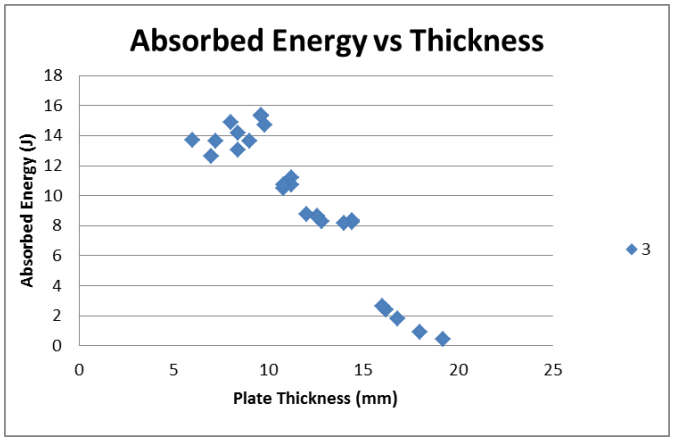

Figure 5.12: Scatter data for the layer configuration 3 for glass/epoxy plates

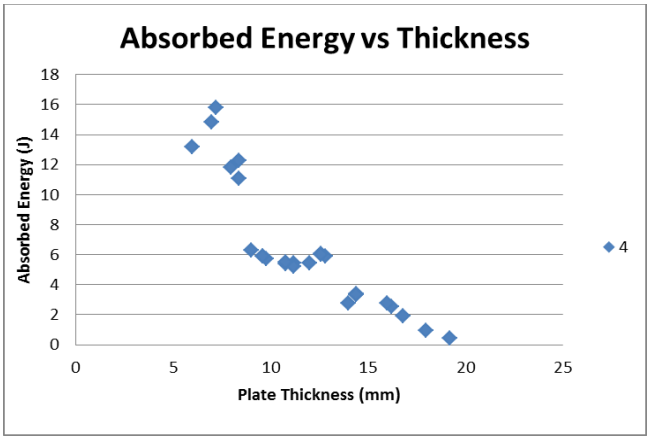

Figure 5.13: Scatter data for the layer configuration 4 for glass/epoxy plates

Physically, this phenomenon can be explained such that when the thickness of the composite plate is small, the plate behaves much more like a membrane and during impact the plate stretches until all the kinetic energy is transferred to the plate and then it pushes back the impactor giving away some of the energy back to the impactor and the rest is dissipated in the form of damage within the plate. The more the thickness of the plate is increased, the stiffer it gets and the ability to bend under impact loads is reduced which increases the bending stress and hence the plate suffers more damage. At very high thickness, the plate becomes very strong and stiff which results in very low amounts of energy absorbed.

This large increase in the absorbed energy at the intermediate thickness range can be explained by the concept that the flat plates with small thickness acts like a membrane and in such thin plates the compression failure in the plane of the plate or through the thickness cannot be observed. In such cases, the maximum deformation is higher than the plate thickness [26]. This can be observed in our case as well, for example, if we consider the cases number 1 and 2 from the Table A. 5, the plate with thickness 6 mm absorbs less energy than the plate with 7.2 mm. The maximum deformation in the case 1 here was found to be 8.7 mm which is more than the plate thickness while the maximum deformation is about 6.5 mm in the case of plate with 7.2 thickness. Another interesting point observed was the calculation of the A, B and D matrices defined in the equations (4.12) to (4.16). It was observed that irrespective of the stacking sequence, the increase in absorbed energy was coincident with the same values of the sum of the members of the extensional stiffness matrix A. It is to be noted that the extensional stiffness matrix

provides the relationship between the strains and the forces for the laminate. This value was quantified to be in the range of 330 to 450 GPa-m.

The same effect can be observed in the carbon/epoxy plates but because the fracture energies are high for carbon, the increase in absorbed energy with the increase in thickness is not high. Although, we do observe some cases in Figure 5.5 to Figure 5.8; where the amount of energy to increase slightly or at least didn't decrease by the same percentage as was expected.

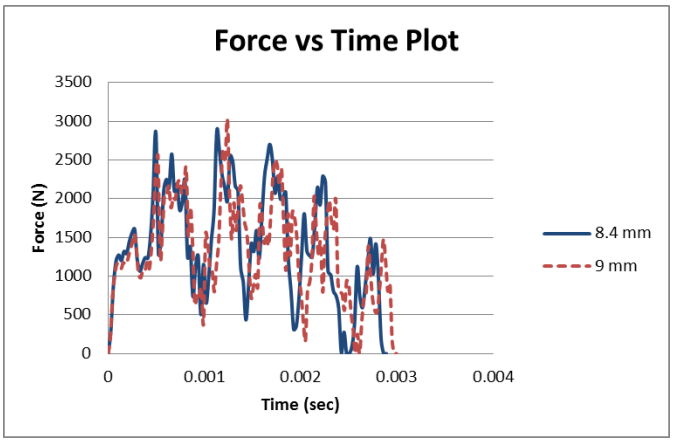

Figure 5.14: Force vs time plot of two different thickness GFRP plates using [45/-45/0/90] laminate configuration

A comparison of force history graphs for two carbon/epoxy laminates and two glass/epoxy laminates show that in the glass/epoxy plates the sharp falls in the force. A sudden fall in the force represents the onset of damage until the impact load is supported by the layers so far remain undamaged. In carbon/epoxy plates, the fall in force is not that high before it starts to increase which shows that after the initiation of damage it doesn't propagate so quickly. This is due to the high fracture energies of the carbon fiber.

Whereas the glass/epoxy plates show a much steeper fall in the force values. This represents that the damage once initiated can propagate quite easily, that is due to the low fracture energies of the glass fiber. A comparison of the fracture energies shows that glass has 1/16th of the fracture energies of the carbon. To better understand this cause, a similar glass/epoxy plate as shown in Figure 5.15 was simulated with 4 times the initial fracture energy only in the tensile fiber direction. The phenomenon that impact performance deteriorates in these samples with the larger thickness was still observed but this time the difference in the amount of absorbed energies is quite low and also the force history graphs are close to the one of carbon/epoxy.

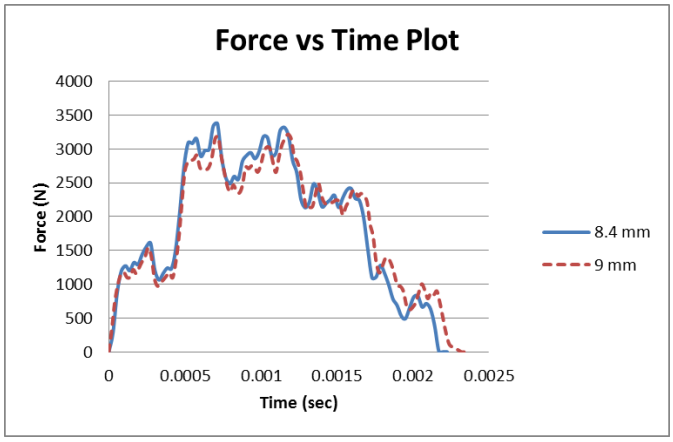

Figure 5.15: Force vs. time plot of two different thickness GFRP plates using [45/-45/0/90] laminate configuration with fracture energy of 40 kJ/m^2

5.2.3 Effects of Stacking Sequence

The stacking sequence of composite laminas is the arrangement of the individual layers in specific orientation. The ability of arranging layers according to the design gives the special advantage to composite materials over the conventional isotropic materials in better load handling capabilities. In this study, four different stacking sequences were

studied. These stacking sequences are arrangement of 4 layers mentioned in Table 5.1 and Table 5.2 in various directions which were then repeated to achieve the desired thickness and number of layers.

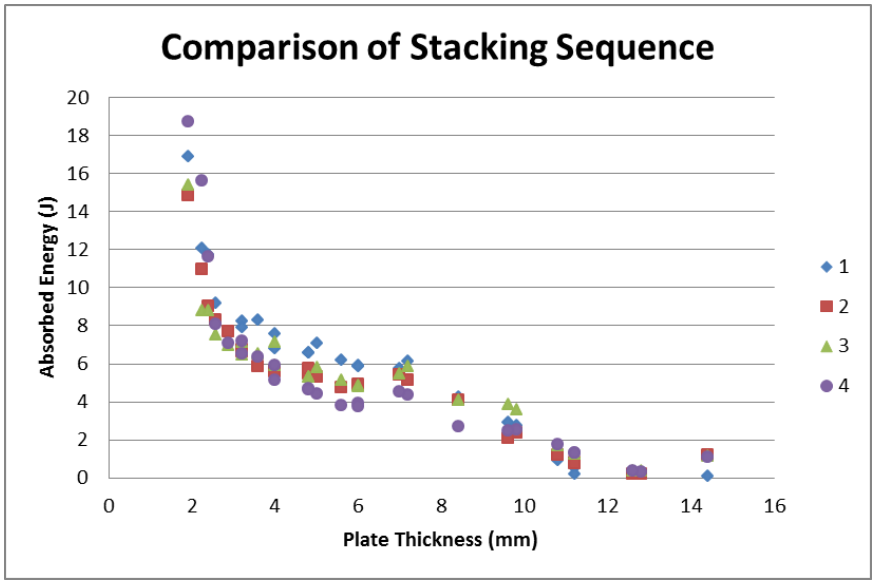

Figure 5.16: Absorbed Energy vs. thickness for all the four stacking sequences for carbon/epoxy system

Figure 5.16 plots the amount of absorbed energy for all the stacking sequences studied for this work. From the plot, it is observed that for the thinnest plates, the worst stacking sequence was 4 while the best was stacking sequence 1. This is in-line with the current research where the quasi-isotropic behavior of laminate configuration of stacking sequence 1 is suggested to be the best against the low-velocity impacts. This suggestion is correct considering the stacking sequence 1 laminate configuration distributes fibers equally in both the principal directions which are the main load bearing component in the composite materials and have equal stiffnesses in the x and y directions. The other two stacking sequences lie in between the stacking sequences of 2 and 4.

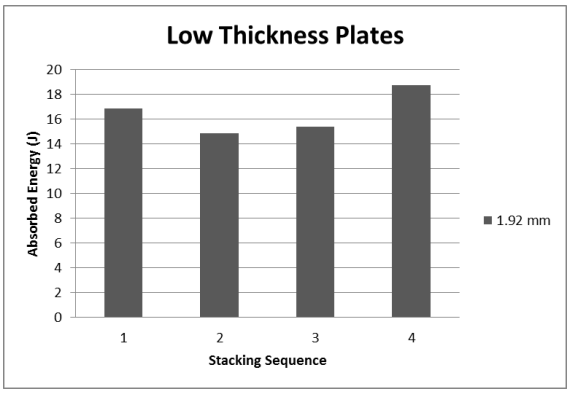

Figure 5.17: Stacking sequence comparison for thin CFRP plates

Further increasing the thickness provides more insight into the effects of stacking sequence. Here, it can be observed that in the intermediate thickness range for the carbon/epoxy plates, the best laminate configuration or the stacking sequence is the sequence number 4. However, at larger thicknesses, there is not much of a difference. Figure 5.18 shows the similar behavior for the glass/epoxy plates.

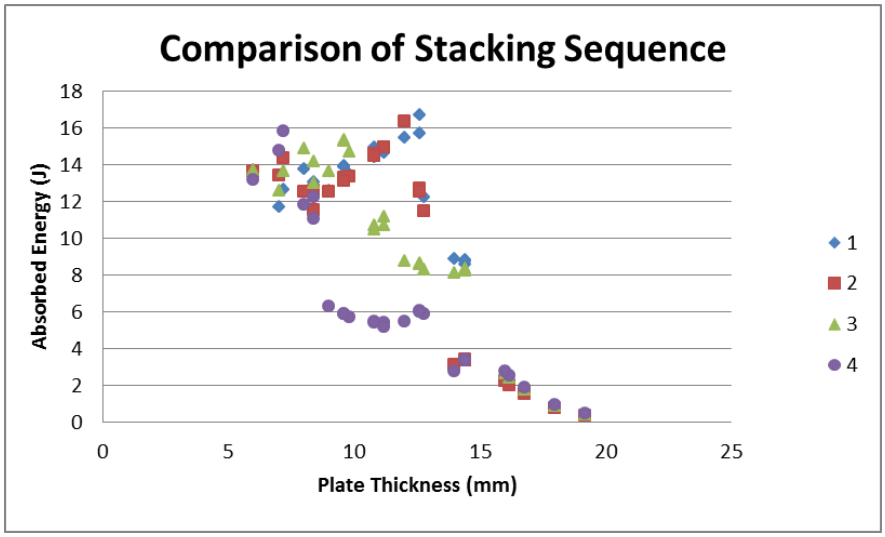

Figure 5.18: Absorbed Energy vs. thickness for all the four stacking sequences for carbon/epoxy system

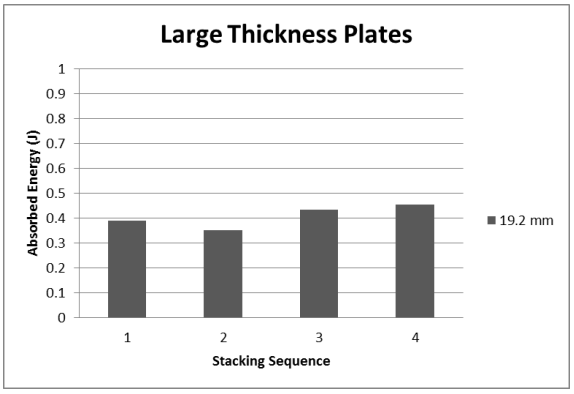

Figure 5.19: Stacking sequence comparison for very thick GFRP plates

Even for the glass/epoxy plates the stacking sequence 4 is better in terms of the absorbed energy for the moderately thick plates. This is due to the fact that the most important factor in the damage limitation is having a high tensile strength in the fiber directions. Therefore, to avoid damage due to the impact loads, the fibers should be aligned in the direction where the maximum stress is observed. If we recall the boundary conditions we applied for our numerical model as shown in Figure 3.7, it was on the two shorter edges of the plate which makes the plate constrained in the global y-axis direction. The reason that the stacking sequence 4 has better performance is down to this reason, since it has more fibers aligned towards the y-axis and it can withstand more loads in this direction. A simple calculation of the transformation of the strengths in the x and y-axis direction show that the stacking sequence 4 has the highest strength in the y-direction followed by sequence 2. Therefore, this stacking sequence offers better performance especially in the intermediate thickness plates where the others were facing more damage.

Alternative explanations for this kind of behavior can be find in the study by Zhao et al. [73], where they observed that the maximum damage size and the maximum deflection of the composite plate decreases with the increase in the bending stiffness of transverse direction. The bending stiffness can be calculated using the equations provided earlier for the A, B and D matrices, where D matrix represents the bending stiffness matrix. Zhao et al. reported that the best stacking sequence would be the one in which the longitudinal and transverse stiffness are equal. This is true in the case where we have similar boundary conditions on all the edges. If, we have boundary conditions different on different directions, then we can optimize the stacking sequence as is in our case the sequence 4 provides the best solution according to the given boundary conditions.

5.2.4 Effects of Layer Thickness and Number of Layers

Sensitivity analysis results suggested that the number of layers have some effect on the impact performance of the composite plates. From the sensitivity analysis, it was observed that if the overall thickness of the plate is remained constant but the numbers of layers vary, then the amount of energy absorbed will be varied. The results as listed in the Table A. 1 to Table A. 8 suggest that this is indeed the case. But, the variation is not always as initially observed from the sensitivity analysis. The variation in the amount of absorbed energy depends upon the orientation of individual layers that are added to or removed from the stacking in compensation to keep the thickness constant.

If we consider the two cases from the carbon/epoxy plates with the same thickness but different number of layers, we observe some interesting results. It can be observed that the in case where we have 20 layers, we have four additional layers of 0˚ and 30˚ two each. As discussed earlier during the effects of stacking sequence, these four additional

layers are just keeping the overall thickness constant but in fact are reducing the number of fibers from the layers of 60˚ and 90˚. As we by now know that these layers when transformed along the principal directions share larger share of the strength in the y-axis where we deduced the majority of the stress would be produced. Hence, the observation in this case is that the additions of these 0˚ and 30˚ layers are doing more harm than good. As can be seen in from the amount of energy absorbed increased in the case of 20 layers compared to the case of 16 layers.

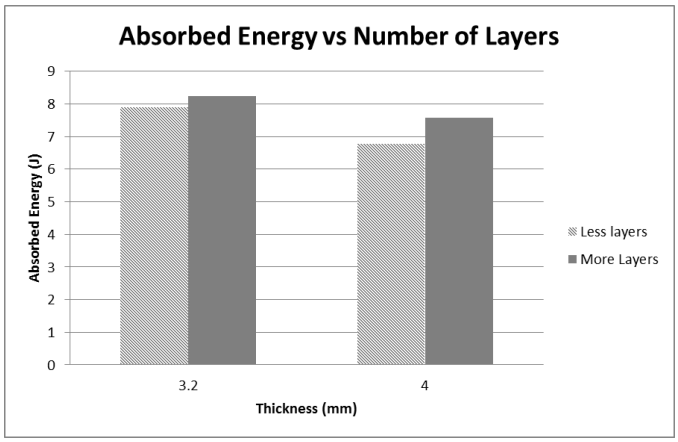

Figure 5.20: Comparison of amount of absorbed energy between 16 layered and 20 layered CFRP plates

Table 5.3: Orientation of individual layers for two cases of carbon/epoxy plate

Thickness of layer (mm)	Number of Layers	Total Thickness (mm)	Absorbed Energy (J)
0.16	20	3.2	8.227648
0.2	16	3.2	7.894729
0.25	16	4	6.78549
0.2	20	4	7.570117

By virtue of the above explanation, it might be argued that if we increase the number of layers keeping the thickness constant in such a way that some of the fibers from the 0˚ and 30˚ layers are removed and added to 60˚ and 90˚ orientated layers, then we might observe improvement in the impact performance. By comparing the results from Table 5.4 and Figure 5.21, it is observed that is indeed the case.

Table 5.4: Orientation of individual layers for two cases of carbon/epoxy plate

Thickness of layer (mm)	**Number of Layers**	**Total Thickness (mm)**	**Absorbed Energy (J)**
0.3	20	6	5.915478
0.25	24	6	5.849285
0.35	32	11.2	0.2031
0.4	28	11.2	0.56125

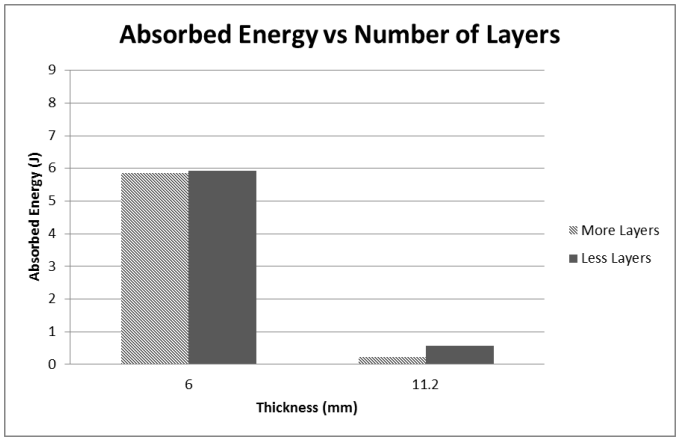

Figure 5.21: Comparison of amount of absorbed energy based on number of layers for a fixed thickness CFRP plates

The same behavior can be observed for the glass/epoxy plates as demonstrated from the results in Table 5.5 and Figure 5.22 for the situation where the addition of layers results in the improvement of impact performance. This is due to the same reason as

explained above that this is due to the addition of layers which can bear more load in the direction of the stress and hence improve the overall impact performance. While Table 5.6 and Figure 5.23 represents the case where the addition of layers decrease performance.

Table 5.5: Orientation angles of GFRP plates where increasing layers increase performance

Thickness of layer (mm)	**Number of Layers**	**Total Thickness (mm)**	**Absorbed Energy (J)**
0.35	24	8.4	14.20262381
0.3	28	8.4	13.02287113
0.3	32	9.6	15.32878983
0.4	24	9.6	15.3788138

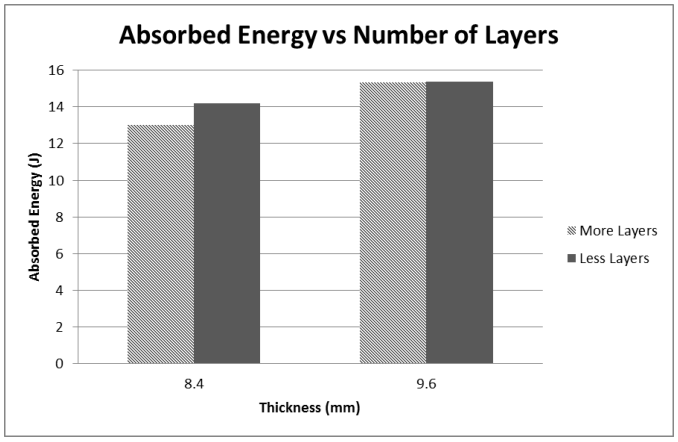

Figure 5.22: Layers comparison in cases where the increase in layers increase performance for GFRP plates

Table 5.6: Orientation angles of GFRP plates where increasing layers decrease performance

Thickness of layer (mm)	Number of Layers	Total Thickness (mm)	Absorbed Energy (J)
0.3	36	10.8	10.72389162
0.45	24	10.8	10.4629225
0.35	36	12.6	8.650227096
0.45	28	12.6	8.588431527

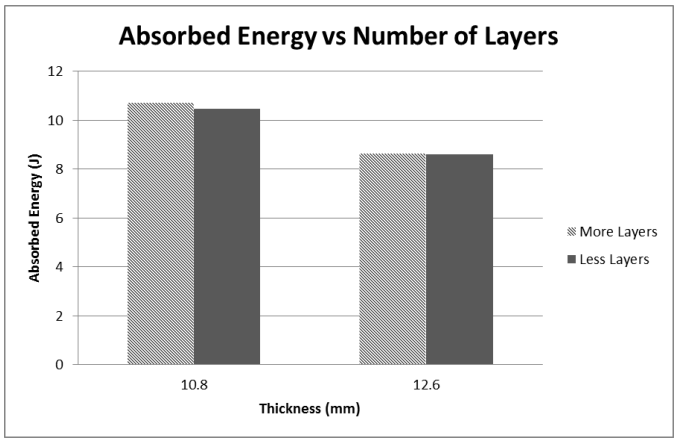

Figure 5.23: Layers comparison in cases where the increase in layers decrease performance for GFRP plates

5.3 NUMERICAL EXPERIMENTS FOR COMPOSITE PIPES

Following on from the study of effects of the parameters on the impact performance of the composite plates, the study is carried out for the composite pipes as well. The factors that have influence on the impact performance are the same as found from the sensitivity analysis study and we also studied their effects for the composite plates as well. The difference between plates and the pipes is in the type of lamina and the

lamina's orientation angle. Since, it is known that the composite pipes are manufactured using the filament winding technique, the type of lamina considered in this study is the unidirectional lamina. The material properties for carbon/epoxy and glass/epoxy are listed in the Tables Table 3.9, Table 3.11 and Table 3.13 and Table 3.10, Table 3.12 and Table 3.14 respectively. Also, the pipes manufactured using filament winding technology have only two orientations, i.e., $\pm\theta$, therefore here we have studied different winding angles rather than a combination of layer orientations as studied for the composite flat plates.

The design of experiments is again applied to gather the results for the composite pipes where the complete damage to the complete survival configurations is selected. The layer thickness is selected based on the commercial availability of carbon and glass fibers. The winding angle was selected from 35˚ to 75˚ with an interval of 10˚. This is selected on the basis of the study of Rosenow [59] in which he studied the effect of variation of winding angles on the filament wound glass fiber reinforced polyester. The author studied winding angles from 15˚ to 85˚. In his study, the author suggested that the winding angle of 55˚ was optimal for the hoop to axial stress ratio of 2, while for only pressure loadings without axial stress the optimal winding angle was 75˚.

Initially, experiments were designed with 4 distinct layer thicknesses, 5 sets of number of layers and 5 different winding angles. This design gave a total of 100 simulations to be carried out. Later on, two additional layer thicknesses and a further set of simulations were run with total number of layers up to 40 for the glass fibers and 16 layers for the carbon fibers. These simulations were added for the reason to have all the variation from maximum damage to minimum damage. Also, after the initial simulations

it was noted that more simulations should be tried around the mean angle of 55˚ and therefore 4 new winding angles were added. Table 5.7 and Table 5.8 give the values for all the selected factors for glass/epoxy and carbon/epoxy pipes respectively.

Table 5.7: DOE table for the GFRP pipes

Thickness	Number of Layers	Winding Angles
0.25	20	35
0.3	24	45
0.35	28	50
0.375	32	52.5
0.4	36	55
0.425	40	57.5
		60
		65
		75

Table 5.8: DOE table for the CFRP pipes

Thickness	Number of Layers	Winding Angles
0.25	16	35
0.3	20	45
0.35	24	50
0.375	28	52.5
0.4	32	55
0.425	36	57.5
		60
		65
		75

The load and the boundary conditions are applied as described in the numerical model earlier. The impact energy of 40 J was applied using an initial velocity given to the

striker. In total, 162 different combinations were simulated for each glass and carbon fiber based composite pipes. The results are tabulated in the appendix A from Table A. 15 to Table A. 30. In total, 162 simulations were performed for each carbon and glass based composite pipes.

5.3.1 Effects of Fiber Material

Two types of materials carbon and glass are used as fiber reinforcement for the composite pipes. It is clear from the material properties tables Table 3.9 to Table 3.14 presented earlier that the carbon fiber is much stronger than the glass fiber and also the fracture energies are higher for the carbon. For this reason, it can be argued that the CFRP pipes will perform better under impact loads than GFRP and indeed this is the case if we look at the results presented in the Table A. 15 to Table A. 30. For the same geometric conditions, the amount of absorbed energy in the CFRP pipes is lower than that of GFRP pipes.

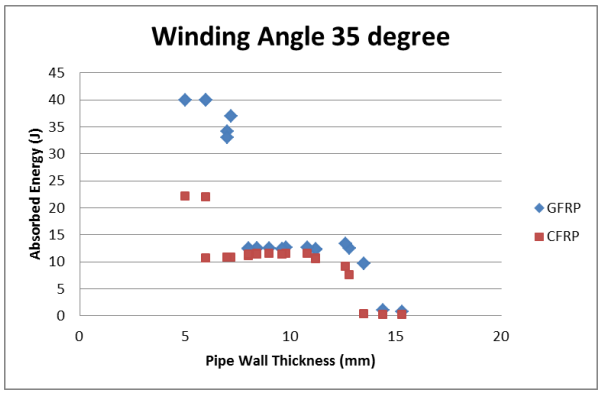

Figure 5.24: Absorbed energies for the CFRP and GFRP pipes for 35˚ winding angle

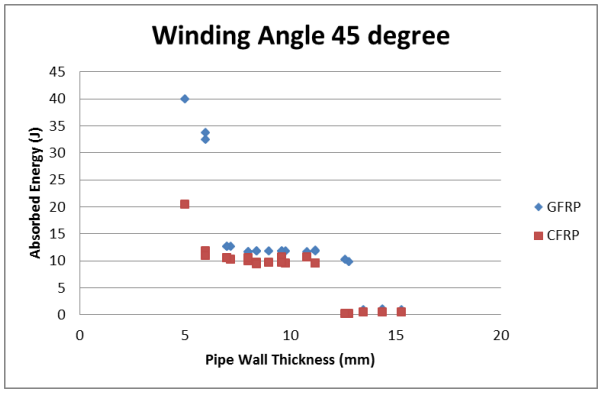

Figure 5.25: Absorbed energies for the CFRP and GFRP pipes for 45˚ winding angle

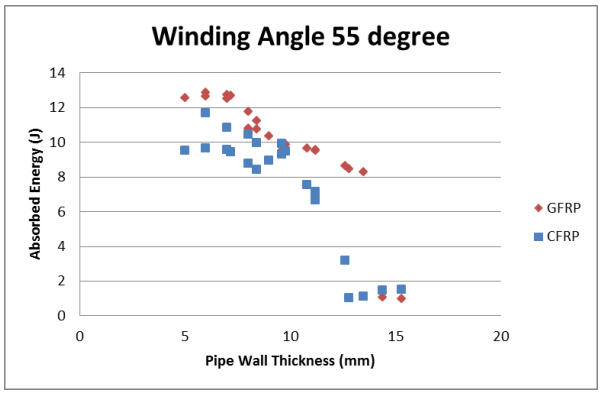

Figure 5.26: Absorbed energies for the CFRP and GFRP pipes for 55˚ winding angle

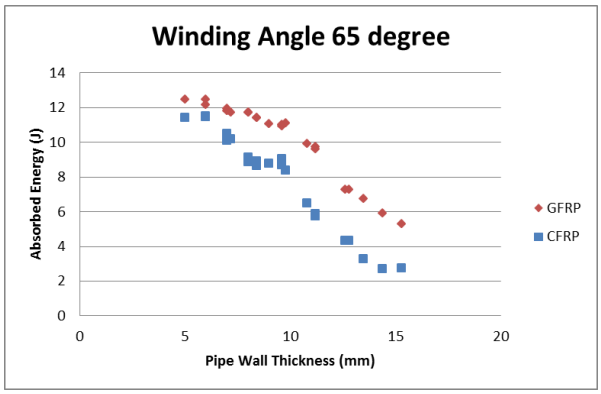

Figure 5.27: Absorbed energies for the CFRP and GFRP pipes for 65˚ winding angle

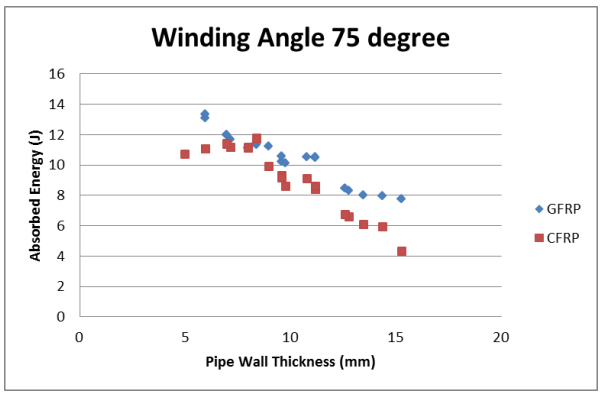

Figure 5.28: Absorbed energies for the CFRP and GFRP pipes for 75˚ winding angle

From the scatter plots of the two types of material presented in the figures from Figure 5.24 to Figure 5.28, the observation that the carbon/epoxy pipes will perform better than the glass/epoxy pipes is correct. From these plots, it can also be observed that the difference in the amount of damage, which is the absorbed energy, is very high in thin walled pipes. But, in the moderately thick walled pipes, although the carbon pipes perform better but the difference is reduced. But, in very thick pipes, again the difference becomes quite significant.

5.3.2 Effects of Thickness

The increase in the overall wall thickness of pipe is assumed to be significant by virtue of the results previously observed in the sensitivity analysis approach and also the results from the analysis of flat plates demonstrated the same phenomenon. Figure 5.29 to Figure 5.38 shows the variation in the amount of absorbed energies for both the GFRP and CFRP pipes vs. thickness. It can be observed from these plots that there is a range of thickness values for all the winding angles and for both material types, during which the increasing thickness doesn't improve the impact performance. The same phenomenon

was observed by Zhao et al. [73] in their study, they noticed that the damage threshold velocity was not affected by the increase in the thickness of the plates. They further reported that although the damage is almost unaffected but the damaged area reduced with the increase in the thickness of the plates. The same results can be deduced for this range of thickness values where there is no improvement in the impact resistance of the pipes. But, we do observe that after crossing this thickness range a sudden drop in the amount of absorbed energy which is not reported in the study of Zhao et al. as they studied only three cases for the thickness variations.

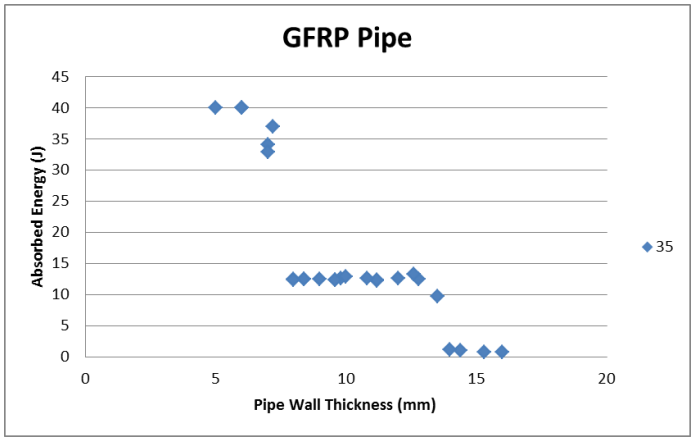

Figure 5.29: Variation of absorbed energy vs. thickness of the plate for 35˚ winding angle GFRP pipes

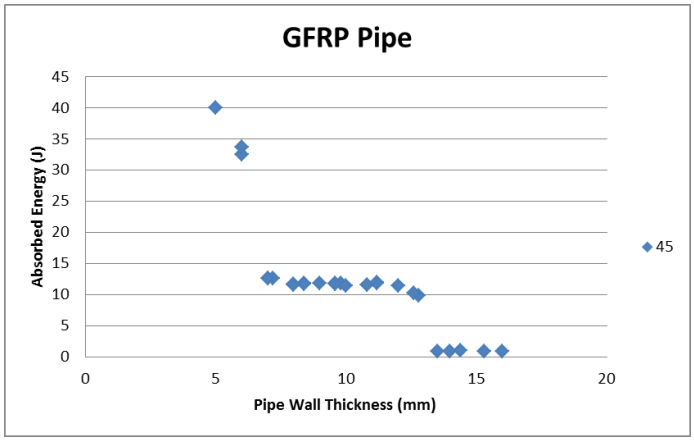

Figure 5.30: Variation of absorbed energy vs. thickness of the plate for 45˚ winding angle GFRP pipes

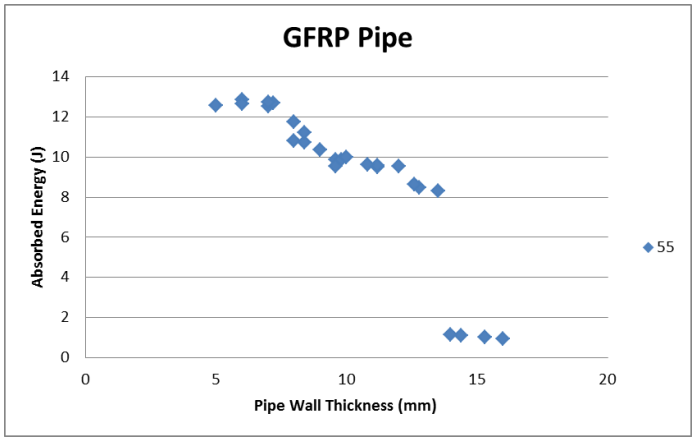

Figure 5.31: Variation of absorbed energy vs. thickness of the plate for 55˚ winding angle GFRP pipes

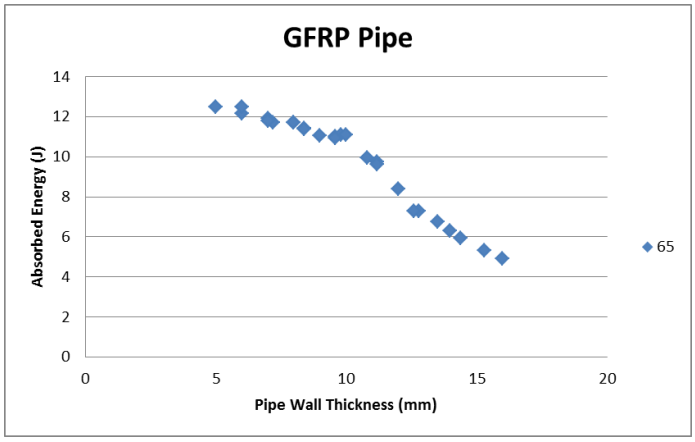

Figure 5.32: Variation of absorbed energy vs. thickness of the plate for 65˚ winding angle GFRP pipes

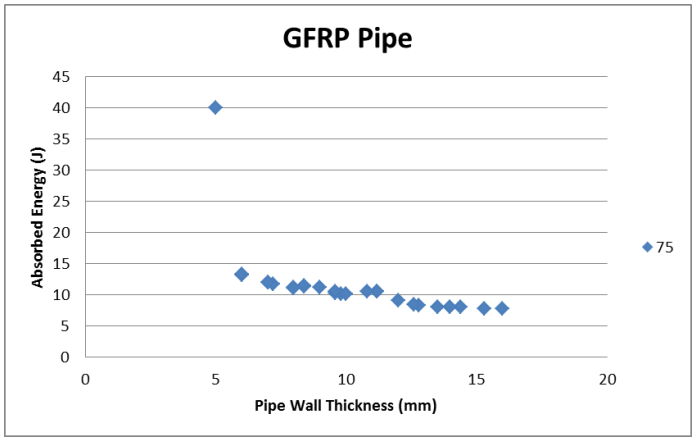

Figure 5.33: Variation of absorbed energy vs. thickness of the plate for 75˚ winding angle GFRP pipes

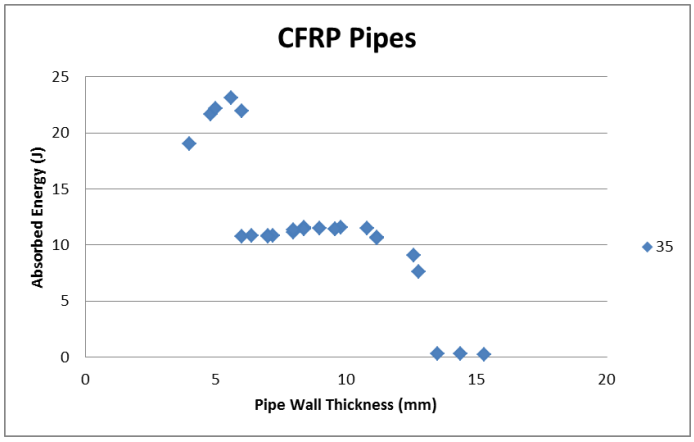

Figure 5.34: Variation of absorbed energy vs. thickness of the plate for 35˚ winding angle CFRP pipes

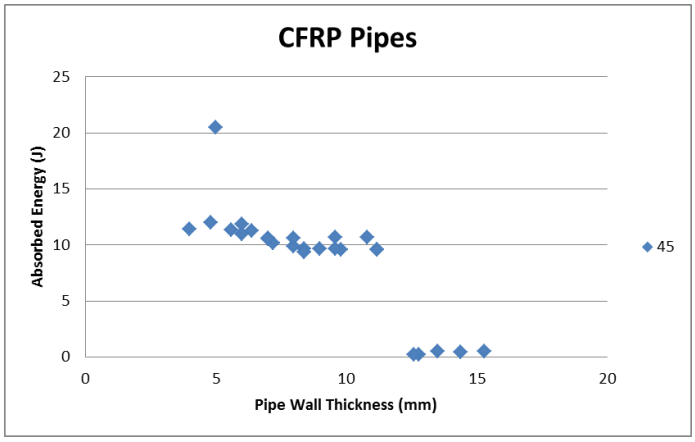

Figure 5.35: Variation of absorbed energy vs. thickness of the plate for 45˚ winding angle CFRP pipes

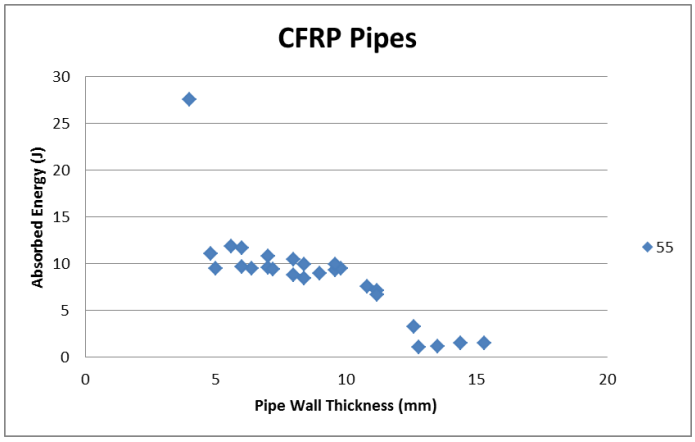

Figure 5.36: Variation of absorbed energy vs. thickness of the plate for 55˚ winding angle CFRP pipes

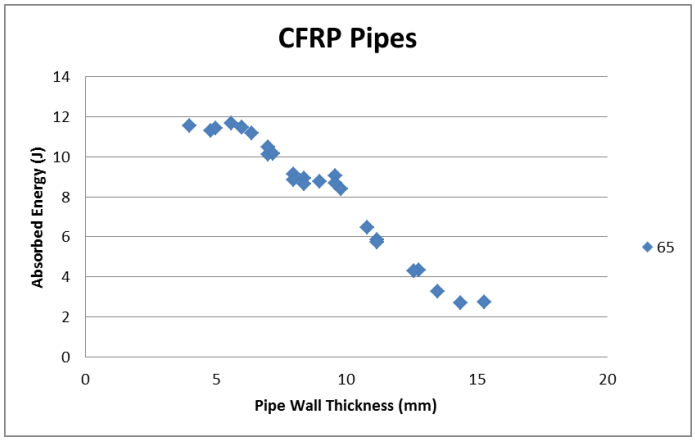

Figure 5.37: Variation of absorbed energy vs. thickness of the plate for 65˚ winding angle CFRP pipes

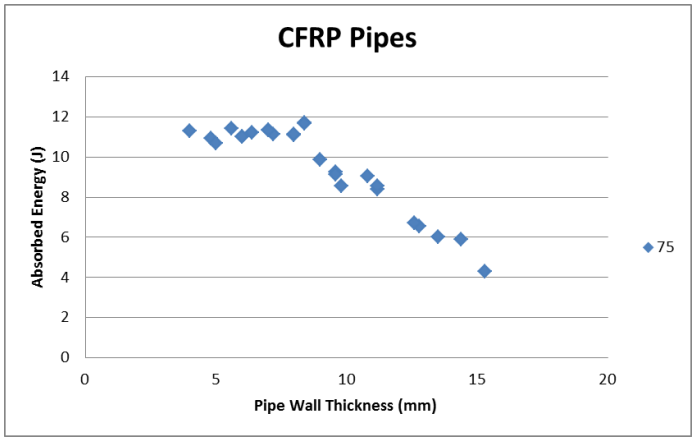

Figure 5.38: Variation of absorbed energy vs. thickness of the plate for 75˚ winding angle CFRP pipes

In all of these cases where the increase in thickness doesn't improve the impact resistance, it was observed that the vibration in the pipe increased. This as explained earlier for the case of flat plates, where we observed an increase in the amount of absorbed energy is due to the fact that the overall stiffness of the structure increases with increase in the thickness but not sufficient enough. Hence, we observe vibrations which is the cause of more absorbed energy as explained by Krishnamurthy et al. [36] in their research that the energy absorbed upon impact is the sum of the strain energy and the kinetic energy of each of the modes of vibration.

5.3.3 Effects of Winding Angle

The choice of the variation of the winding angle depended upon the study by Rosenow [59]. Based on the conclusions provided by Rosenow, we selected 5 different winding angles from 35˚ to 75˚ with an interval of 10˚. The results show that the pipes with winding angles of 35˚ and 75˚ are particularly worse than the rest in handling the impact loads. The results are represented in the Figure 5.39 and Figure 5.40 it is observed

that in most of the cases the pipes with winding angle of 55˚ have the least absorbed energy and better impact resistance.

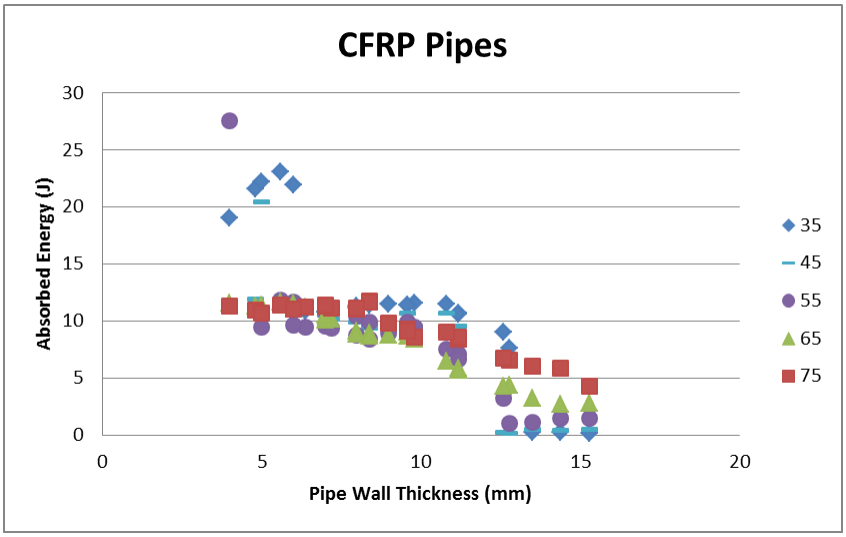

Figure 5.39: Comparison of absorbed energy for different winding angles of CFRP pipes

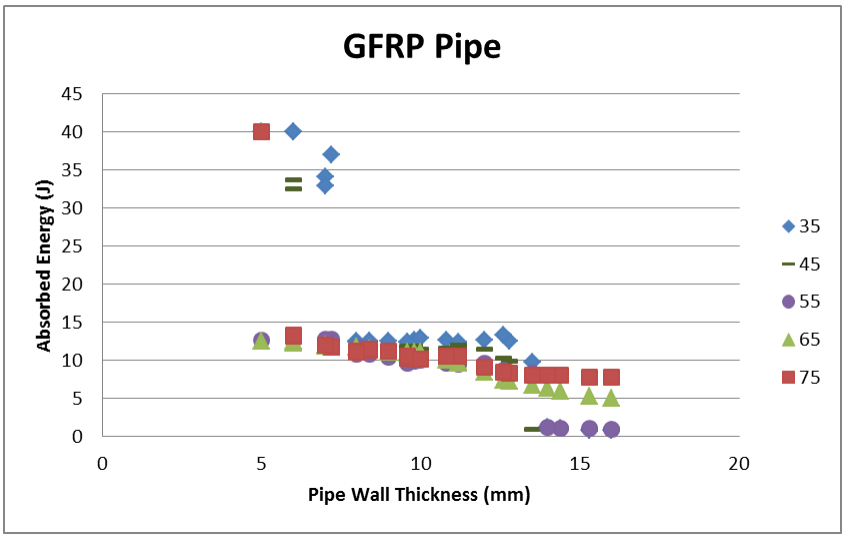

Figure 5.40: Comparison of absorbed energy for different winding angles of GFRP pipes

From the above graphs, it is clear that for most of the pipe thickness irrespective of the fiber material, the orientation of 55˚ performs better. In some cases, 45˚ and 65˚ winding angles were slightly better. In order to further examine, a further cases were simulated with angles ranging from 50˚, 52.5˚, 57.5˚ and 60˚.

Close observation of these figures and the relevant tables in the appendix show that for glass fiber pipes, there is not much of a difference in terms of absorbed energy for smaller thickness pipes. However, when the thickness is increased the 55˚ winding angle pipes were better in performance compared to the rest. The observation is reversed for the carbon based pipes where at smaller thickness 55˚ were slightly better and increasing thickness results in slightly worse performance but the difference is not that much.

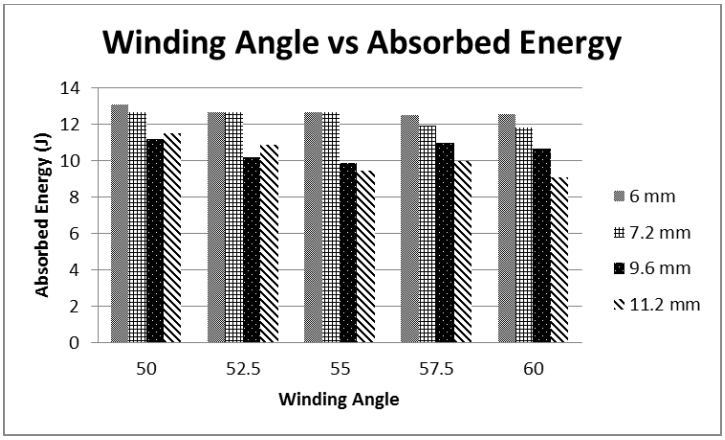

Figure 5.41: Bar Graph representing variation of Absorbed Energy w.r.t. to winding angle for GFRP pipes

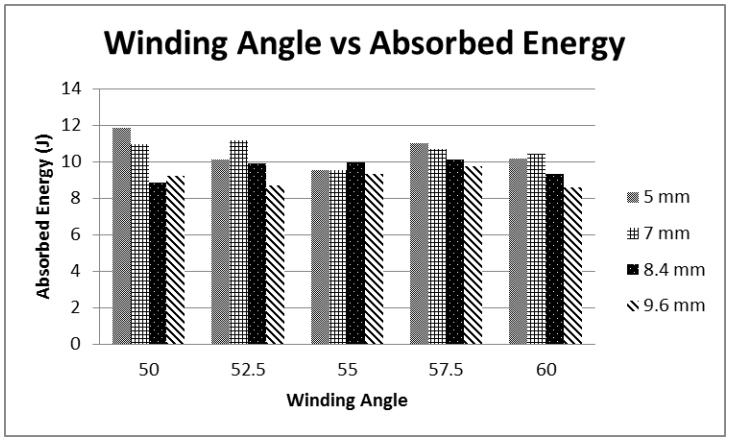

Figure 5.42: Bar Graph representing variation of Absorbed Energy w.r.t. to winding angle for CFRP pipes

The reason for the better performance of 55˚ winding angle pipes is that the impact force tries to bend the pipe near the impact point, hence winding angles of 55˚ which is reported to perform better when loaded with both hoop stress and axial stress performs better in the case of impact loads as well. The slight difference can be attributed to other reasons such as the number of layers, thickness of the wall or the boundary conditions.

The fiber orientation in the 55˚ winding angles is better in terms of performance because it can carry both axial and hoop stresses effectively as stated earlier and during impact, the bending due to the loads creates stress in both the longitudinal and circumferential directions. Hence, 55˚ winding angle is preferred. If we base further analysis on this assumption, it can be inferred that the winding angles of 35˚ or even less are since more aligned with the longitudinal axis of the pipe can withstand more longitudinal or axial stresses but will be weaker in the circumferential direction. On the other hand 75˚ winding angles are more close to the hoop winding which is known to

handle internal pressure and hoop stresses will perform better in the loadings that put the pipe under circumferential stresses but will fail in the axial loadings.

5.3.4 Effects of Layer Thickness and Number of Layers

It is reported in the work of Zhao et al. [73] that the stacking sequence has some major influence on the impact performance of the curved shells. It is reported in their work that the damage is reduced with the increase in the interface number in the laminated shells. The interface number can be understood as the number of time the fiber orientations are changed within a laminate. For example, in a laminate where [45/-45/0/90] is the stacking of layers, we have 4 interface changes while in a laminate where $[45_2/-45_2/0_2/90_2]$ is the stacking of layers the interface number is still 4 in spite of the fact that the number of layers are twice that of the earlier sample.

The above result suggests that in the pipes where the individual layers have less thickness and to achieve the overall thickness of the pipe numbers of layers are increased will be better than the other way round. The simulations we performed however, suggested that the increase in number of layers keeping the overall thickness constant has little effect on the amount of absorbed energy or in some cases it has adverse effect. This can be observed in the graphs of Figure 5.43 to Figure 5.52. Here, the results are not always in the favor of more layers. This can be due to a fact that the results described in the study of Zhao et al. [73] is for curved shell and the current study is for pipes, therefore, the geometry and the boundary changes may affect the influence of number of layers differently than for flat plates or curved plates.

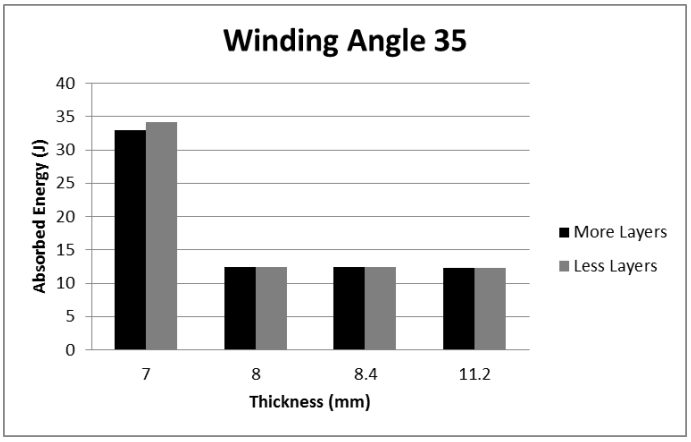

Figure 5.43: Comparison of absorbed energy in equal thickness plates with varying number of layers for 35˚ GFRP pipes

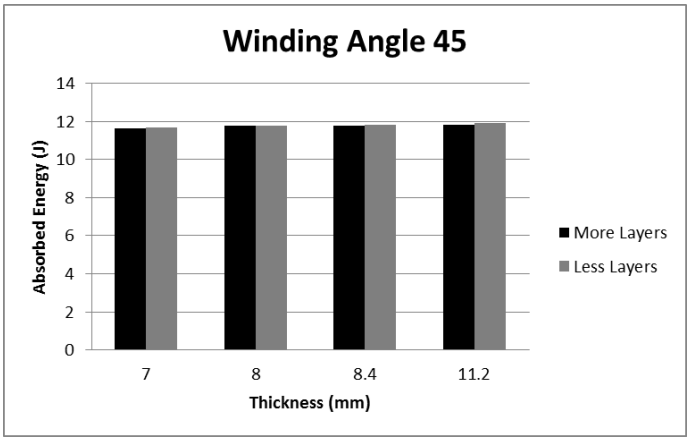

Figure 5.44: Comparison of absorbed energy in equal thickness plates with varying number of layers for 45˚ GFRP pipes

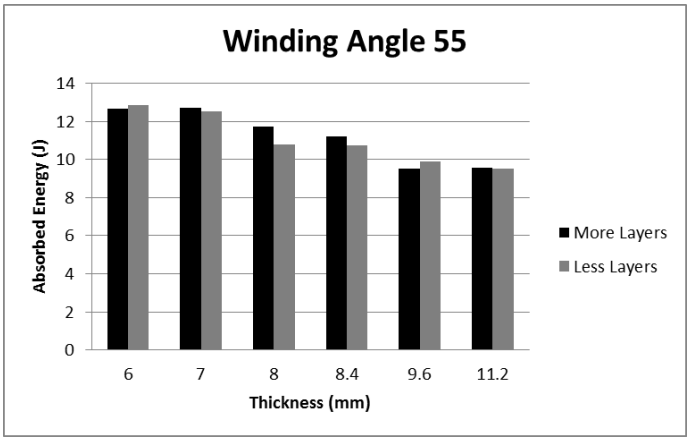

Figure 5.45: Comparison of absorbed energy in equal thickness plates with varying number of layers for 55˚ GFRP pipes

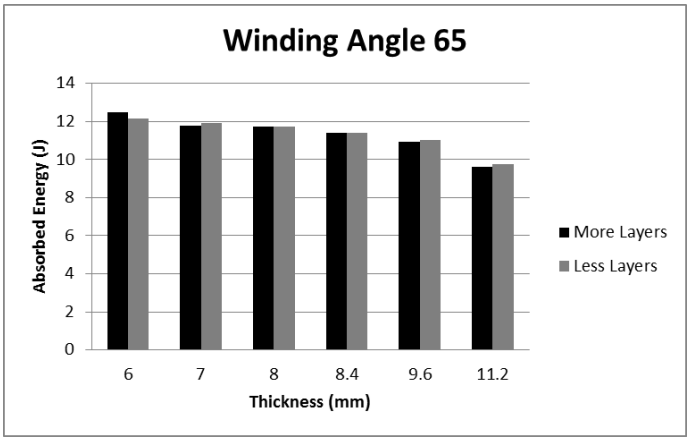

Figure 5.46: Comparison of absorbed energy in equal thickness plates with varying number of layers for 65˚ GFRP pipes

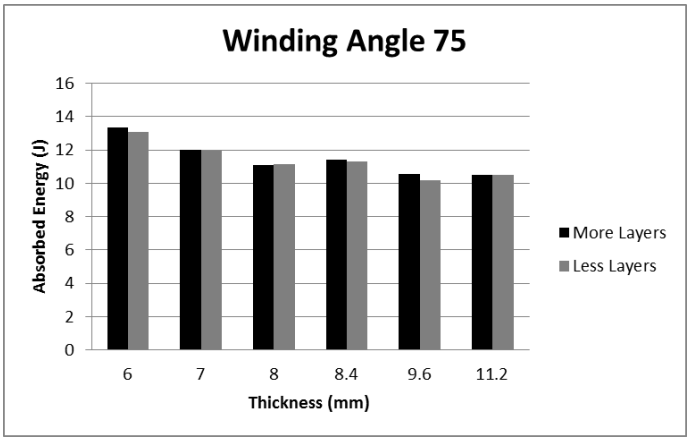

Figure 5.47: Comparison of absorbed energy in equal thickness plates with varying number of layers for 75˚ GFRP pipes

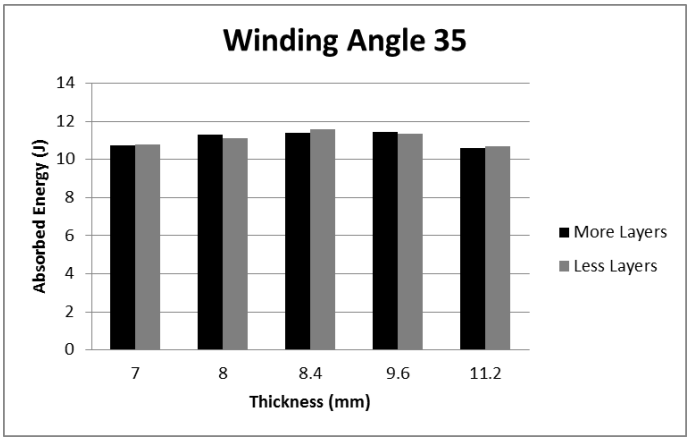

Figure 5.48: Comparison of absorbed energy in equal thickness plates with varying number of layers for 35˚ CFRP pipes

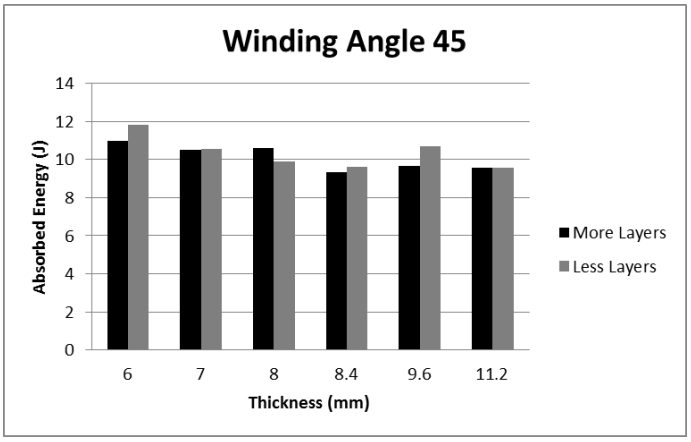

Figure 5.49: Comparison of absorbed energy in equal thickness plates with varying number of layers for 45˚ CFRP pipes

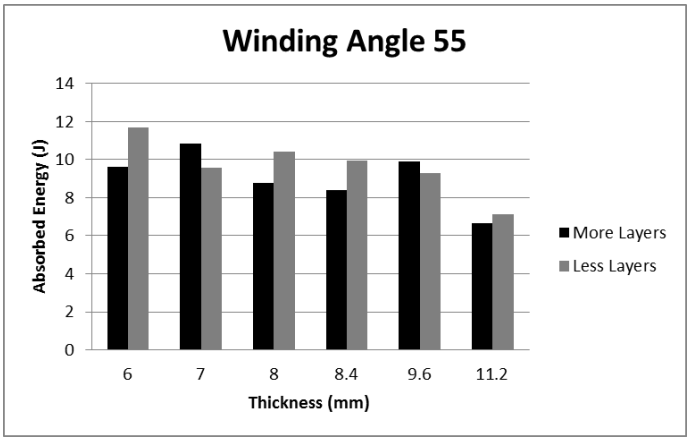

Figure 5.50: Comparison of absorbed energy in equal thickness plates with varying number of layers for 55˚ CFRP pipes

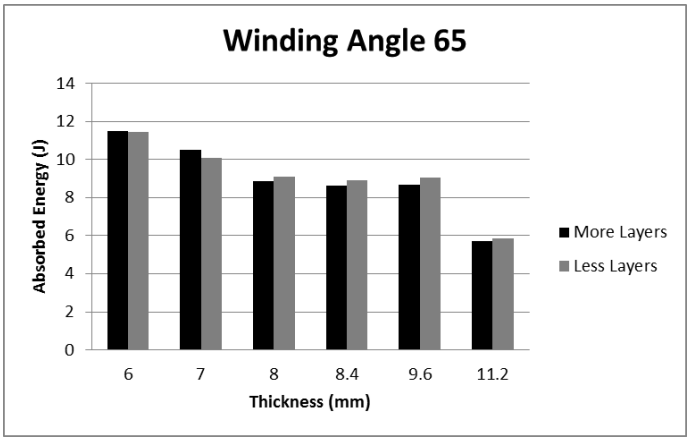

Figure 5.51: Comparison of absorbed energy in equal thickness plates with varying number of layers for 65˚ CFRP pipes

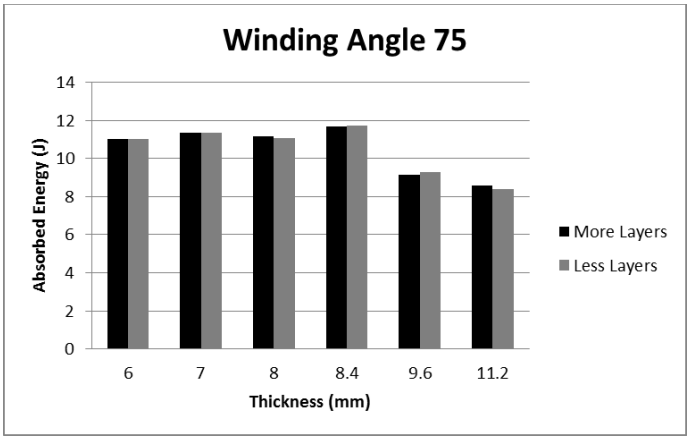

Figure 5.52: Comparison of absorbed energy in equal thickness plates with varying number of layers for 75˚ CFRP pipes

5.4 INCLUSION OF EMBEDDING

From the study so far, it is understood that the tensile strength of the fiber and the fracture energies of the fiber materials are one of the important contributors. In order to improve the performance of the composite plates and pipes, it is therefore advisable to

use materials such as carbon or graphite which have higher tensile strengths and fracture energies. But, the cost factor is also important since the idea is to design such that the performance is optimal with respect to the minimum costs.

To achieve better impact resistance at a lower cost is the main aim. We know that the glass/epoxy systems are less expensive compared to carbon/epoxy. In this section, we will discuss the kinds of materials included and their placement in the glass/epoxy plates and pipes to enhance the overall impact performance of the structures.

5.4.1 Embedding Type

For the composite flat plates, the main fiber material is chosen to be glass with addition of carbon fibers. Since, the flat plates are manufactured using the woven fabric only the carbon/epoxy woven fabric was used along with the glass/epoxy fabric. From the material properties tables listed in Chapter 3, it is known that the carbon/epoxy laminas are much stronger than the glass/epoxy. Also, from the simulations run for both type of materials and the results listed in the tables in the Appendix A confirmed that the carbon/epoxy plates perform much better than the glass/epoxy. Therefore, some layers from the composite plate were replaced by carbon fibers. The studies prior to this one already concluded that for the case considered in this thesis for composite plates, the best stacking sequence will be number 4, i.e., [60/45/-45/-60], which were used in order to study the effects of inclusion of other fiber materials. The other conditions of the load and the boundary conditions and the impactor remain the same as in the study for the composite plates.

Similarly, for pipes the results already studied were utilized to enhance the impact resistance of the composite pipes made using glass fiber filament winding by the addition of other materials in the winding process. Usually, the pipes are manufactured using continuous filament winding of one type of fiber material impregnated with the epoxy resin but it is not impossible to break the fibers after completion of layers and then include other fibers with the same epoxy resin to improve the performance. Infact, it is a common practice in the aerospace industry to manufacture composite rocket motor casings with different winding angles and different kinds of fibers to achieve the desired design criteria which is mostly dependent upon multi-loads situation to be encountered during service. For the composite pipes, it was observed that the pipes with carbon fiber offer quite an advantage over the pipes with glass fiber. But for both the types of material the best winding angle was the same as 55˚. Also, inclusion of a layer of woven fabric can be studied as it can be beneficial considering the woven fabric has better strength characteristic in both the directions compared to the unidirectional lamina. Therefore, for this study inclusion of unidirectional carbon/epoxy and woven carbon/epoxy layers in the glass/epoxy composite pipes have been studied. For the study, the loads and the boundary conditions are kept the same as in the previous studies and as stated earlier in Chapter 3.

5.4.2 Effects of Placement of Embedding

The inclusion of other materials alone cannot guarantee an increase in the performance of the structure, the placement of the embedding is also necessary. Since, the material to be included is based on the superior strength and better performance, it should be placed where the damage initiates. To understand the relation between the placement of the inclusions and the impact performance, different placements were tried

for the carbon layers in the composite plate that mainly consisted of glass fibers. Following different combinations were tried with the position of woven carbon lamina as:

1) Top and Bottom layers
2) Middle 2 layers
3) Top 2 layers
4) Bottom 2 layers
5) Single top and bottom layers and 2 middle layers
6) Single Top and Middle layers

In addition to different positions, different thickness of the carbon layers and glass layers were considered. As described earlier, the stacking sequence considered is number 4 i.e., [60/45/-45/-60].

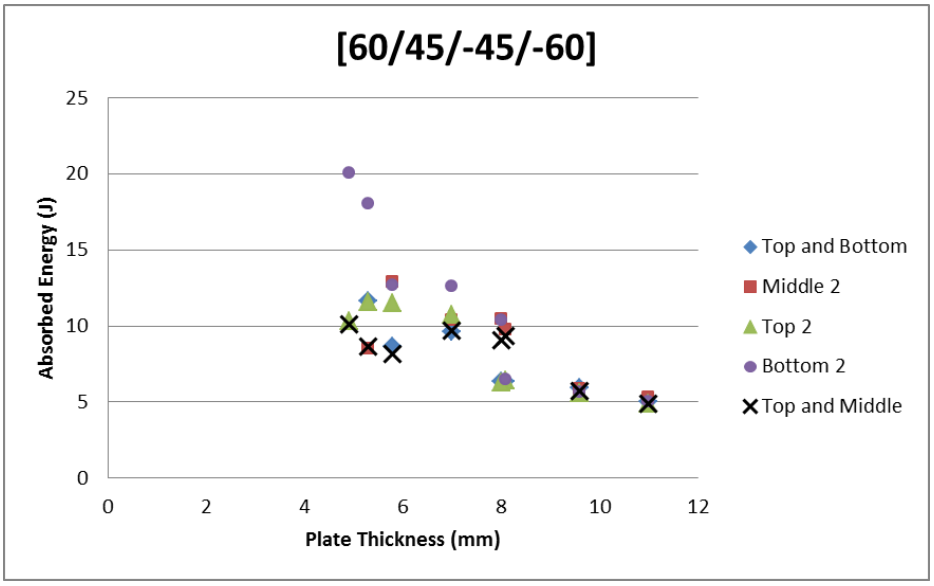

Figure 5.53: Comparison of the amount of absorbed energy in all the combinations tried

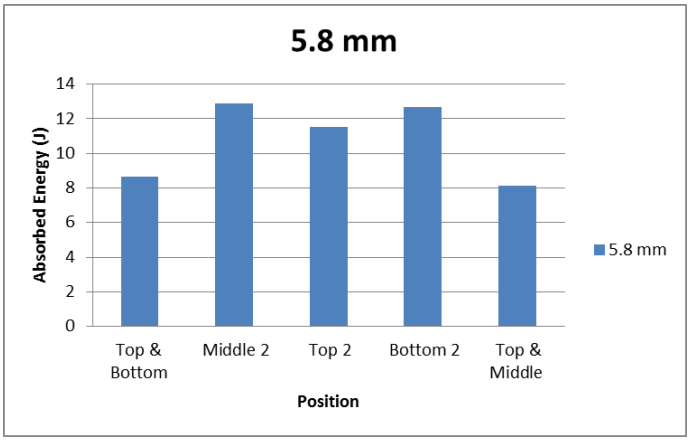

Figure 5.54: Comparison of the effect of position of the carbon layer for 5.8 mm plate

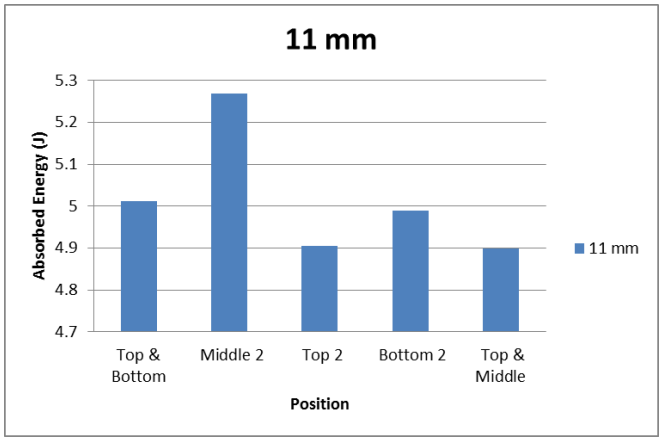

Figure 5.55: Comparison of the effect of position of the carbon layer for 11 mm plate

The results for these simulations are tabulated in the Appendix A. Table A. 9 to Table A. 14 and the graphical representation is provided in the figures Figure 5.53 to Figure 5.55. From the results, it is evident that the greatest effect of the inclusion and placement of the carbon layers is when the overall plate thickness is small. Once, the plate thickness is increased most of the load bearing capacity is taken by the glass fiber layers and hence we can't measure the effectiveness. In the low thickness plates, the placement of the carbon fiber layers is thus important and it is observed that the most

efficient placement is when we place one carbon layer at the top and one in the middle. The top 2 layers of carbon perform slightly worse but this can be attributed to the fact that the first layer is 60˚ while the second one was only 45˚ compared to the case where one top and one middle layers are replaced both of them being the 60˚ layers. Another important result to be noticed that the increase in the absorbed energy observed for the glass/epoxy systems Figure 5.13 with the increase in thickness was negated quite a bit by the introduction of carbon/epoxy layers especially when these layers are replaced at the top only, top and middle and cases with top and bottom. Therefore, it can be deduced that the carbon layers introduction at the top and middle gives the better impact performance at a slightly higher cost.

Similar procedure was adopted to study the effect of carbon/epoxy layers, both woven and unidirectional layers, on the impact performance of the composite pipes. From the results presented earlier, it is inferred that the damage initiates at the top layer that is the closest layer to the impact point. Therefore, different layer combinations with woven fabric and unidirectional fibers were tried and the results are presented in the Appendix A. Table A. 31 to Table A. 34. The winding angle was kept at 55˚ as it was found out to be the optimal angle of winding against the impact loads.

The results suggest that the inclusion of top layers as the woven carbon fabric doesn't improve the impact performance. This is due to the reason that the most important strength factor in withstanding impact loads is the tensile strength and in this case the tensile strength of unidirectional glass fiber is slightly more than the woven carbon fabric. The inclusion of woven carbon fabric is thus not recommended as it will increase the costs without increasing the impact performance. On the other hand, the inclusion of

unidirectional carbon layers suggests that there is an advantage especially when top 4 layers were replaced. In the case of top 4 layers of carbon fibers, the impact performance is in fact better than the pure carbon based pipes. This is therefore highly recommended configuration considering less expensive with better resistance against impact loads. The results are graphically represented in Figure 5.56 and Figure 5.57.

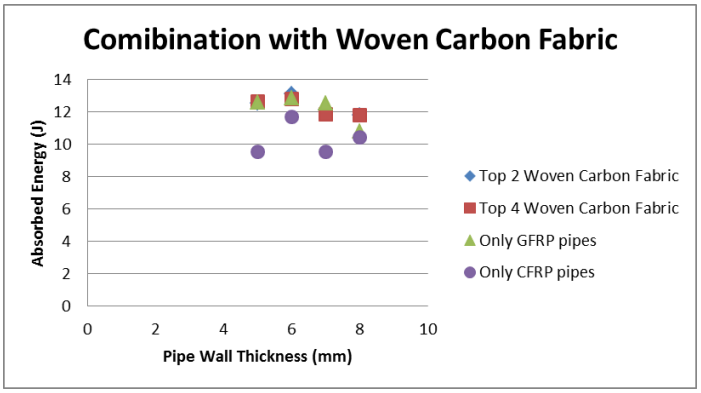

Figure 5.56: Comparison of different combinations of woven carbon fabric layers with GFRP and CFRP pipes of comparable configurations

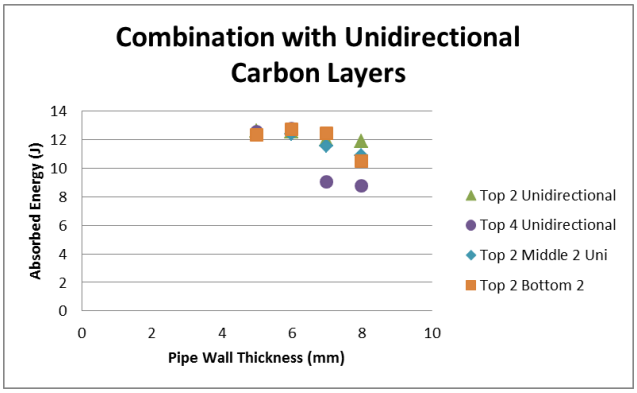

Figure 5.57: Comparison of absorbed energies in different configurations for the hybrid CFRP and GFRP pipes

5.5 CONCLUSIONS

This chapter includes the results and discussion for the simulations carried out in order to study the effects of various parameters upon the impact performance of the composite structures. These parameters were identified by the sensitivity analysis but their exact nature and the explanation of their behavior cannot be provided by the sensitivity analysis. The approach considered in this chapter was to design a set of experiments to be performed numerically. Simulations were performed using ABAQUS explicit for both flat plates and pipes. The design variables and their effects have been studied in detail. Few of these parameters have already been studied in the available literature and the results from the current work is studied and compared with the already available literature. The parameters studied in this chapter were selected after the sensitivity analysis and were selected such that they are directly related to the designing of the composite plates and pipes. Factors such as the impactor mass, geometry and the boundary conditions were kept constant as most of the times in real life applications these factors will be outside the control of the designer. The simulations were performed in two phases initially a complete DOE table was constructed but later on more variations of the factors were added to complete the analysis in a way that the complete range of variables is selected from being safe to complete penetration of the impactor. The main conclusions drawn from this chapter are summarized as follows:

- The most profound effect of all the variables was that of the thickness of the plates and the pipes. The crucial observation in the analysis of this factor is that the dependence of impact performance on the thickness of the structure is

not directly proportional. In fact, it was found that there was a range of thickness where actually the performance is worse than before. This observation is explained by the ability of the thin structures to withstand bending without undergoing vibrations. The increase in thickness increases the structural rigidity which in turn effects adversely due to the unnecessary induced vibrations upon impact.

- The stacking sequence of the composite plates has a significant role in the impact performance. Although not directly studied, this is due to the boundary conditions effect. It is suggested that during the design phase knowledge of the kind of boundary conditions is better. Hence, it is recommended that the more fiber should be aligned in the direction where the boundary conditions are such that they restraint the bending of the plate.
- The conclusion from the chapter 4 that the numbers of layers have an effect but they have to be chosen carefully is further explained based on the orientation of the added layers. It is important to have as more as possible fibers in the direction of the maximum stress during the impact to delay the damage initiation process.
- The material properties which have a significant effect on the impact resistance of any composite structures are the tensile strength of the fiber and the energy release rates during damage propagation. Care must be taken in the selection of material and designing of the composite structures as to maximum utilize the tensile strength of the fibers.

- The improvement in the impact resistance of the composite plates without increasing costs by much can be achieved through the introduction of carbon/epoxy layers in place of glass/epoxy layers. These layers of carbon/epoxy should be introduced in places where the damage initiates. Also, the layers to be replaced should be selected carefully keeping in mind that those layers should be replaced that increases the bending stiffness of the plate.
- The best stacking sequence or the orientation angles of the layers is the one that aligns more fibers in the direction of maximum stress caused due to the presence of boundary condition effects.
- The inclusion of woven fabric in the filament wound composite pipes can be beneficial if the woven fabric selected has a higher tensile strength than the unidirectional glass or carbon fibers.

CHAPTER 6

OPTIMIZATION OF DESIGN PARAMETERS

The optimization of the impact resistance of the composite plates and pipes against low velocity impact loads is important in terms of a number of advantages. Optimized solutions are lighter in terms of weight hence saving materials and resulting in low cost efficient products. Generally, optimization is performed on a selected function commonly termed as the cost function which is the function of several variables. The cost function, if properly defined, can be used with a variety of techniques of optimization. The basic optimization idea is to minimize or maximize this cost function by choosing the input variables in such manner that it forms the best possible solution among a set of possible solutions. The history of optimization dates back to the first known optimization technique of Steepest Descent pioneered by Gauss. With the advent of last century the available techniques are more refined and now find themselves being employed in a multitude of scientific and technological fields. Mathematically, we can represent the problem as:

$$\text{Optimize } y = f\left(x_1, x_2, ..., x_n\right) \tag{6.1}$$

$$\text{Subject to } g_j\left(x_1, x_2, ..., x_n\right)\begin{Bmatrix}\leq\\=\\\geq\end{Bmatrix} b_j \quad j = 1, 2, ..., m \tag{6.2}$$

6.1 OPTIMIZATION PROBLEM

In our problem, the cost function represented in Eq. (6.1) by 'y' is the amount of absorbed energy and the cost of the plate or the pipe. The dependent variables x_1, x_2 etc. are the layer thickness, orientation angles or stacking sequence, number of layers and the material type. We have two objectives to minimize simultaneously which makes the problem as multi-objective optimization, but the objectives here are not contradictory, therefore, can be combined in one single function.

There are a number of optimization techniques available as described in the literature review section. Any optimization technique is based upon the cost function, which in our case is not defined analytically. To get the cost function, we have to use models like linear regression model or any other similar techniques. Because the data is not well structured and has a lot of variations from point to point, regression models were unable to predict the empirical mathematical equation. To obtain a function that can predict the amount of absorbed energy which will then be used as the cost function, artificial neural networks were utilized. The ANN model available with the commercially available software MATLAB®, the ANN model can be used for function fitting of highly non-linear data. This technique was then used and optimized to get the best possible model that can predict the amount of absorbed energy.

6.2 ARTIFICIAL NEURAL NETWORKS

Artificial Neural Network (ANN) or sometimes called Neural Network is an interconnected group of artificial neurons that uses a mathematical model or computational model for information processing based on a connectionist approach to computation. It is an adaptive system whose structure is modifiable based on the external or internal information that flows through the network. The name is given because of its ability to learn like human brain by examples. This technique is useful in pattern recognition, model fitting or data classification. Once trained; ANN can be used to predict the outcome of new independent data different from the training set. The ability of ANN model to learn by example highly non-linear and noisy data is useful in our approach where we are dealing with statistical data. This feature is very useful in our problem where a mathematical relationship of the factors considered by sensitivity analysis with the absorbed impact energy is not available but with the help of FEA simulations a lot of training data is available to us.

A neural network is a set of connected neurons, these neurons receive impulses from either input cells or other neurons and apply a function and transmit the output to other neurons or the final output cells. The neural networks can be multi-layered in which case one layer receives information from the preceding layer of neurons and passes the output to the subsequent layers.

A neuron is a real function of the input vector (y1, y2, … , yk). The output is a function described as:

$$f(x_j) = f\left(\alpha_j + \sum_{i=1}^{k} w_{ij} y_j\right) \tag{6.3}$$

Where, f is a typically a function as sigmoid (log or tanh) function. A graphical representation of neuron is

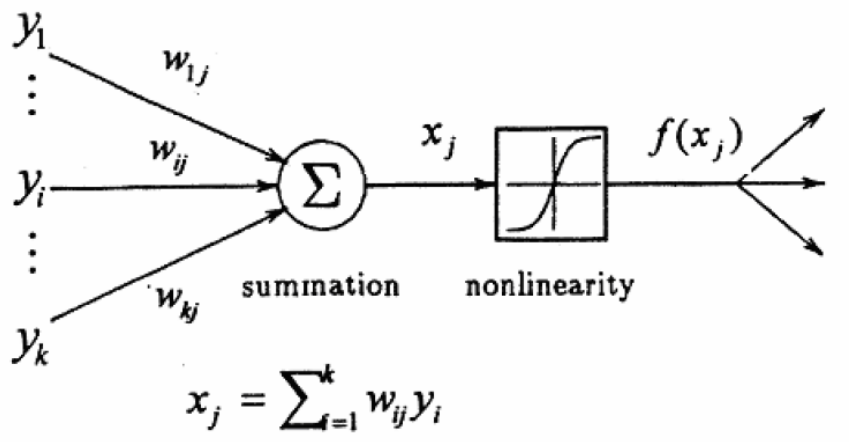

Figure 6.1: A single neuron

6.2.1 Feed Forward Networks

A feed forward network works in the forward direction i.e. the flow of information is in only one direction along the connections from the input layer through the hidden layers of neurons to the final output layer. There is no feedback loop in these networks and hence the output does not affect the performance of the previous layers or the same layer.

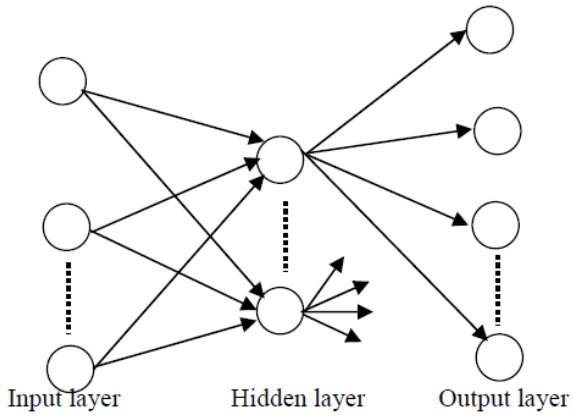

Figure 6.2: A multi-layered feed forward neural network

6.2.2 ANN Model for Flat Plates

Two separate ANN models were generated for the carbon/epoxy and the glass/epoxy plates. In total we had 108 different simulation data for each type of material.

Data set available for training ANN in this study is 108 samples, few iterations of ANN models were tried coupled with a differential evolution algorithm for the optimization of the ANN model in terms of the number of neurons and the hidden layers. The data set was randomly distributed in three sets, for the training, testing and validation of the model. The training was carried out by randomly selecting 94 data points and the rest were divided equally for the testing and validation.

The optimization algorithm of differential evolution was used to find the best ANN model, an objective function was defined which computes the maximum error from one ANN model at a time which was based on the number of neurons. This optimization of the ANN model was necessary to find the best possible configuration of ANN models which depend upon the number of hidden layers and neurons. The ANN model

configuration thus obtained was then train to predict the amount of absorbed energy for the composite plates. Two separate models were used to predict the behavior of composite plates based on carbon or glass fibers.

The carbon/epoxy composite plates' impact behavior was well defined compared to the glass/epoxy composite plates. It is noted that the more the data follows a pattern, the better the correlation will be, as the ANN model described earlier uses the target response to calculate the weights of each neurons. The model for carbon/epoxy plates needed only 21 neurons and a single hidden layer containing all the neurons. The model is generally supposed to predict the behavior accurately when the absolute error between the predicted and the targeted values is at least 2 orders less in magnitude.

The ANN model for carbon/epoxy system has a root mean square error of just 0.08 J with the maximum error of 0.6242 J.

Table 6.1: Testing ANN for 21 neurons for CFRP plates

Input1 (thickness mm)	Input2 (Number of Layers)	Input3 (Stacking Sequence)	Actual response (Abaqus) J	Simulated Response (ANN) J	Difference
0.3	20	1	5.9155	6.105	-0.1895
0.25	16	1	6.7855	6.8955	-0.11
0.25	20	3	5.7807	5.6217	0.159
0.35	28	1	2.7507	2.5044	0.2463
0.16	16	3	7.5475	7.3142	0.2333
0.3	16	1	6.5986	6.4669	0.1317
0.25	20	1	7.074	7.0582	0.0158
0.18	16	1	7.7121	8.0439	-0.3318
0.25	28	1	5.7693	5.7452	0.0241
0.18	16	4	7.1083	7.08	0.0283
0.4	28	3	1.2529	1.3213	-0.0684
0.4	32	1	0.2346	0.0313	0.2033
0.2	24	4	4.631	4.7639	-0.1329
0.25	20	2	5.3035	5.3961	-0.0926

A separate verification was carried out with simulations from ABAQUS and the ANN model for the cases presented in Table 6.2. The verification gives the further confidence in the ANN model and its use in generating the population for the optimization process. Figure 6.3 shows the correlation between the target and the predicted response while Figure 6.4 represents the difference between the actual and the predicted response.

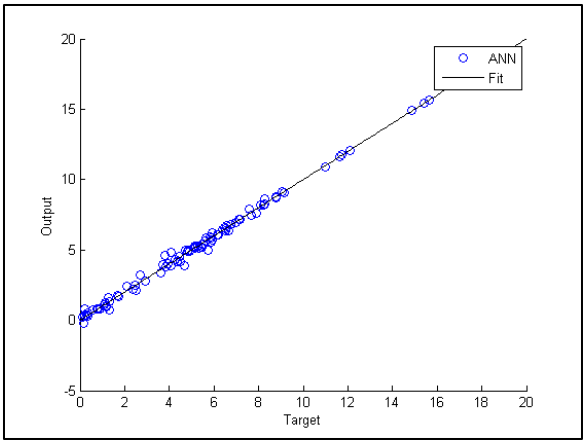

Figure 6.3: Correlation between the predicted and the target response for CFRP plates

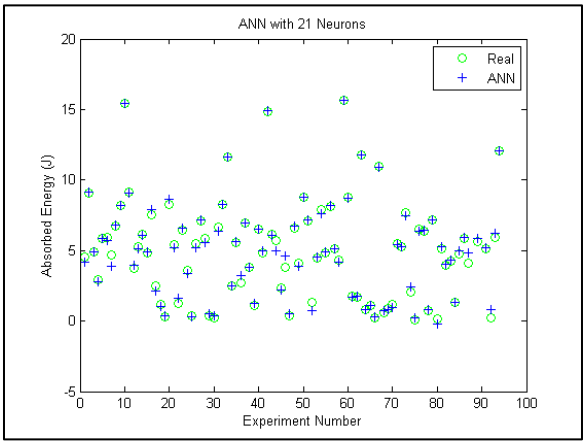

Figure 6.4: Actual response and the predicted response for CFRP plates

Table 6.2: Independent test cases to verify ANN model

Input1 (thickness mm)	**Input2 (No. of Layers)**	**Input3 (Stacking Sequence)**	**Actual response (Abaqus) J**	**Simulated Response (ANN) J**	**Difference**
0.24	24	1	5.9006	5.9836	-0.083
0.16	30	4	4.6322	5.0069	-0.3747
0.22	26	2	4.6903	4.9347	-0.2444
0.14	18	3	7.7589	8.5684	-0.8095
0.36	32	2	0.5093	0.6132	-0.1039

A similar ANN model was trained to predict the glass/epoxy composite plates. The ANN model for glass fiber plates uses 24 neurons in a single layer and is able to predict the amount of absorbed energy with maximum error of 1.1047 J and root mean square error of 0.33 J.

Table 6.3: Testing ANN for 24 neurons for GFRP plates

Input1 (thickness mm)	**Input2 (Number of Layers)**	**Input3 (Stacking Sequence)**	**Actual response (Abaqus) J**	**Simulated Response (ANN) J**	**Difference**
0.6	28	1	1.6022	1.6531	-0.0509
0.25	32	3	14.8979	14.9839	-0.086
0.4	28	3	11.1732	11.0837	0.0895
0.25	32	1	13.8011	12.9575	0.8436
0.45	36	4	2.5115	2.4935	0.018
0.35	36	3	8.6502	8.2851	0.3651
0.4	36	1	8.5923	8.8273	-0.235
0.4	28	2	14.9456	14.0875	0.8581
0.35	32	4	5.187	5.7195	-0.5325
0.45	32	3	8.2871	8.5516	-0.2645
0.5	36	2	0.7561	0.7411	0.015
0.3	24	1	12.686	12.8399	-0.1539
0.25	36	4	6.3016	5.7934	0.5082
0.35	24	4	11.046	11.6601	-0.6141

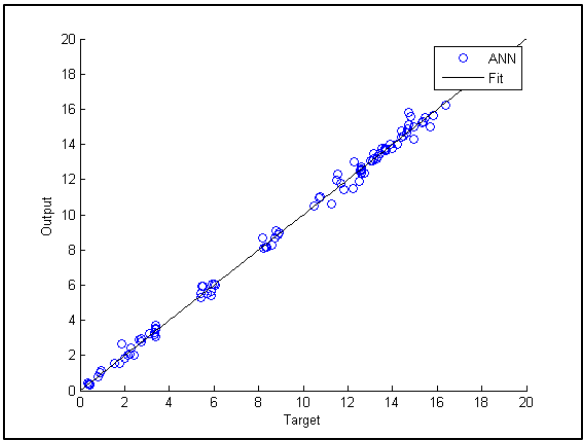

Figure 6.5: Correlation between the predicted and the target response for GFRP plates

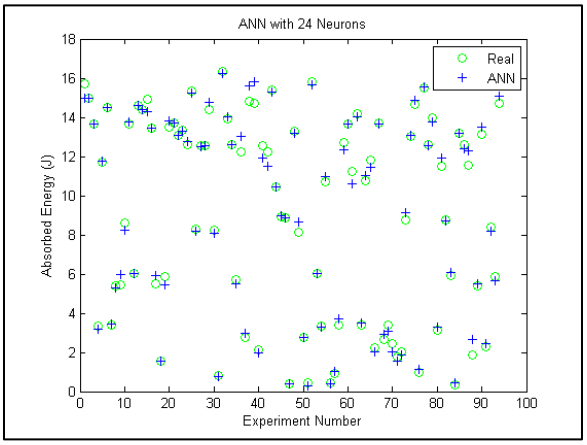

Figure 6.6: Actual response and the predicted response for GFRP plates

Table 6.4: Independent test cases to verify ANN model for GFRP plates

Input1 (thickness mm)	**Input2 (No. of Layers)**	**Input3 (Stacking Sequence)**	**Actual response (Abaqus) J**	**Simulated Response (ANN) J**	**Difference**
0.26	24	2	13.37359	15.5417	2.1681
0.42	30	4	6.14928	6.2809	0.1316
0.35	26	1	12.69973	13.153	0.4532
0.54	34	2	0.602984	0.6865	0.0835
0.36	36	3	8.449098	8.3282	-0.1209

The number of data samples for training is the same for carbon and glass fiber plates but the error is more pronounced for the glass fiber plates due to the reason that the data for the response is not following a pattern which makes it harder to model ANN. This error can be reduced by introducing more data for training purposes.

6.2.3 ANN Model for Pipes

The training of ANN models for composite pipes is trickier as can be observed from the graphs presented earlier. It can be observed that in most of the cases for carbon and glass fiber pipes, there is a range where the absorbed energy value remains more or less the same and then it decreases suddenly. This sudden change is modeled using more neurons in the ANN models. In total there are 162 points for the training and validation which is almost 1.5 times that of the plates.

For the carbon fiber pipes, the ANN model is particularly worse in the correlation. Even with 100 neurons distributed a single hidden layer; the root mean square error is as high as 0.32 J and the maximum error is about 1.49 J.

Table 6.5: Testing ANN for 100 neurons for CFRP pipes

Input1 (thickness mm)	**Input2 (Number of Layers)**	**Input3 (Stacking Sequence)**	**Actual response (Abaqus) J**	**Simulated Response (ANN) J**	**Difference**
0.425	55	36	0.3935	1.3454	-0.9519
0.35	55	32	6.646	6.3746	0.2714
0.3	45	16	11.9603	11.9681	-0.0078
0.4	55	28	7.1349	6.9401	0.1948
0.4	65	32	4.3499	4.0834	0.2665
0.35	57.5	20	10.6618	9.8097	0.8521
0.25	75	32	11.1477	11.1986	-0.0509
0.425	45	36	0.5237	0.5876	-0.0639
0.35	75	32	8.5637	7.654	0.9097
0.25	57.5	24	11.1164	9.6288	1.4876
0.3	35	28	11.3783	11.3015	0.0768
0.25	45	28	10.5071	10.5036	0.0035
0.25	52.5	24	11.3505	11.233	0.1175
0.3	65	28	8.6457	8.3328	0.3129

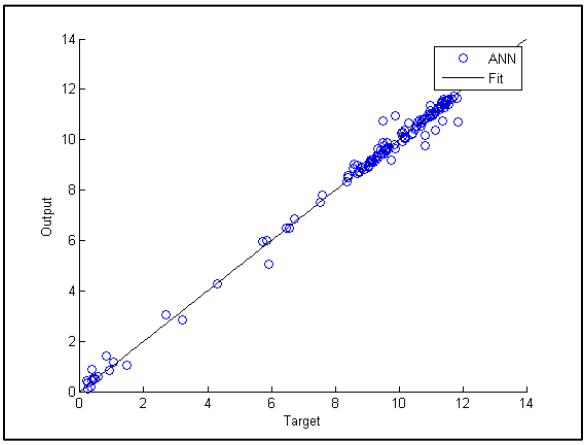

Figure 6.7: Correlation for predicted and target data for CFRP pipes

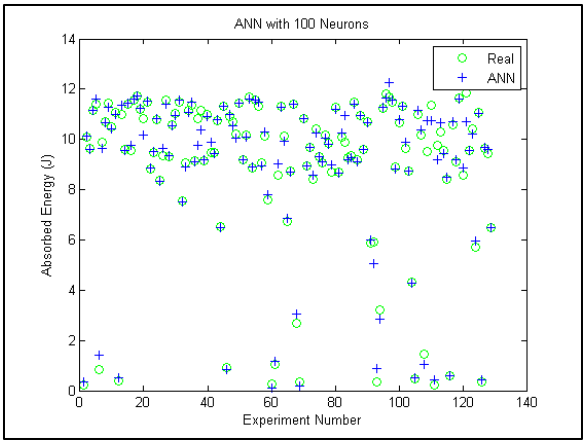

Figure 6.8: Actual response and the predicted response for CFRP pipes

The prediction performance of ANN model for the glass fiber pipes is much better with a maximum error of 1.026 J and root mean square error of only 0.26 J. These results from ANN model are not accurate enough but the absolute error in most of the cases is small enough to consider the model for prediction. The numbers of neurons used in this model are 37 and the number of hidden layer is 1.

Table 6.6: Testing ANN for 37 neurons for GFRP pipes

Input1 (thickness mm)	Input2 (Number of Layers)	Input3 (Stacking Sequence)	Actual response (Abaqus) J	Simulated Response (ANN) J	Difference
0.3	55	40	9.5385	9.6133	-0.0748
0.35	65	28	11.1121	11.1812	-0.0691
0.35	65	20	11.9186	11.8575	0.0611
0.25	65	36	11.0703	11.0599	0.0104
0.375	65	36	6.7361	6.7112	0.0249
0.35	55	36	8.6462	9.2142	-0.568
0.4	50	28	11.5286	11.5219	0.0067
0.3	57.5	28	11.4357	11.6259	-0.1902
0.35	75	40	7.9836	8.1484	-0.1648
0.25	35	32	12.4234	12.1281	0.2953
0.25	57.5	28	12.0485	12.1576	-0.1091
0.425	35	36	0.8283	0.6212	0.2071
0.35	75	32	10.4983	10.4393	0.059
0.25	65	28	11.7907	11.7143	0.0764

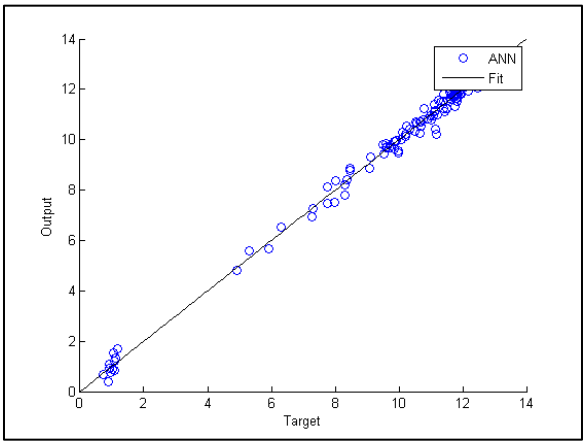

Figure 6.9: Correlation for predicted and target data for GFRP pipes

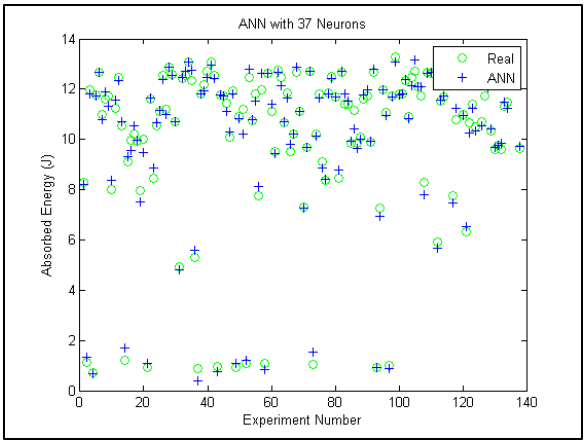

Figure 6.10: Actual response and the predicted response for GFRP pipes

6.3 COST MODELS

Composite materials and their production is an expensive process. It has always been the focus of major design and development teams to reduce the costs while simultaneously achieve maximum performance. The idea for this study is optimizing the impact performance with respect to the costs. To estimate the costs related to the composite plates and pipes, it is necessary to develop a cost model which can relate the costs of the material and the production with the samples. A simple yet realistic cost model is proposed in this section, the cost model we adopted here is given by:

$$CF = X + \left[(C1/100) + \left(C2/100 \right) \right] * X \tag{6.4}$$

In this equation, CF represents the total costs, whereas we assume X to be the material costs. In general, material costs are considered to be the maximum and the other costs like labor costs ‘C1’ and the other overheads ‘C2’ are considered to be some fraction of the material costs.

An online survey for the prices of the different types of fibers gave a basic idea of the material costs. The prices listed in the Table 6.7 are for a reference and may vary depending upon a number of factors ranging from the supplier to the texture of the fiber.

Table 6.7: Material costs of different types of fibers

Material	**Type**	**Price**
Carbon fiber	Woven fabric	200 USD per m^2
Glass fiber	Woven fabric	12 USD per m^2
Carbon fiber	Unidirectional	900 USD per kg
Glass fiber	Unidirectional	30 USD per kg

Based on these prices for the materials used in the manufacturing of composite plates and pipes, it is obvious that the optimization with respect to the cost is important.

6.4 DIFFERENTIAL EVOLUTION ALGORITHMS

Differential evolution algorithms were developed in mid 90s as an optimization technique by Rainer Storn and Kenneth Price. It is a simple and robust population based optimization technique with few control variables and fast convergence. Being an evolutionary algorithm, the DE technique is suited for solving non-linear and non-differentiable optimization problems. DE is a kind of search technique which works on finding the candidate solution among a population. DE algorithms generate new populations from the existing one based on certain parameters like mutations and crossovers. The details about the differential evolution algorithm are not discussed here. For our problem, we use an initial population size of 200, with a crossover of 0.8 and a total of 100 generations to find the optimal solution.

6.4.1 Cost Optimization

The results from the all the analysis as discussed in previous chapters indicate that the improvement in impact resistance is not linearly dependent on the factors considered. Thus, it is necessary to study the cost optimization of both the composite plates and the composite pipes. A differential evolution algorithm was adopted to optimize the amount of absorbed energy by the plate or the pipe and the cost model was used to predict the cost of making that sample.

Separate optimizations for the CFRP plates and the GFRP plates was carried out and compared with the costs for both types of materials. It is assumed here that in addition to the cost and the impact performance, the weight of the structure and the thickness of the plate should also be a factor in finding the best compromise.

For GFRP plates, a series of runs of the optimization algorithm, it was found that the optimal solution is a plate having 36 number of layers using stacking sequence 4 with the thickness of each layer to be about 0.57 mm. At this configuration, the ANN model predicts the absorbed energy by the plate to be 0.004 J. The weight of the composite plate with this configuration is 0.56 kg and assuming the price listed in Table 6.7, the cost is estimated to be 14 USD. But it is known that the sheets of 0.57 mm may not be available commercially while 0.6 mm thick woven fabrics are available. Therefore, we propose a design of composite plate with glass fiber to be used with 0.6 mm thick layers and 36 layers in total with the stacking sequence 4. This configuration will weigh about 0.59 kg and cost of 14.75 USD.

Similarly, for CFRP plates, the optimal solution was found to be plate with 32 layers of stacking sequence 1 and the thickness of each layer to 0.38 mm. This configuration will weigh about 0.29 kg and the amount of absorbed energy as predicted by our ANN model is 0.102 J. The cost of this plate would be around 260 USD which is a lot as compared to just 14 USD for the glass plate although it saves almost half of the weight of the glass plate. Simulations were performed for both CFRP plates and the GFRP plates with absorbed energy of 0.21 J and 0.31 J respectively. The results show that the ANN prediction model and optimization algorithm performs really well.

As we concluded earlier, a best configuration would be to use the stacking sequence 4 with mainly GFRP layers and replacing top and middle layers with the CFRP layers. This configuration is believed to perform better in terms of less weight and thickness with some increase in price.

Also, the same optimization procedure is applied to the composite pipes. The results from ANN in this case have some error but the procedure in general is applicable. This ANN model may skip some of the better results but due to the error in estimation of the absorbed energy, the optimization algorithm would reject a better one in favor of a worse but reliable solution. About 10 runs of optimization algorithm were performed and the most repeated configuration was selected. It was found from the optimization routine for the carbon fiber pipes; the best solution would be to have winding angle of 42.5˚ with total 36 layers and having each layer of 0.425 mm thick. According to ANN model this configuration would absorb energy of about 0.2 J. The price estimate for this type of pipe is about 1370 USD while the weight is about 6.8 kg. A simulation was performed in ABAQUS for this configuration which reports absorbed energy of 0.3 J.

Optimization for the glass fiber pipes suggested that optimal solution to be pipes with winding angle of 51˚ with total of 40 layers and each layer of about 0.4 mm thick. According to the ANN model this configuration would absorb around 0.965 J of energy. The cost estimate for this configuration of pipe is about 250 USD. This pipe weighs around 9 kgs. Simulation of GFRP pipe with the optimized configuration using ABAQUS suggests our results are quite accurate as the predicted absorbed energy is close to the one from simulation which is 0.88 J.

A simulation in the ABAQUS environment of the proposed solution from the optimization algorithm confirmed the results for all the cases. As was the case with plates, the compromise between price and the weight can be achieved by replacing top layers of GFRP pipes with the carbon fiber layers as suggested in Chapter 4.

6.5 CONCLUSIONS

This chapter discusses the optimization techniques and the ANN models for prediction of the amount of absorbed energy. The main conclusions from this chapter can be summarized as:

- ANN models are very strong and useful tools for the function fitting of non-linear behavior and as observed in the case of CFRP plates are able to predict the absorbed energy with very little error.
- The accuracy of the ANN models depend upon the behavior of the training data sets, if there are too much sudden variations in the training data as was

observed in the results from the composite pipes then the model can be prone to errors.

- A better way to model ANN with training data as in our case is to simulate and generate a very big training data. In our study, we had around 100 data each for the flat plates and about 150 for the pipes apart from the ones that were used to validate the results. As a rule of thumb, it is suggested that the data size should be in the range of 500-1000 for a very accurate model.

CHAPTER 7

CONCLUSIONS AND RECOMMENDATIONS

7.1 CONCLUSIONS

This chapter includes the major conclusions drawn from this study. The results and discussions about the findings were already discussed in detail with each chapter along with the major conclusions. The following can be summarized as the conclusions:

- The Hashin damage model used as the damage initiation model in this research is accurate enough to predict the onset of damage without loss of much accuracy.
- Sensitivity analysis is a useful tool in determining the factors influencing the most on the impact performance of the FRP plates and pipes.
- The amount of absorbed energy considered as an indication for the amount of damage is affected mainly by the thickness of the layers, number of layers, stacking sequence and the material properties.
- Material properties like the tensile strength of the fiber and the fracture energies of the laminate during the tensile loading in the longitudinal direction

are more influential than other mechanical properties of the fiber or the binder material used.

- Quasi isotropic laminates show good performance in all conditions. But, the stacking sequence other than quasi isotropic laminates can have optimal performance if the boundary conditions are such that they restrict deformation in any particular direction and allow in the other directions.
- Influence of boundary conditions can be controlled by aligning more layers to counter the stress produced as a result of bending.
- The numbers of layers also have an effect on the impact resistance and should be selected carefully as to not just increase the layers which result in more contact force and hence greater damage.
- Design of experiment is a useful method to statistically study the variation in the impact performance of the FRP plates and pipes with respect to the variables identified using sensitivity analysis.
- The effect of thickness of the laminate is the most interesting one compared to the other factors. The thickness is not directly proportional to the impact performance of the plates or the pipes. Thin plates have better performance compared to plates that are thick but not rigid enough.
- The amount of dissipated energy transferred to the specimen is not always in the form of damage dissipation but some of the energy is transferred to the specimen which generates unnecessary vibration. Based on the above two conclusions, the specimen thickness should be such that it is stiff and thick enough to withstand the impact loads without suffering from the vibrations.

- It is important to have as more fibers as possible in the direction of the maximum stress during the impact to delay the damage initiation process.
- The design of the structure and the choice of material should be such that the maximum utilization of the tensile strength of the fiber materials can be achieved.
- The inclusion of woven fabric in the filament wound composite pipes can be beneficial if the woven fabric selected has a higher tensile strength than the unidirectional glass or carbon fibers.
- Using the optimization algorithm, it was suggested that the optimal stacking sequence for the flat plates would be the sequence number 4 from this study.
- The inclusion of carbon fibers in the flat plates and the pipes can enhance the impact resistance quite a lot with the added advantage of weight savings as well as reduced thickness at a slightly higher price.

7.2 FUTURE DIRECTION

There is a lot of room for research in this topic; following are some of the recommendations for the future research in this area:

- One of the most important studies would be to understand the behavior of the composite structures under the influence of other loads such as the internal pressure, thermal strain and multi-axial loads.
- It is well known fact that the composite materials are good in tensile loading conditions and after impact events still can perform at a reasonable level but

after impact the compressive strength is significantly reduced. Compression after impact tests are widely used in the industry to study the amount of damage after the impact loads. An experimental study can be carried out using CAI tests to better understand the damage.

- Modes of damage can be quantified and a study can be performed to understand the nature and modes of damage after low-velocity impacts.
- Further research can be performed in the impact behavior of hybrid composites.
- More simulations can be performed with more input data in order to get better accuracy from the ANN models.
- Developing mathematical and empirical relations for the damage can be targeted as an advanced study into the impact behavior of composite structures.

APPENDICES

A.1 RESULTS FOR THE COMPOSITE PLATES

Table A. 1: List of experiments numerically solved for the layer configuration 1 for Carbon/Epoxy plates

S. No.	Layer Thickness (mm)	Number of Layers	Total Thickness of Plate (mm)	Rebound Velocity (m/s)	Absorbed Energy (J)
1	0.12	16	1.92	3.7716	16.8809
2	0.14	16	2.24	4.5403	12.0893
3	0.16	16	2.56	4.9512	9.1643
4	0.18	16	2.88	5.1430	7.71212
5	0.12	20	2.4	4.5898	11.7503
6	0.16	20	3.2	5.0757	8.2276
7	0.18	20	3.6	5.0685	8.2824
8	0.2	16	3.2	5.1193	7.8947
9	0.25	16	4	5.2618	6.7855
10	0.3	16	4.8	5.2854	6.5986
11	0.2	20	4	5.1614	7.5701
12	0.25	20	5	5.2251	7.0740
13	0.3	20	6	5.3709	5.9155
14	0.2	24	4.8	5.2905	6.5578
15	0.25	24	6	5.3791	5.8493
16	0.3	24	7.2	5.3403	6.1606
17	0.2	28	5.6	5.3385	6.1756
18	0.25	28	7	5.3890	5.7693
19	0.3	28	8.4	5.5732	4.2549
20	0.35	28	9.8	5.7503	2.7507
21	0.4	28	11.2	5.9987	0.56125
22	0.3	32	9.6	5.7284	2.9391
23	0.35	32	11.2	6.0384	0.2031
24	0.4	32	12.8	6.0349	0.2346
25	0.3	36	10.8	5.9588	0.9193
26	0.35	36	12.6	6.0409	0.18073
27	0.4	36	14.4	6.0486	0.11064

Table A. 2: List of experiments numerically solved for the layer configuration 2 for Carbon/Epoxy plates

S. No.	Layer Thickness (mm)	Number of Layers	Total Thickness of Plate (mm)	Rebound Velocity (m/s)	Absorbed Energy (J)
1	0.12	16	1.92	4.11064	14.8770
2	0.14	16	2.24	4.69889	10.9903
3	0.16	16	2.56	5.06889	8.2798
4	0.18	16	2.88	5.14636	7.6862
5	0.12	20	2.4	4.96802	9.0391
6	0.16	20	3.2	5.2784	6.6539
7	0.18	20	3.6	5.37821	5.8561
8	0.2	16	3.2	5.26623	6.7501
9	0.25	16	4	5.40544	5.6359
10	0.3	16	4.8	5.42364	5.4881
11	0.2	20	4	5.41088	5.5918
12	0.25	20	5	5.44628	5.3035
13	0.3	20	6	5.49541	4.9003
14	0.2	24	4.8	5.39271	5.7390
15	0.25	24	6	5.50199	4.8461
16	0.3	24	7.2	5.46472	5.1526
17	0.2	28	5.6	5.51426	4.7447
18	0.25	28	7	5.43048	5.4324
19	0.3	28	8.4	5.59542	4.0685
20	0.35	28	9.8	5.79284	2.3823
21	0.4	28	11.2	5.97076	0.8125
22	0.3	32	9.6	5.82705	2.0841
23	0.35	32	11.2	5.97504	0.7742
24	0.4	32	12.8	6.03607	0.2244
25	0.3	36	10.8	5.93021	1.1745
26	0.35	36	12.6	6.03809	0.2061
27	0.4	36	14.4	5.92846	1.1900

Table A. 3: List of experiments numerically solved for the layer configuration 3 for Carbon/Epoxy plates

S. No.	Layer Thickness (mm)	Number of Layers	Total Thickness of Plate (mm)	Rebound Velocity (m/s)	Absorbed Energy (J)
1	0.12	16	1.92	4.02354	15.4083
2	0.14	16	2.24	5.00151	8.7887
3	0.16	16	2.56	5.1643	7.5475
4	0.18	16	2.88	5.23933	6.9621
5	0.12	20	2.4	5.00133	8.7900
6	0.16	20	3.2	5.30247	6.4629
7	0.18	20	3.6	5.29392	6.5308
8	0.2	16	3.2	5.21854	7.1251
9	0.25	16	4	5.21853	7.1252
10	0.3	16	4.8	5.44782	5.2909
11	0.2	20	4	5.37119	5.9127
12	0.25	20	5	5.38755	5.7807
13	0.3	20	6	5.50416	4.8282
14	0.2	24	4.8	5.44647	5.3020
15	0.25	24	6	5.50308	4.8371
16	0.3	24	7.2	5.37818	5.8564
17	0.2	28	5.6	5.46656	5.1375
18	0.25	28	7	5.42745	5.4571
19	0.3	28	8.4	5.59528	4.0696
20	0.35	28	9.8	5.64996	3.6085
21	0.4	28	11.2	5.92138	1.2529
22	0.3	32	9.6	5.62214	3.8437
23	0.35	32	11.2	5.91947	1.2699
24	0.4	32	12.8	6.02044	0.3657
25	0.3	36	10.8	5.87043	1.7035
26	0.35	36	12.6	6.02154	0.3560
27	0.4	36	14.4	5.93517	1.1303

Table A. 4: List of experiments numerically solved for the layer configuration 4 for Carbon/Epoxy plates

S. No.	Layer Thickness (mm)	Number of Layers	Total Thickness of Plate (mm)	Rebound Velocity (m/s)	Absorbed Energy (J)
1	0.12	16	1.92	3.42872	18.7329
2	0.14	16	2.24	3.98288	15.6525
3	0.16	16	2.56	5.09185	8.1048
4	0.18	16	2.88	5.22069	7.1083
5	0.12	20	2.4	4.60535	11.6431
6	0.16	20	3.2	5.21299	7.1686
7	0.18	20	3.6	5.31472	6.3653
8	0.2	16	3.2	5.2942	6.5286
9	0.25	16	4	5.46716	5.1326
10	0.3	16	4.8	5.522	4.6806
11	0.2	20	4	5.37021	5.9206
12	0.25	20	5	5.55184	4.4328
13	0.3	20	6	5.61302	3.9205
14	0.2	24	4.8	5.52799	4.6310
15	0.25	24	6	5.63551	3.7308
16	0.3	24	7.2	5.56273	4.3420
17	0.2	28	5.6	5.62726	3.8005
18	0.25	28	7	5.543	4.5064
19	0.3	28	8.4	5.75417	2.7171
20	0.35	28	9.8	5.77615	2.5271
21	0.4	28	11.2	5.91357	1.3223
22	0.3	32	9.6	5.78399	2.4591
23	0.35	32	11.2	5.9137	1.3211
24	0.4	32	12.8	6.02662	0.3099
25	0.3	36	10.8	5.86668	1.7365
26	0.35	36	12.6	6.02121	0.3588
27	0.4	36	14.4	5.94022	1.0853

Table A. 5: List of experiments numerically solved for the layer configuration 1 for Glass/Epoxy plates

S. No.	Layer Thickness (mm)	Number of Layers	Total Thickness of Plate (mm)	Rebound Velocity (m/s)	Absorbed Energy (J)
1	0.25	24	6	4.29654	13.7048
2	0.3	24	7.2	4.45182	12.6860
3	0.35	24	8.4	4.38999	13.0960
4	0.4	24	9.6	4.25182	13.9915
5	0.45	24	10.8	4.1855	14.4112
6	0.5	24	12	4.01153	15.4807
7	0.6	24	14.4	5.00643	8.7517
8	0.25	28	7	4.59771	11.6958
9	0.3	28	8.4	4.46418	12.6033
10	0.35	28	9.8	4.32582	13.5155
11	0.4	28	11.2	4.14263	14.6790
12	0.25	32	8	4.28157	13.8011
13	0.3	32	9.6	4.26511	13.9066
14	0.35	32	11.2	4.13433	14.7305
15	0.25	36	9	4.46612	12.5903
16	0.3	36	10.8	4.09504	14.9730
17	0.35	36	12.6	3.80239	16.7064
18	0.4	32	12.8	4.51516	12.2600
19	0.4	36	14.4	5.02762	8.5923
20	0.45	28	12.6	3.97484	15.7005
21	0.45	32	14.4	4.99326	8.8505
22	0.45	36	16.2	5.81877	2.1564
23	0.5	28	14	4.98613	8.9039
24	0.5	32	16	5.80594	2.2683
25	0.5	36	18	5.97269	0.7952
26	0.6	28	16.8	5.88193	1.6022
27	0.6	32	19.2	6.01784	0.3892

Table A. 6: List of experiments numerically solved for the layer configuration 2 for Glass/Epoxy plates

S. No.	Layer Thickness (mm)	Number of Layers	Total Thickness of Plate (mm)	Rebound Velocity (m/s)	Absorbed Energy (J)
1	0.25	24	6	4.3052	13.6489
2	0.3	24	7.2	4.18788	14.3962
3	0.35	24	8.4	4.46527	12.5960
4	0.4	24	9.6	4.35886	13.3003
5	0.45	24	10.8	4.15121	14.6256
6	0.5	24	12	3.86215	16.3628
7	0.6	24	14.4	5.67396	3.4046
8	0.25	28	7	4.3385	13.4331
9	0.3	28	8.4	4.61759	11.5584
10	0.35	28	9.8	4.35215	13.3441
11	0.4	28	11.2	4.0995	14.9456
12	0.25	32	8	4.47352	12.5407
13	0.3	32	9.6	4.38341	13.1393
14	0.35	32	11.2	4.10035	14.9403
15	0.25	36	9	4.47352	12.5407
16	0.3	36	10.8	4.17267	14.4916
17	0.35	36	12.6	4.44619	12.7235
18	0.4	32	12.8	4.62489	11.5078
19	0.4	36	14.4	5.67654	3.3827
20	0.45	28	12.6	4.4747	12.5328
21	0.45	32	14.4	5.6774	3.3753
22	0.45	36	16.2	5.83351	2.0276
23	0.5	28	14	5.70682	3.1242
24	0.5	32	16	5.81129	2.2217
25	0.5	36	18	5.97706	0.7561
26	0.6	28	16.8	5.88858	1.5435
27	0.6	32	19.2	6.02185	0.3530

Table A. 7: List of experiments numerically solved for the layer configuration 3 for Glass/Epoxy plates

S. No.	Layer Thickness (mm)	Number of Layers	Total Thickness of Plate (mm)	Rebound Velocity (m/s)	Absorbed Energy (J)
1	0.25	24	6	4.29723	13.7004
2	0.3	24	7.2	4.30629	13.6419
3	0.35	24	8.4	4.21859	14.2026
4	0.4	24	9.6	4.02843	15.3788
5	0.45	24	10.8	4.77313	10.4629
6	0.5	24	12	5.0023	8.7827
7	0.6	24	14.4	5.05658	8.3732
8	0.25	28	7	4.46288	12.6120
9	0.3	28	8.4	4.40108	13.0229
10	0.35	28	9.8	4.13868	14.7035
11	0.4	28	11.2	4.67287	11.1732
12	0.25	32	8	4.10725	14.8979
13	0.3	32	9.6	4.0367	15.3288
14	0.35	32	11.2	4.73406	10.7415
15	0.25	36	9	4.30269	13.6651
16	0.3	36	10.8	4.73654	10.7240
17	0.35	36	12.6	5.01993	8.6502
18	0.4	32	12.8	5.0657	8.3040
19	0.4	36	14.4	5.07679	8.2197
20	0.45	28	12.6	5.02813	8.5884
21	0.45	32	14.4	5.06793	8.2871
22	0.45	36	16.2	5.78836	2.4212
23	0.5	28	14	5.08497	8.1573
24	0.5	32	16	5.76298	2.6410
25	0.5	36	18	5.96128	0.8974
26	0.6	28	16.8	5.86131	1.7838
27	0.6	32	19.2	6.01275	0.4351

Table A. 8: List of experiments numerically solved for the layer configuration 4 for Glass/Epoxy plates

S. No.	Layer Thickness (mm)	Number of Layers	Total Thickness of Plate (mm)	Rebound Velocity (m/s)	Absorbed Energy (J)
1	0.25	24	6	4.37745	13.1785
2	0.3	24	7.2	3.95406	15.8241
3	0.35	24	8.4	4.69099	11.0460
4	0.4	24	9.6	5.37575	5.8760
5	0.45	24	10.8	5.43519	5.3940
6	0.5	24	12	5.42735	5.4579
7	0.6	24	14.4	5.68184	3.3375
8	0.25	28	7	4.1224	14.8044
9	0.3	28	8.4	4.51686	12.2485
10	0.35	28	9.8	5.39647	5.7086
11	0.4	28	11.2	5.433	5.4119
12	0.25	32	8	4.57902	11.8244
13	0.3	32	9.6	5.37565	5.8768
14	0.35	32	11.2	5.46052	5.1870
15	0.25	36	9	5.3227	6.3016
16	0.3	36	10.8	5.4226	5.4966
17	0.35	36	12.6	5.35458	6.0464
18	0.4	32	12.8	5.3718	5.9078
19	0.4	36	14.4	5.67569	3.3899
20	0.45	28	12.6	5.35868	6.0134
21	0.45	32	14.4	5.67957	3.3569
22	0.45	36	16.2	5.77795	2.5115
23	0.5	28	14	5.75044	2.7493
24	0.5	32	16	5.75055	2.7484
25	0.5	36	18	5.95438	0.9590
26	0.6	28	16.8	5.84955	1.8871
27	0.6	32	19.2	6.01049	0.4555

Table A. 9: Combinations for Top and Bottom layers of Carbon/epoxy and Results

No.	Carbon layer thickness (mm)	Glass layer thickness (mm)	Total Plate Thickness (mm)	Number of Layers	Rebound Velocity (m/s)	Absorbed Energy (J)
1	0.2	0.35	16	5.3	4.6045	11.6491
2	0.2	0.3	20	5.8	5.0184	8.6616
3	0.2	0.3	24	7	4.8861	9.6449
4	0.2	0.35	24	8.1	5.3202	6.3213
5	0.25	0.35	28	9.6	5.3720	5.9063
6	0.25	0.25	32	8	5.3137	6.3734
7	0.25	0.35	32	11	5.4819	5.0114

Table A. 10: Combinations for Middle 2 layers of Carbon/epoxy and Results

No.	Carbon layer thickness (mm)	Glass layer thickness (mm)	Total Plate Thickness (mm)	Number of Layers	Rebound Velocity (m/s)	Absorbed Energy (J)
1	0.2	0.35	16	5.3	5.0352	8.5348
2	0.2	0.3	20	5.8	4.4225	12.8813
3	0.2	0.3	24	7	4.7797	10.4161
4	0.2	0.35	24	8.1	4.8720	9.7481
5	0.25	0.35	28	9.6	5.37442	5.8867
6	0.25	0.25	32	8	4.77254	10.4671
7	0.25	0.35	32	11	5.45069	5.2675

Table A. 11: Combinations for Top 2 layers of Carbon/epoxy and Results

No.	Carbon layer thickness (mm)	Glass layer thickness (mm)	Total Plate Thickness (mm)	Number of Layers	Rebound Velocity (m/s)	Absorbed Energy (J)
1	0.2	0.35	16	5.3	4.61488	11.5772
2	0.2	0.25	20	4.9	4.78974	10.3438
3	0.2	0.3	20	5.8	4.62342	11.5180
4	0.2	0.3	24	7	4.73144	10.7601
5	0.2	0.35	24	8.1	5.30862	6.4139
6	0.25	0.35	28	9.6	5.41414	5.5653
7	0.25	0.25	32	8	5.3265	6.2713
8	0.25	0.35	32	11	5.49488	4.9047

Table A. 12: Combinations for Bottom 2 layers of Carbon/epoxy and Results

No.	Carbon layer thickness (mm)	Glass layer thickness (mm)	Total Plate Thickness (mm)	Number of Layers	Rebound Velocity (m/s)	Absorbed Energy (J)
1	0.2	0.35	16	5.3	3.55864	18.05206
2	0.2	0.25	20	4.9	3.15915	20.06483
3	0.2	0.3	20	5.8	4.45159	12.68751
4	0.2	0.3	24	7	4.46224	12.61631
5	0.2	0.35	24	8.1	5.29749	6.50245
6	0.25	0.35	28	9.6	5.39965	5.682835
7	0.25	0.25	32	8	4.7856	10.37352
8	0.25	0.35	32	11	5.4845	4.9899

Table A. 13: Combinations for Top, Bottom and Middle 2 layers of Carbon/epoxy

No.	Carbon layer thickness (mm)	Glass layer thickness (mm)	Total Plate Thickness (mm)	Number of Layers	Rebound Velocity (m/s)	Absorbed Energy (J)
1	0.2	0.25	16	3.8	5.03532	8.5342
2	0.2	0.35	16	5	5.1643	7.5479
3	0.2	0.3	20	5.6	5.00095	8.7929
4	0.2	0.3	24	6.8	4.9959	8.8309
5	0.2	0.35	24	7.8	5.31015	6.4017

Table A. 14: Combinations for Top and Middle layers of Carbon/epoxy and Results

No.	Carbon layer thickness (mm)	Glass layer thickness (mm)	Total Plate Thickness (mm)	Number of Layers	Rebound Velocity (m/s)	Absorbed Energy (J)
1	0.2	0.35	16	5.3	5.02165	8.6373
2	0.2	0.25	20	4.9	4.82216	10.1101
3	0.2	0.3	20	5.8	5.08829	8.1320
4	0.2	0.3	24	7	4.87564	9.7211
5	0.2	0.35	24	8.1	4.9283	9.3339
6	0.25	0.35	28	9.6	5.39191	5.7455
7	0.25	0.25	32	8	4.96792	9.0398
8	0.25	0.35	32	11	5.4955	4.8993

A.2 RESULTS FOR THE COMPOSITE PIPES

Table A. 15: Results of numerical simulation for the Carbon/epoxy pipes having 20 layers

S. No.	Layer Thickness (mm)	Winding Angle (degree)	Total Thickness of Plate (mm)	Rebound Velocity (m/s)	Absorbed Energy (J)
1	0.25	35	5	1.88815	22.1744
2	0.3	35	6	2.42007	10.7163
3	0.35	35	7	2.41699	10.7908
4	0.4	35	8	2.40259	11.1378
5	0.25	45	5	1.97629	20.4714
6	0.3	45	6	2.37435	11.8123
7	0.35	45	7	2.42622	10.5673
8	0.4	45	8	2.45385	9.8931
9	0.25	55	5	2.46942	9.5098
10	0.3	55	6	2.37988	11.6809
11	0.35	55	7	2.46786	9.5483
12	0.4	55	8	2.43165	10.4354
13	0.25	65	5	2.39083	11.4197
14	0.3	65	6	2.38887	11.4665
15	0.35	65	7	2.4453	10.1025
16	0.4	65	8	2.48513	9.1206
17	0.25	75	5	2.422	10.6696
18	0.3	75	6	2.40684	11.0356
19	0.35	75	7	2.39423	11.3383
20	0.4	75	8	2.40487	11.0830

Table A. 16: Results of numerical simulation for the Carbon/epoxy pipes having 24 layers

S. No.	Layer Thickness (mm)	Winding Angle (degree)	Total Thickness of Plate (mm)	Rebound Velocity (m/s)	Absorbed Energy (J)
1	0.25	35	6	1.90173	21.9171
2	0.3	35	7.2	2.41621	10.8096
3	0.35	35	8.4	2.38414	11.5794
4	0.4	35	9.6	2.39278	11.3730
5	0.25	45	6	2.40896	10.9846
6	0.3	45	7.2	2.44188	10.1861
7	0.35	45	8.4	2.46463	9.6280
8	0.4	45	9.6	2.42102	10.6933
9	0.25	55	6	2.46441	9.6334
10	0.3	55	7.2	2.47285	9.4251
11	0.35	55	8.4	2.45131	9.9554
12	0.4	55	9.6	2.47772	9.3045
13	0.25	65	6	2.38813	11.4842
14	0.3	65	7.2	2.44234	10.1749
15	0.35	65	8.4	2.49357	8.9105
16	0.4	65	9.6	2.48778	9.0548
17	0.25	75	6	2.40684	11.0356
18	0.3	75	7.2	2.40243	11.1417
19	0.35	75	8.4	2.37773	11.7320
20	0.4	75	9.6	2.47919	9.2681

Table A. 17: Results of numerical simulation for the Carbon/epoxy pipes having 28 layers

S. No.	Layer Thickness (mm)	Winding Angle (degree)	Total Thickness of Plate (mm)	Rebound Velocity (m/s)	Absorbed Energy (J)
1	0.25	35	7	2.41827	10.7599
2	0.3	35	8.4	2.39256	11.3783
3	0.35	35	9.8	2.38517	11.5548
4	0.4	35	11.2	2.42129	10.6868
5	0.25	45	7	2.4287	10.5071
6	0.3	45	8.4	2.47588	9.3501
7	0.35	45	9.8	2.46703	9.5688
8	0.4	45	11.2	2.46637	9.5851
9	0.25	55	7	2.41547	10.8275
10	0.3	55	8.4	2.51334	8.4156
11	0.35	55	9.8	2.47131	9.4631
12	0.4	55	11.2	2.56379	7.1349
13	0.25	65	7	2.42896	10.5008
14	0.3	65	8.4	2.50417	8.6457
15	0.35	65	9.8	2.51416	8.3950
16	0.4	65	11.2	2.61311	5.8583
17	0.25	75	7	2.39331	11.3603
18	0.3	75	8.4	2.38041	11.6682
19	0.35	75	9.8	2.50703	8.5740
20	0.4	75	11.2	2.51475	8.3802

Table A. 18: Results of numerical simulation for the Carbon/epoxy pipes having 32 layers

S. No.	Layer Thickness (mm)	Winding Angle (degree)	Total Thickness of Plate (mm)	Rebound Velocity (m/s)	Absorbed Energy (J)
1	0.25	35	8	2.39549	11.3081
2	0.3	35	9.6	2.39064	11.4242
3	0.35	35	11.2	2.42538	10.5877
4	0.4	35	12.8	2.54531	7.6070
5	0.25	45	8	2.42531	10.5894
6	0.3	45	9.6	2.46261	9.6778
7	0.35	45	11.2	2.46798	9.5453
8	0.4	45	12.8	2.82109	0.2073
9	0.25	55	8	2.49993	8.7517
10	0.3	55	9.6	2.45368	9.8973
11	0.35	55	11.2	2.58279	6.6460
12	0.4	55	12.8	2.79102	1.0510
13	0.25	65	8	2.49593	8.8517
14	0.3	65	9.6	2.50256	8.6860
15	0.35	65	11.2	2.61836	5.7210
16	0.4	65	12.8	2.67021	4.3510
17	0.25	75	8	2.40218	11.1477
18	0.3	75	9.6	2.48446	9.1373
19	0.35	75	11.2	2.50744	8.5637
20	0.4	75	12.8	2.58654	6.5491

Table A. 19: Results of numerical simulation for the Carbon/epoxy pipes having 36 layers

S. No.	Layer Thickness (mm)	Winding Angle (degree)	Total Thickness of Plate (mm)	Rebound Velocity (m/s)	Absorbed Energy (J)
1	0.25	35	9	2.38755	11.4980
2	0.3	35	10.8	2.3883	11.4801
3	0.35	35	12.6	2.4877	9.0567
4	0.4	35	14.4	2.81955	0.2507
5	0.25	45	9	2.46453	9.6305
6	0.3	45	10.8	2.42175	10.6756
7	0.35	45	12.6	2.82005	0.2366
8	0.4	45	14.4	2.81233	0.4540
9	0.25	55	9	2.49248	8.9377
10	0.3	55	10.8	2.5481	7.5359
11	0.35	55	12.6	2.71305	3.1968
12	0.4	55	14.4	2.77641	1.4577
13	0.25	65	9	2.49985	8.7537
14	0.3	65	10.8	2.58909	6.4831
15	0.35	65	12.6	2.67148	4.3160
16	0.4	65	14.4	2.73159	2.6921
17	0.25	75	9	2.45539	9.8553
18	0.3	75	10.8	2.48717	9.0699
19	0.35	75	12.6	2.57949	6.7312
20	0.4	75	14.4	2.61093	5.9152
21	0.375	35	13.5	2.81827	0.2868
22	0.425	35	15.3	2.8215	0.1957
23	0.375	45	13.5	2.81148	0.4779
24	0.425	45	15.3	2.80985	0.5237
25	0.375	55	13.5	2.78844	1.1230
26	0.425	55	15.3	2.77505	1.4955
27	0.375	65	13.5	2.70996	3.2806
28	0.425	65	15.3	2.72913	2.7592
29	0.375	75	13.5	2.60633	6.0352
30	0.425	75	15.3	2.67199	4.3023

Table A. 20: Results of numerical simulation for the Carbon/epoxy pipes having 16 layers

S. No.	Layer Thickness (mm)	Winding Angle (degree)	Total Thickness of Plate (mm)	Rebound Velocity (m/s)	Absorbed Energy (J)
1	0.25	35	4	2.04884	19.0113
2	0.3	35	4.8	1.91739	21.6181
3	0.35	35	5.6	1.83941	23.0829
4	0.4	35	6.4	2.41512	10.8360
5	0.25	45	4	2.39079	11.4206
6	0.3	45	4.8	2.36811	11.9603
7	0.35	45	5.6	2.3956	11.3055
8	0.4	45	6.4	2.39885	11.2276
9	0.25	55	4	1.57573	27.5854
10	0.3	55	4.8	2.40525	11.0739
11	0.35	55	5.6	2.37488	11.7997
12	0.4	55	6.4	2.47032	9.4876
13	0.25	65	4	2.38487	11.5620
14	0.3	65	4.8	2.39637	11.2871
15	0.35	65	5.6	2.38004	11.6770
16	0.4	65	6.4	2.40016	11.1962
17	0.25	75	4	2.39583	11.3000
18	0.3	75	4.8	2.41153	10.9226
19	0.35	75	5.6	2.39003	11.4388
20	0.4	75	6.4	2.39868	11.2317

Table A. 21: Results of numerical simulation for the Carbon/epoxy pipes having 20 layers and angles between 50˚ and 60˚

S. No.	Layer Thickness (mm)	Winding Angle (degree)	Total Thickness of Plate (mm)	Rebound Velocity (m/s)	Absorbed Energy (J)
1	0.25	50	5	2.37267	11.8522
2	0.3	50	6	2.39215	11.3881
3	0.35	50	7	2.41011	10.9568
4	0.4	50	8	2.48405	9.1475
5	0.25	52.5	5	2.44559	10.0954
6	0.3	52.5	6	2.40921	10.9785
7	0.35	52.5	7	2.40164	11.1606
8	0.4	52.5	8	2.44105	10.2064
9	0.25	57.5	5	2.4085	10.9956
10	0.3	57.5	6	2.4444	10.1245
11	0.35	57.5	7	2.42232	10.6618
12	0.4	57.5	8	2.42097	10.6945
13	0.25	60	5	2.44265	10.1673
14	0.3	60	6	2.47024	9.4896
15	0.35	60	7	2.43268	10.4103
16	0.4	60	8	2.47767	9.3058

Table A. 22: Results of numerical simulation for the Carbon/epoxy pipes having 24 layers and angles between 50˚ and 60˚

S. No.	Layer Thickness (mm)	Winding Angle (degree)	Total Thickness of Plate (mm)	Rebound Velocity (m/s)	Absorbed Energy (J)
1	0.25	50	6	2.38059	11.6640
2	0.3	50	7.2	2.46575	9.6004
3	0.35	50	8.4	2.49698	8.8255
4	0.4	50	9.6	2.48156	9.2093
5	0.25	52.5	6	2.39372	11.3505
6	0.3	52.5	7.2	2.48235	9.1897
7	0.35	52.5	8.4	2.4537	9.8968
8	0.4	52.5	9.6	2.50164	8.7090
9	0.25	57.5	6	2.40348	11.1164
10	0.3	57.5	7.2	2.41616	10.8109
11	0.35	57.5	8.4	2.4444	10.1245
12	0.4	57.5	9.6	2.45988	9.7450
13	0.25	60	6	2.43162	10.4361
14	0.3	60	7.2	2.43659	10.3151
15	0.35	60	8.4	2.4763	9.3397
16	0.4	60	9.6	2.5066	8.5848

Table A. 23: Results of numerical simulation for the Glass/epoxy pipes having 20 layers

S. No.	Layer Thickness (mm)	Winding Angle (degree)	Total Thickness of Plate (mm)	Rebound Velocity (m/s)	Absorbed Energy (J)
1	0.25	35	5	0	Penetrate
2	0.3	35	6	0	Penetrate
3	0.35	35	7	1.08274	34.1384
4	0.4	35	8	2.3477	12.4415
5	0.25	45	5	0	Penetrate
6	0.3	45	6	1.22598	32.4849
7	0.35	45	7	2.33975	12.6278
8	0.4	45	8	2.37994	11.6794
9	0.25	55	5	2.34227	12.5689
10	0.3	55	6	2.32993	12.8571
11	0.35	55	7	2.34418	12.5241
12	0.4	55	8	2.41696	10.7915
13	0.25	65	5	2.34617	12.4774
14	0.3	65	6	2.35908	12.1737
15	0.35	65	7	2.36987	11.9186
16	0.4	65	8	2.37815	11.7220
17	0.25	75	5	0	Penetrate
18	0.3	75	6	2.31988	13.0908
19	0.35	75	7	2.36784	11.9667
20	0.4	75	8	2.40273	11.1344

Table A. 24: Results of numerical simulation for the Glass/epoxy pipes having 24 layers

S. No.	Layer Thickness (mm)	Winding Angle (degree)	Total Thickness of Plate (mm)	Rebound Velocity (m/s)	Absorbed Energy (J)
1	0.25	35	6	0	Penetrate
2	0.3	35	7.2	0.77370	37.0070
3	0.35	35	8.4	2.34652	12.4692
4	0.4	35	9.6	2.35183	12.3445
5	0.25	45	6	1.12588	33.6620
6	0.3	45	7.2	2.33701	12.6919
7	0.35	45	8.4	2.37526	11.7907
8	0.4	45	9.6	2.37449	11.8090
9	0.25	55	6	2.33816	12.6650
10	0.3	55	7.2	2.33665	12.7003
11	0.35	55	8.4	2.41873	10.7487
12	0.4	55	9.6	2.45415	9.8857
13	0.25	65	6	2.34628	12.4749
14	0.3	65	7.2	2.37862	11.7108
15	0.35	65	8.4	2.39118	11.4113
16	0.4	65	9.6	2.40827	11.0012
17	0.25	75	6	2.3087	13.3495
18	0.3	75	7.2	2.37866	11.7099
19	0.35	75	8.4	2.39493	11.3216
20	0.4	75	9.6	2.4412	10.2027

Table A. 25: Results of numerical simulation for the Glass/epoxy pipes having 28 layers

S. No.	Layer Thickness (mm)	Winding Angle (degree)	Total Thickness of Plate (mm)	Rebound Velocity (m/s)	Absorbed Energy (J)
1	0.25	35	7	1.18648	32.9613
2	0.3	35	8.4	2.34749	12.4465
3	0.35	35	9.8	2.34058	12.6084
4	0.4	35	11.2	2.35438	12.2845
5	0.25	45	7	2.33806	12.6674
6	0.3	45	8.4	2.37643	11.7629
7	0.35	45	9.8	2.37471	11.8038
8	0.4	45	11.2	2.36973	11.9219
9	0.25	55	7	2.33516	12.7351
10	0.3	55	8.4	2.39867	11.2319
11	0.35	55	9.8	2.45515	9.8612
12	0.4	55	11.2	2.46985	9.4992
13	0.25	65	7	2.37526	11.7907
14	0.3	65	8.4	2.392	11.3917
15	0.35	65	9.8	2.40366	11.1121
16	0.4	65	11.2	2.45935	9.7580
17	0.25	75	7	2.36673	11.9929
18	0.3	75	8.4	2.39012	11.4366
19	0.35	75	9.8	2.44531	10.1023
20	0.4	75	11.2	2.42834	10.5158

Table A. 26: Results of numerical simulation for the Glass/epoxy pipes having 32 layers

S. No.	Layer Thickness (mm)	Winding Angle (degree)	Total Thickness of Plate (mm)	Rebound Velocity (m/s)	Absorbed Energy (J)
1	0.25	35	8	2.34847	12.4234
2	0.3	35	9.6	2.35175	12.3464
3	0.35	35	11.2	2.35126	12.3579
4	0.4	35	12.8	2.34264	12.5602
5	0.25	45	8	2.38248	11.6189
6	0.3	45	9.6	2.37675	11.7553
7	0.35	45	11.2	2.37343	11.8342
8	0.4	45	12.8	2.45558	9.8506
9	0.25	55	8	2.37704	11.7484
10	0.3	55	9.6	2.4683	9.5375
11	0.35	55	11.2	2.46654	9.5809
12	0.4	55	12.8	2.51122	8.4689
13	0.25	65	8	2.37831	11.7182
14	0.3	65	9.6	2.41152	10.9229
15	0.35	65	11.2	2.46551	9.6063
16	0.4	65	12.8	2.5584	7.2729
17	0.25	75	8	2.40355	11.1147
18	0.3	75	9.6	2.4265	10.5605
19	0.35	75	11.2	2.42906	10.4983
20	0.4	75	12.8	2.51793	8.3001

Table A. 27: Results of numerical simulation for the Glass/epoxy pipes having 36 layers

S. No.	Layer Thickness (mm)	Winding Angle (degree)	Total Thickness of Plate (mm)	Rebound Velocity (m/s)	Absorbed Energy (J)
1	0.25	35	9	2.34385	12.5318
2	0.3	35	10.8	2.34026	12.6159
3	0.35	35	12.6	2.31136	13.2881
4	0.4	35	14.4	2.7913	1.0432
5	0.25	45	9	2.3753	11.7897
6	0.3	45	10.8	2.38331	11.5992
7	0.35	45	12.6	2.44123	10.2020
8	0.4	45	14.4	2.79047	1.0664
9	0.25	55	9	2.43497	10.3546
10	0.3	55	10.8	2.46449	9.6314
11	0.35	55	12.6	2.50415	8.6462
12	0.4	55	14.4	2.7895	1.0934
13	0.25	65	9	2.4054	11.0703
14	0.3	65	10.8	2.45222	9.9331
15	0.35	65	12.6	2.55745	7.2972
16	0.4	65	14.4	2.61074	5.9202
17	0.25	75	9	2.39953	11.2113
18	0.3	75	10.8	2.42708	10.5464
19	0.35	75	12.6	2.5115	8.4618
20	0.4	75	14.4	2.53095	7.9715
21	0.375	35	13.5	2.46227	9.6861
22	0.425	35	15.3	2.79899	0.8283
23	0.375	45	13.5	2.79539	0.9290
24	0.425	45	15.3	2.79574	0.9192
25	0.375	55	13.5	2.51755	8.3097
26	0.425	55	15.3	2.79256	1.0080
27	0.375	65	13.5	2.5793	6.7361
28	0.425	65	15.3	2.63406	5.3086
29	0.375	75	13.5	2.52931	8.0130
30	0.425	75	15.3	2.53922	7.7618

Table A. 28: Results of numerical simulation for the Glass/epoxy pipes having 40 layers

S. No.	Layer Thickness (mm)	Winding Angle (degree)	Total Thickness of Plate (mm)	Rebound Velocity (m/s)	Absorbed Energy (J)
1	0.25	35	10	2.32956	12.8658
2	0.3	35	12	2.34196	12.5761
3	0.35	35	14	2.78597	1.1919
4	0.4	35	16	2.80272	0.7238
5	0.25	45	10	2.38761	11.4966
6	0.3	45	12	2.39204	11.3907
7	0.35	45	14	2.79567	0.9211
8	0.4	45	16	2.79667	0.8932
9	0.25	55	10	2.45024	9.9816
10	0.3	55	12	2.46826	9.5385
11	0.35	55	14	2.78827	1.1278
12	0.4	55	16	2.79438	0.9572
13	0.25	65	10	2.40469	11.0873
14	0.3	65	12	2.51472	8.3809
15	0.35	65	14	2.59576	6.3102
16	0.4	65	16	2.64831	4.9323
17	0.25	75	10	2.44626	10.0791
18	0.3	75	12	2.48627	9.0923
19	0.35	75	14	2.53047	7.9836
20	0.4	75	16	2.53942	7.7567

Table A. 29: Results of numerical simulation for the Glass/epoxy pipes having 24 layers with winding angles between 50˚ and 60˚

S. No.	Layer Thickness (mm)	Winding Angle (degree)	Total Thickness of Plate (mm)	Rebound Velocity (m/s)	Absorbed Energy (J)
1	0.25	50	6	2.31991	13.0901
2	0.3	50	7.2	2.33779	12.6737
3	0.35	50	8.4	2.3796	11.6875
4	0.4	50	9.6	2.40056	11.1866
5	0.25	52.5	6	2.33659	12.7017
6	0.3	52.5	7.2	2.33785	12.6723
7	0.35	52.5	8.4	2.34672	12.4645
8	0.4	52.5	9.6	2.4401	10.2296
9	0.25	57.5	6	2.34376	12.5339
10	0.3	57.5	7.2	2.36829	11.9560
11	0.35	57.5	8.4	2.38649	11.5233
12	0.4	57.5	9.6	2.40847	10.9964
13	0.25	60	6	2.3424	12.5658
14	0.3	60	7.2	2.37386	11.8239
15	0.35	60	8.4	2.40307	11.1263
16	0.4	60	9.6	2.42099	10.6940

Table A. 30: Results of numerical simulation for the Glass/epoxy pipes having 28 layers with winding angles between 50˚ and 60˚

S. No.	Layer Thickness (mm)	Winding Angle (degree)	Total Thickness of Plate (mm)	Rebound Velocity (m/s)	Absorbed Energy (J)
1	0.25	50	7	2.34138	12.5897
2	0.3	50	8.4	2.37784	11.7294
3	0.35	50	9.8	2.40265	11.1364
4	0.4	50	11.2	2.38627	11.5286
5	0.25	52.5	7	2.33777	12.6742
6	0.3	52.5	8.4	2.36277	12.0866
7	0.35	52.5	9.8	2.42132	10.6860
8	0.4	52.5	11.2	2.41214	10.9079
9	0.25	57.5	7	2.36438	12.0485
10	0.3	57.5	8.4	2.39016	11.4357
11	0.35	57.5	9.8	2.42214	10.6662
12	0.4	57.5	11.2	2.44986	9.9909
13	0.25	60	7	2.37223	11.8626
14	0.3	60	8.4	2.38314	11.6032
15	0.35	60	9.8	2.42183	10.6737
16	0.4	60	11.2	2.48559	9.1092

Table A. 31: Combinations for Top 2 layers of Woven Carbon/epoxy and Results for 55˚ filament wound pipes

No.	Carbon layer thickness (mm)	Glass layer thickness (mm)	Total Plate Thickness (mm)	Number of Layers	Rebound Velocity (m/s)	Absorbed Energy (J)
1	0.25	0.25	20	5	2.34429	12.5215
2	0.3	0.3	20	6	2.3181	13.1320
3	0.35	0.35	20	7	2.36128	12.1218
4	0.4	0.4	20	8	2.37573	11.7795

Table A. 32: Combinations for Top 4 layers of Woven Carbon/epoxy and Results for 55˚ filament wound pipes

No.	Carbon layer thickness (mm)	Glass layer thickness (mm)	Total Plate Thickness (mm)	Number of Layers	Rebound Velocity (m/s)	Absorbed Energy (J)
1	0.25	0.25	20	5	2.33811	12.66621
2	0.3	0.3	20	6	2.33318	12.78136
3	0.35	0.35	20	7	2.3728	11.8491
4	0.4	0.4	20	8	2.37544	11.78642

Table A. 33: Combinations for Top 2 layers of Unidirectional Carbon/epoxy and Results for 55˚ filament wound pipes

No.	Carbon layer thickness (mm)	Glass layer thickness (mm)	Total Plate Thickness (mm)	Number of Layers	Rebound Velocity (m/s)	Absorbed Energy (J)
1	0.25	0.25	20	5	2.34126	12.59251
2	0.3	0.3	20	6	2.34276	12.55738
3	0.35	0.35	20	7	2.36739	11.97732
4	0.4	0.4	20	8	2.3716	11.87757

Table A. 34: Combinations for Top 4 layers of Unidirectional Carbon/epoxy and Results for 55˚ filament wound pipes

No.	Carbon layer thickness (mm)	Glass layer thickness (mm)	Total Plate Thickness (mm)	Number of Layers	Rebound Velocity (m/s)	Absorbed Energy (J)
1	0.25	0.25	20	5	2.34404	12.52738
2	0.3	0.3	20	6	2.33466	12.74681
3	0.35	0.35	20	7	2.48928	9.017425
4	0.4	0.4	20	8	2.50019	8.74525

NOMENCLATURE

E_{11}	Elastic Modulus in Longitudinal Direction	[N/m^2]
E_{22}	Elastic Modulus in Transverse Direction	[N/m^2]
E_{33}	Elastic Modulus in Transverse Direction	[N/m^2]
ν_{12}	Poisson's Ratio in plane containing fiber	[Unitless]
ν_{13}	Poisson's Ratio in plane containing fiber	[Unitless]
ν_{23}	Poisson's Ratio in transverse plane	[Unitless]
G_{12}	Shear Modulus in plane containing fiber	[N/m^2]
G_{13}	Shear Modulus in plane containing fiber	[N/m^2]
G_{23}	Shear Modulus in transverse plane	[N/m^2]
X_t	Tensile strength in fiber direction	[N/m^2]
X_c	Compressive strength in fiber direction	[N/m^2]
Y_t	Tensile strength in transverse direction	[N/m^2]
Y_c	Compressive strength in transverse direction	[N/m^2]

S_{12}	In-Plane Shear Strength	[N/m^2]
G_f^t	Fracture Toughness in longitudinal tensile direction	[J/m^2]
G_f^c	Fracture Toughness in longitudinal compressive direction	[J/m^2]
G_m^t	Fracture Toughness in transverse tensile fracture mode	[J/m^2]
G_m^c	Fracture Toughness in transverse compressive fracture mode	[J/m^2]
G_s	In-Plane Fracture Toughness	[J/m^2]
NSC	Normalized Sensitivity Coefficient	[Unitless]
CFRP	Carbon Fiber Reinforced Polymer	
GFRP	Glass Fiber Reinforced Polymer	

REFERENCES

[1] S. Abrate, Impact on Composite Structures, Cambridge University Press, Cambridge, UK, 1998.

[2] M. Aktas, C. Atas, B. Icten, R. Karakuzu, An experimental investigation of the impact response of composite laminates, Composite Structures. 87 (2009) 307–313.

[3] E. Al-Momani, I. Rawabdeh, An application of finite element method and design of experiments in the optimization of sheet metal blanking process, Jordan Journal of Mechanical and Industrial Engineering. 2 (2008) 53–63.

[4] F.S. Almeida, a. M. Awruch, Design optimization of composite laminated structures using genetic algorithms and finite element analysis, Composite Structures. 88 (2009) 443–454.

[5] A.Z. Arturas KERSYS, Neringa KERSIENE, Experimental Research of the Impact Response of E-Glass/Epoxy and Carbon/Epoxy Composite Systems, Materials Science. 16 (2010) 324–329.

[6] Z. Aslan, R. Karakuzu, B. Okutan, The response of laminated composite plates under low-velocity impact loading, Composite Structures. 59 (2003) 119–127.

[7] Y. Bai, Pipelines and Risers, Elsevier Ltd, Oxford, UK, 2001.

[8] H. Bakaiyan, H. Hosseini, E. Ameri, Analysis of multi-layered filament-wound composite pipes under combined.pdf, Composite Structures. 88 (2009) 532–541.

[9] K.-J. Bathe, Finite Element Procedures, Prentice Hall, New York, 1996.

[10] A. Bezazi, S. Pierce, K. Worden, E. Harkati, Fatigue life prediction of sandwich composite materials under flexural tests using a Bayesian trained artificial neural network, International Journal of Fatigue. 29 (2007) 738–747.

[11] E.M. Bezerra, a. C. Ancelotti, L.C. Pardini, J. a. F.F. Rocco, K. Iha, C.H.C. Ribeiro, Artificial neural networks applied to epoxy composites reinforced with carbon and E-glass fibers: Analysis of the shear mechanical properties, Materials Science and Engineering: A. 464 (2007) 177–185.

[12] K. Brownlee, C. Alexander, Methodology for Assessing the Effects of Plain Dents, Wrinkle Bends, and Mechanical Damage on Pipeline Integrity, in: NACE International Corrosion 2007 Conference & Expo, Nashville, Tennessee, USA, 2007: pp. 1–19.

[13] W.J. Cantwell, Geometrical effects in the low velocity impact response of GFRP, Composites Science and Technology. 67 (2007) 1900–1908.

[14] A. Chib, Parametric Study of Low Velocity Impact Analysis on Compsoite Tubes, Wichita State University, 2006.

[15] J. Dolbow, T. Belytschko, Numerical Integration of the Galerkin Weak Form in Meshfree Methods 1 Introduction, Computational Mechanics. 23 (1999) 219–230.

[16] M. V. Donadon, B.G. Falzon, L. Iannucci, J.M. Hodgkinson, Intralaminar toughness characterisation of unbalanced hybrid plain weave laminates, Composites Part A: Applied Science and Manufacturing. 38 (2007) 1597–1611.

[17] U. Farooq, K. Gregory, Finite Element Simulation of Low Velocity Impact Damage Morphology in Quasi _ Isotropic Composite Panels Under Variable Shape Impactors, European Journal of Scientific Research. 25 (2009) 636–648.

[18] U. Farooq, K. Gregory, Explicit Dynamic Simulation of Drop-Weight Low Velocity Impact on Carbon Fibrous Composite Panels, ARPN Journal of Engineering and Applied Sciences. 5 (2010) 50–61.

[19] J. Fish, A. Ghouali, Multiscale analytical sensitivity analysis for composite materials, International Journal for Numerical Methods in Engineering. 50 (2001) 1501–1520.

[20] B. Gershon, G. Marom, Fracture toughness and mechanical properties of glass fibre-epoxy composites, Journal of Material Science. 10 (1975) 1549–1556.

[21] H.M. Gomes, A.M. Awruch, P.A.M. Lopes, Reliability based optimization of laminated composite structures using genetic algorithms and Artificial Neural Networks, Structural Safety. 33 (2011) 186–195.

[22] S. Heimbs, S. Heller, P. Middendorf, Simulation of Low Velocity Impact on Composite Plates with Compressive Preload, Material II-Composites. (2008) 11–24.

[23] S.-C. Her, Y.-C. Liang, The finite element analysis of composite laminates and shell structures subjected to low velocity impact, Composite Structures. 66 (2004) 277–285.

[24] P. Hopkins, The Structural Integrity Of Oil And Gas Transmission Pipelines, Comprehensive Structural Integrity. 1 (2002) 1–62.

[25] R. Hosseinzadeh, M.M. Shokrieh, L. Lessard, Damage behavior of fiber reinforced composite plates subjected to drop weight impacts, Composites Science and Technology. 66 (2006) 61–68.

[26] L. Iannucci, M.L. Willows, An energy based damage mechanics approach to modelling impact onto woven composite materials—Part I: Numerical models, Composites Part A: Applied Science and Manufacturing. 37 (2006) 2041–2056.

[27] S.I. Ibekwe, G. Li, S.-S. Pang, B.H. Smith, Low Velocity Impact Response of a Laminated Composite Tube with a Metallic Bumper Layer, in: ICCE-14 FOURTEENTH ANNUAL INTERNATIONAL CONFERENCE ON COMPOSITES/NANO ENGINEERING, 2006: pp. 3–4.

[28] Z. Jiang, L. Gyurova, Z. Zhang, K. Friedrich, A.K. Schlarb, Neural network based prediction on mechanical and wear properties of short fibers reinforced polyamide composites, Materials & Design. 29 (2008) 628–637.

[29] H. El Kadi, Modeling the mechanical behavior of fiber-reinforced polymeric composite materials using artificial neural networks—A review, Composite Structures. 73 (2006) 1–23.

[30] M. Kamiński, Sensitivity analysis of homogenized characteristics for some elastic composites, Computer Methods in Applied Mechanics and Engineering. 192 (2003) 1973–2005.

[31] M.M. Kamiński, Computational mechanics of composite materials, 1st ed., Springer, Lodz, Poland, 2004.

[32] S.M.R. Khalili, M. Soroush, a. Davar, O. Rahmani, Finite element modeling of low-velocity impact on laminated composite plates and cylindrical shells, Composite Structures. 93 (2011) 1363–1375.

[33] M. Kleiber (Ed.), Handbook of Computational Solid Mechanics, 1st ed., Springer Verlag, Warsaw, Poland, 1998.

[34] K. Krishnamurthy, Impact response and damage in laminated composite cylindrical shells, Composite Structures. 59 (2003) 15–36.

[35] K.S. Krishnamurthy, P. Mahajan, R.K. Mittal, A parametric study of the impact response and damage of laminated cylindrical composite shells, Composites Science and Technology. 61 (2001) 1655–1669.

[36] K.S. Krishnamurthy, P. Mahajan, R.K. Mittal, A parametric study of the impact response and damage of laminated cylindrical composite shells, Composites Science and Technology. 61 (2001) 1655–1669.

[37] P. Laney, Use of Composite Pipe Materials in the Transportation of Natural Gas, Renewable Energy. (n.d.).

[38] D.S. Lee, C. Morillo, G. Bugeda, S. Oller, E. Onate, Multilayered composite structure design optimisation using distributed/parallel multi-objective evolutionary algorithms, Composite Structures. 94 (2012) 1087–1096.

[39] M. Lefik, D.P. Boso, B. a. Schrefler, Artificial Neural Networks in numerical modelling of composites, Computer Methods in Applied Mechanics and Engineering. 198 (2009) 1785–1804.

[40] C. Li, N. Hu, Y. Yin, H. Sekine, Low-velocity impact-induced damage of continuous fiber-reinforced composite laminates. Part I. An FEM numerical model, Composites Part A: Applied Science and Manufacturing. 33 (2002) 1055–1062.

[41] C. Li, N. Hu, J. Cheng, H. Fukunaga, H. Sekine, Low-velocity impact-induced damage of continuous fiber-reinforced composite laminates. Part II. Verification

and numerical investigation, Composites Part A: Applied Science and Manufacturing. 33 (2002) 1063–1072.

[42] P. a. M. Lopes, H.M. Gomes, a. M. Awruch, Reliability analysis of laminated composite structures using finite elements and neural networks, Composite Structures. 92 (2010) 1603–1613.

[43] G.-M. Luo, Y.-J. Lee, Quasi-static simulation of constrained layered damped laminated curvature shells subjected to low-velocity impact, Composites Part B: Engineering. 42 (2011) 1233–1243.

[44] E.-S. Mahdi, H. El Kadi, Crushing behavior of laterally compressed composite elliptical tubes: Experiments and predictions using artificial neural networks, Composite Structures. 83 (2008) 399–412.

[45] H. Man, G. Prusty, Neural network modelling for damage behaviour of composites using full-field strain measurements, Composite Structures. 93 (2011) 383–391.

[46] L. Marín, D. Trias, P. Badalló, G. Rus, J. a. Mayugo, Optimization of composite stiffened panels under mechanical and hygrothermal loads using neural networks and genetic algorithms, Composite Structures. 94 (2012) 3321–3326.

[47] M. Masi, S. Fogliani, S. Carra, Sensitivity Analysis on Indium Phosphide Liquid Encapsulated Czochralski Growth, Crystal Research and Technology. 34 (1999) 1157–1167.

[48] A.S. for T. and Materials, Standard Test Method for Determination of the Impact Resistance of Thermoplastic Pipe and Fittings by Means of a Tup (Falling Weight) 1, Book of Standards. 08 (1999) 1–8.

[49] C. Menna, D. Asprone, G. Caprino, V. Lopresto, A. Prota, Numerical simulation of impact tests on GFRP composite laminates, International Journal of Impact Engineering. 38 (2011) 677–685.

[50] M.J. Moeller, R.S. Thomas, H. Maruvada, N.S. Chandra, M. Zebrowski, F.M. Company, An Assessment of an FEA Body Model for Design Capability, Sounds and Vibrations. (2004) 24–28.

[51] S.S.P. Montestruc A.N., M.A. Stubblefield, R.H.L. V.A. Cundy, Composite Piping Systems to Improve Oil and Gas Production, Corrosion. (1995) 47–53.

[52] M.K. Naik, The Effect of Environmental Conditions on the Hydrostatic Burst Pressure and Impact Performance of Glass Fiber Reinforced Thermoset Pipes, King Fahd University of Petroleum and Minerals, 2005.

[53] N.K. Naik, S. Meduri, Polymer-matrix composites subjected to low-velocity impact: effect of laminate configuration, Composites Science and Technology. 61 (2001) 1429–1436.

[54] A.K. Noor, R.S. Shah, Effective thermoelastic and thermal properties of unidirectional fiber-reinforced composites and their sensitivity coefficients, Composite Structures. 26 (1993) 7–23.

[55] M. Peer, M. Mahdyarfar, T. Mohammadi, Evaluation of a mathematical model using experimental data and artificial neural network for prediction of gas separation, 17 (2008) 135–141.

[56] P.K. Pinnoji, P. Mahajan, Analysis of impact-induced damage and delamination in the composite shell of a helmet, Materials and Design. 31 (2010) 3716–3723.

[57] B.A. Qureshi, S.M. Zubair, A comprehensive design and rating study of evaporative coolers and condensers. Part II. Sensitivity analysis, International Journal of Refrigeration. 29 (2006) 659–668.

[58] N.F. Rilo, L.M.S. Ferreira, Experimental study of low-velocity impacts on glass-epoxy laminated composite plates, International Journal of Mechanics and Materials in Design. 4 (2008) 291–300.

[59] M.W.K. Rosenow, Wind Angle Effects in Glass Fibre-reinforced Polyester Filament Wound Pipes, Composites. 15 (1984) 144–152.

[60] D. Roylance, Laminated composite plates, in: Mechanics of Materials, John Wiley & Sons, Cambridge, MA, USA, 2000: pp. 1–17.

[61] Z. Salibi, Performance of reinforced thermosetting resin pipe systems in desalination applications: a long-term solution to corrosion - The Arabian Gulf example, Desalination. 138 (2001) 379–384.

[62] A.R. Setoodeh, P. Malekzadeh, K. Nikbin, Low velocity impact analysis of laminated composite plates using a 3D elasticity based layerwise FEM, Materials & Design. 30 (2009) 3795–3801.

[63] B. Sun, D. Hu, B. Gu, Transverse impact damage and energy absorption of 3-D multi-structured knitted composite, Composites Part B: Engineering. 40 (2009) 572–583.

[64] S. Suresh, P.B. Sujit, a. K. Rao, Particle swarm optimization approach for multi-objective composite box-beam design, Composite Structures. 81 (2007) 598–605.

[65] R. Tiberkak, M. Bachene, S. Rechak, B. Necib, Damage prediction in composite plates subjected to low velocity impact, Composite Structures. 83 (2008) 73–82.

[66] V. Tita, J. de Carvalho, D. Vandepitte, Failure analysis of low velocity impact on thin composite laminates: Experimental and numerical approaches, Composite Structures. 83 (2008) 413–428.

[67] A. Vassilopoulos, E. Georgopoulos, V. Dionysopoulos, Artificial neural networks in spectrum fatigue life prediction of composite materials, International Journal of Fatigue. 29 (2007) 20–29.

[68] S.B. Visweswaraiah, H. Ghiasi, D. Pasini, L. Lessard, Multi-objective optimization of a composite rotor blade cross-section, Composite Structures. (2012).

[69] S.E. Watkins, F. Akhavan, R. Dua, K. Chandrashekhara, D.C. Wunsch, Impact-induced damage characterization of composite plates using neural networks, Smart Materials and Structures. 16 (2007) 515–524.

[70] G. Xiao, Z. Zhu, Friction materials development by using DOE/RSM and artificial neural network, Tribology International. 43 (2010) 218–227.

[71] F.J. Yang, W.J. Cantwell, Impact damage initiation in composite materials, Composites Science and Technology. 70 (2010) 336–342.

[72] N.O. Yokoyama, M.V. Donadon, S.F.M. de Almeida, A numerical study on the impact resistance of composite shells using an energy based failure model, Composite Structures. 93 (2010) 142–152.

[73] G.P. Zhao, C.D. Cho, Damage initiation and propagation in composite shells subjected to impact, Composite Structures. 78 (2007) 91–100.

VITAE

Name: Muhammad Haris Malik

Date of Birth: 6th January, 1986

Place of Birth: Karachi, Pakistan

Address: Flat F-8, Block "L", North Nazimabad, Karachi 74700, Pakistan

Phone: +966-508017957, +92-333-3751670

Email: mharis@kfupm.edu.sa, haris.malik@hotmail.com

ACADEMICS

Master of Science (Mechanical Engineering) Sep 2010-Dec 2012

King Fahd University of Petroleum and Minerals, Dhahran, KSA

CGPA 3.94/4

Field of Research

Engineering Mechanics, Non-linear Finite Element Analysis, Materials

Thesis

Optimization of the Impact Resistance of Composite Laminated Plates and Pipes

Bachelor of Engineering (Aerospace) Sep 2003-Sep 2007

Institute of Space Technology, Islamabad, Pakistan

CGPA 3.85/4 (1st Position) Honors: Megna cum Lauda, Presidential Gold Medal

Final Year Project

Buckling analysis of filament wound thin walled cylinder under axial compression and bending moment using analytical and FE techniques with application of softwares like MATLAB and ANSYS